EUROPEAN COMMISSION

Community Research

MATISSE

Materials' Innovations for Safe and Sustainable nuclear

FP7-Fission-2013
Combination of Collaborative project (CP) and Coordination and Support Actions (CSA)

Grant agreement no: 604862
Start date: 01/11/2013 Duration: 48 Months

D2.41

Analysis and assessment of mechanisms of irradiation creep

MatISSE – Contract Number: 604862

Document title	Analysis and assessment of mechanisms of irradiation creep
Author(s)	Vladimir Borodin (guest scientists at KIT), Jia-Chao Chen (PSI), Maxime Sauzay (CEA), Pavel Vladimirov (KIT)
Number of pages	111
Document type	
Work Package	MOIRA
Document number	
Issued by	KIT
Date of completion	05/12/2014
Dissemination level	Confidential, only for consortium members (including the Commission Services)

Summary

Experimental results and theoretical models of irradiation creep accumulated for more than 50 years are reviewed. The influence of experimental conditions on parametric dependencies of irradiation creep are discussed and associated with the underlying microstructual evolution. The analysis of the experimental data accumulated during this period allows confident correlation of the dislocation structure evolution in irradiated materials with various stages of irradiation creep, thus providing a reliable basis for analytical description of this complicated phenomenon.

The existing theoretical models of irradiation creep are reviewed and their ability to reproduce the dose, stress and temperature dependencies of irradiation creep are critically assessed. It is demonstrated that theoretical models are able to give reasonable description of irradiation creep in a broad range of irradiation doses, external stresses and test temperatures, both qualitatively and, often, even quantitatively.

Approval

Rev.	Date	First author	WP leader	Project Coordinator
0	05/12/2014	V. Borodin, KIT	L. Malerba, SCK•CEN	A. Michaux, CEA
1	29/04/2015	V. Borodin, KIT	L. Malerba, SCK•CEN	A. Michaux, CEA
			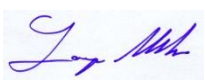	

Distribution list

Name	Organisation	Comments
All beneficiaries	MatISSE	

Table of contents

1. Introduction

Irradiation is known to deteriorate mechanical properties of materials, either modifying the out-of-reactor effects (e.g. creep or phase decomposition), or leading to completely new phenomena (irradiation swelling, low-temperature embrittlement). The change of material behaviour under irradiation is related to a type of defect microstructure evolution, that would not occur in the absence of irradiation. The understanding of these mechanisms is important to prevent undesirable consequences of irradiation on the reliability of structural materials.

This review is restricted to irradiation creep. Creep in general means irreversible long-term deformation of a material subject to the action of external loads. Due to its irreversibility, this effect has some resemblance to plastic deformation, but it is a different phenomenon because it takes place at loads below the yield stress of the studied material. In metals, creep is observed at high temperatures even in the absence of irradiation (this is often referred to as thermal creep). The rate of thermal creep sharply falls with temperature decrease and at low temperatures (below approximately half the melting temperature of the material, T_m), the thermal creep is usually negligible for practical applications of nuclear reactor structural materials. Irradiation, however, pronouncedly accelerates creep in the low temperature range where thermal creep is negligible. The irradiation induced strain rate can reach 10 %/hour at applied loads of hundreds of MPa, being orders of magnitude higher than that of thermal creep. The functional dependence of the irradiation creep rate on experimental and material parameters (test time, temperature, load level, material composition) sharply changes as well. For example, the scaling of creep rate with the value of applied stress and test temperature is completely different under irradiation and without it [1]. Moreover, the steady-state irradiation creep rates in different materials are very similar, whereas the thermal creep rates of the same materials can differ by many orders of magnitude [2]. The material pre-processing can completely differently affect the irradiation and thermal creep; e.g. preliminary aging of a material results in the suppression of thermal creep and the acceleration of irradiation creep [3]. All these observations point to an inherently different origin and mechanisms for irradiation and thermal creep, despite the similarity of the macroscopic effects.

Irradiation changes the microstructural mechanisms involved in material deformation so significantly, that irradiation creep should be considered as an independent physical phenomenon, rather than a simple acceleration of thermal creep by irradiation. Interestingly, the essential difference between irradiation and thermal creep was realized early in the irradiation creep investigations (see e.g. [4]), which started in the early sixties of the last century, when in-reactor

deformation of fuel pins became a serious technological problem. A typical map of deformation mechanisms as a function of irradiation temperature and applied load is shown in Fig. 1.1.

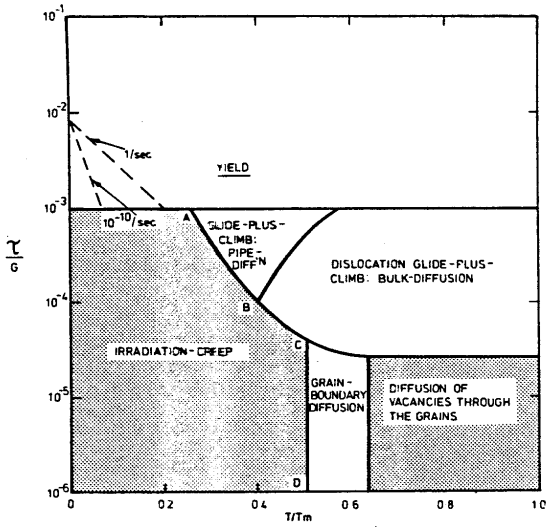

Fig. 1.1 Notional deformation map for a bcc metal under stress in a fast-breeder reactor. Irradiation creep gives way to thermal creep at about one-half the absolute melting point. τ - shear stress; *G* - shear modulus; *T* - absolute temperature; T_m - melting point. Contours enclose dominant creep mechanisms. ABCD = boundary between irradiation creep (shaded) and various mechanisms of "thermal" creep. According to [5].

The first experimental results [6-10] gave contradictory information on the existence and the magnitude of irradiation creep. However, already by the beginning of the 1970s, when sufficient data for high irradiation doses in fast reactors (~10^{21} -10^{22} n/cm^2) had been accumulated, it became evident that the creep acceleration under irradiation is a universal phenomenon inherent to a wide class of nuclear materials, including steels, nickel-based and zirconium-based alloys. Further investigations expanded the range of investigated materials to ferritic-martensitic steels, to various pure metals (see Table 1.1) and 'pure' metallic alloys (e.g. V-Fe-Ti [11-13], Ni-Al [14], Cu-W [15,16]), as well as some non-metallic materials (graphite, SiC).

Irradiation creep was intensively studied in the 1970s and 1980es, as can be noticed in Fig. 1.2. These studies have largely clarified the creep behaviour of structural and functional materials in typical rector operation environments and suggested ways to circumvent the most unpleasant consequences of it in stressed metallic components of reactor core (such as fuel pin claddings and wrappers). In parallel, the basic microscopic mechanisms of irradiation creep were studied intensively.

Table 1.1 Pure metals, where irradiation creep was investigated.

Material	**References**
Aluminum (Al)	[17-26]
Beryllium (Be)	[27]
Copper (Cu)	[28-33]
Iron (Fe)	[34]
Molybdenum (Mo)	[10,35-37]
Nickel (Ni)	[8,10,27,31,35,38-66]
Niobium (Nb)	[27,67,68]
Platinum (Pt)	[27,31]
Silver (Ag)	[31]
Titanium (Ti)	[10,50,69,70]
Tungsten (W)	[27,71]
Vanadium (V)	[72,73]
Zirconium (Zr)	[34,69,74-78]

By the end of the 1980s irradiation creep became "predictable", even if not fully understood. Reactor developers got at least a "qualitatively feeling" of what one should expect in relevant operation conditions. Accompanied by the general decrease of public interest to nuclear power and the corresponding funding decline at the end of the 1980, this fact led to a considerable decrease of experimental research in the field of irradiation creep, starting from the mid-1990s. At this time, experiments were oriented either towards new materials (in particular - ferritic-martensitic steels [79-86], including oxide-dispersion strengthened (ODS) ones [87-93]) that raised in importance in nuclear power industry, or on the better understanding of the topics that remained unclear from the basic point of view (first of all – the correlation between irradiation creep and swelling [94-99]). Theoretical studies in the last two decades were extremely rare.

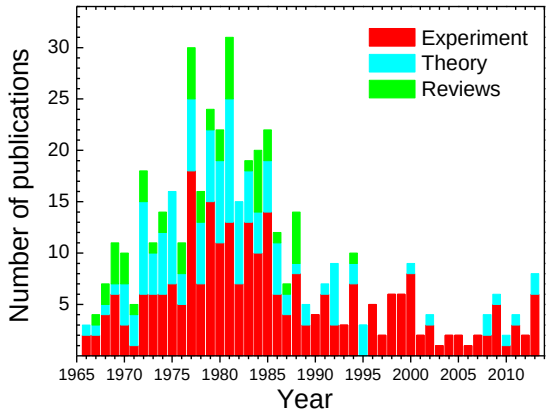

Fig.1.2. Publication activity on irradiation creep

Due to the noticeable decline in research activity, the general picture of the irradiation creep phenomenon remains far from complete, despite the large amount of already accumulated experimental data. Because the creep tests are primarily carried out in fast reactors, where the acquisition of experimental points requires significant time of irradiation (months and years) and expensive equipment, the studies of irradiation creep are predominantly application-relevant and thus the largest amount of data is accumulated for austenitic stainless steels, that is the most complicated system for physical interpretation (so, in this review data on these steels will unavoidably be the main reference). In order to better understand the basic features of irradiation creep in metals, more investigations in better controlled conditions and on simpler systems (such as pure metals) are required. Experiments of this type are possible with the help of charged particle accelerators and high-voltage electronic microscopes (HVEM). The damage creation rates in these facilities are usually higher than in reactors (sometimes even several orders of magnitude higher, e.g. in 1 MV electron microscopes) and it is possible to monitor experimental parameters (deformation, loading, temperature and intensity of irradiation) with high accuracy. The radioactivity of irradiated samples is very low and the microstructure development can be quickly analyzed. Though simulation experiment results cannot be directly extrapolated to in-reactor material behaviour, they are very useful for the elucidation of the basic mechanisms of irradiation creep.

Though simpler than other radiation-induced effects, irradiation creep remains a complex and ambiguous phenomenon, sensitive to many parameters of irradiation and material. Comparison of results for various experimental conditions and techniques, as well as extrapolation of results over wide ranges of material loading and irradiation parameters, can be reliably carried out only provided the physical mechanisms underlying irradiation creep are clear. Although the first theoretical models of irradiation creep were proposed soon after detection of this effect (see reviews [100-102]), an unequivocal theoretical description is not yet achieved. The currently widespread models have their areas of applicability and are not universal for all experimental conditions.

This review presents a systematic overview of the basic features and underlying physical mechanisms of irradiation creep. In section 2 the basic experimental laws describing irradiation creep are presented and related to the kinetics of defect microstructure responsible for the long-term straining of simultaneously loaded and irradiated metals. Section 3 summarizes the current models for the material microstructure development resulting at the macroscopic level in irradiation creep.

2. The laws of irradiation creep

Irradiation creep is, as already said, the irreversible deformation of irradiated materials under the action of applied subyield loads. However, creep is not the only mode of strain accumulation in irradiated materials. For instance, the whole volume of the material often increases under irradiation (the effect is called swelling) and it is usually desirable to separate the effects of swelling and creep. The common way to do so is to describe the isotropic volume change of the material as swelling and the volume-conserving part of strain as creep. It should be kept in mind, however, that this division is no more than a formal agreement, because the mechanisms leading to both kinds of deformation are strongly interrelated at the microstructural level and cannot be separated easily into those causing swelling and those causing creep. The application of loads to a material is known to affect swelling and the changes in swelling would definitely keep the material shape unchanged only provided the material has cubic lattice, the applied loads are hydrostatic and the essential microstructural features causing strain are isotropic. Non-hydrostatic stresses and non-isotropic dislocation distributions can cause swelling-induced shape modification even in cubic lattice materials [103]. In non-cubic (e.g. hcp) materials, shape modifications can take place under irradiation even without external loading; the effect is referred to as radiation growth. For this reason, the volume-conserving deformation is usually additionally separated into two parts, namely radiation growth and irradiation creep. As a consequence, any material deformation that is not due to the effect of applied stresses is not classified as creep. The evident consequence is that in an unloaded material the irradiation creep vanishes by definition.

The second circumstance that should be taken into account when dealing with irradiation creep is that, as already mentioned, creep can occur in metals even in the absence of irradiation. It has thermofluctuative nature and is usually quite pronounced at temperatures exceeding approximately half of the material melting temperature, T_m. Irradiation creates in the material microscopic damage that can additionally contribute to the matter transfer even at those temperatures, where thermal creep is negligible. Hence, it is a common practice to further separate the creep strain into irradiation-free (thermal) and irradiation-induced contributions.

It is experimentally established that creep in crystalline metals is a macroscopic manifestation of the defect microstructure rearrangement under the effect of external loading. Most often, the shape change of material is related to dislocation system evolution (see e.g. [104,105]). The mechanisms not involving dislocation kinetics are more rare but still possible and can be of importance in e.g. ultra-fine grained materials (with the grain size < 0.1 μm, e.g. [15,16]) or at super-high levels of

plastic deformation. In these cases the strain is governed by grain boundary kinetics, involving such effects as grain boundary sliding, point defect diffusion directly between grain boundaries [106,107], or dislocation annihilation in low-angle boundaries [108,109]. However, in the majority of application-relevant materials, where the average grain size is well above 1 μm, the contribution of grain boundaries to creep is of secondary importance. Hence, in the discussion below the known parametric scaling of irradiation creep (on radiation fluence and flux, external load, irradiation temperature, etc.) are correlated to the dislocation system kinetics and to possible effects from other microscopic defects, such as secondary phase precipitates, voids, gas bubbles, etc. [110, 111].

2.1 Dose dependence of irradiation creep

First of all, let us consider the dependence of irradiation creep strain on the irradiation dose, which is the product of irradiation time by irradiation intensity. The latter is usually measured either in terms of the total number of particles penetrating the sample through a unit surface per unit time (irradiation flux, Φ), or in terms of the average number of times (per unit time) a material atom is displaced from its lattice site by bombarding fast particles (damage production rate, G). These values can be related as

$$G = \Phi \int \nu(E)\sigma(E)S(E)dE\,, \qquad (2.1)$$

where σ is the lattice atom displacement cross-section and ν – the cascade function, i.e. the average number of vacancy–interstitial pairs, created by a recoil with the energy E. Typically, each irradiation produces its own energy spectrum $S(E)$ of primary recoils and so the product $\nu\sigma$ should be averaged over all energies of all types of primary recoils caused by incident particles.

Damage production expressed in displacements per atom (dpa) provides a universal characterization of primary damage, which is insensitive to particular types and energies of irradiating particles used and allows a straightforward comparison of predictions from different experiments. Unfortunately, an accurate conversion of irradiation exposure into dpa is not an easy task and is sensitive to many factors, such as the type and the energy spectrum of the incident particles, the chemical composition of the irradiated material, the energy spectra of secondary and higher-order recoils, the efficiency of cascade production of displaced atoms, etc. An even more complicated situation is met for simulation experiments in charged particle accelerators, where radiation damage is non-uniform over the sample depth and is very sensitive to the incident particle parameters. As a matter of fact, displacements per atom should be recalculated for each particular experiment, using the same reference technique of the cascade function calculation. Depending on the conversion procedure

adopted, the errors in the dpa calculation can easily reach tens percent, which should be kept in mind when quantitatively comparing the results of experiments performed in different irradiation facilities and even in different places of the same facility (e.g. in different location in the fission reactor core).

It is a common practice to normalize the measured creep rate to the "standard" point defect generation rate. For fission reactors one typically applies the so called NRT-standard [112]. It is well known, however, that the displacement rates in the case of cascade-forming irradiation can strongly differ from the NRT value, G_{NRT}. Often the 'true' damage generation rate is expressed in terms of G_{NRT} as,

$$G = \zeta G_{NRT}, \tag{2.2}$$

the correction factor ζ can vary from ~ 0.1-0.2 for fast-reactor neutron irradiation [113-120] to ~ 1 for irradiation with 1-2 MeV electrons [113,121].

Having in mind the difficulties with the quantitative interpretation of the data from different sources, attention is paid below mainly to qualitative features of the creep dependence on irradiation dose.

Judging from the experimental observations, at least three markedly different stages of irradiation creep can be distinguished within the fluence range up to ~150 dpa. These stages can be more or less pronounced depending on particular experimental conditions. In the first stage (transient), the creep rate continually decreases, tending to a steady-state value. The latter persists in a certain range of doses, constituting the second stage (steady-state) of irradiation creep. In a certain range of experimental parameters the third stage of irradiation creep can be observed, where the creep rate first increases as compared to the second stage, but then can appreciably decrease or even be completely suppressed later on.

2.1.1 Primary transient creep (stage I)

A typical pattern of the loaded material response to the onset of irradiation is shown in Fig. 2.1(a). The onset of irradiation results in fast acceleration of the strain rate of pre-loaded material [61,67, 68,124-127]. The time required for the creep rate to increase to the new value is usually so short, in comparison to the typical time scale of reactor and simulation experiments, that the increase of the creep rate looks "jump-like". However, a detailed kinetics of the creep rate acceleration stage can be observed in experiments with very low-rate damage production, see Fig. 2.1(b). Actually, the initial creep acceleration on the irradiation switch is not always observed, being sometimes replaced by an

'incubation period' [128,129] or even some amount of 'negative creep' [45,123,130], see e.g. Fig.2.1(c). However such observations are rare and result usually from the action of some competing processes of sample contraction or densification that are promoted by the onset of irradiation.

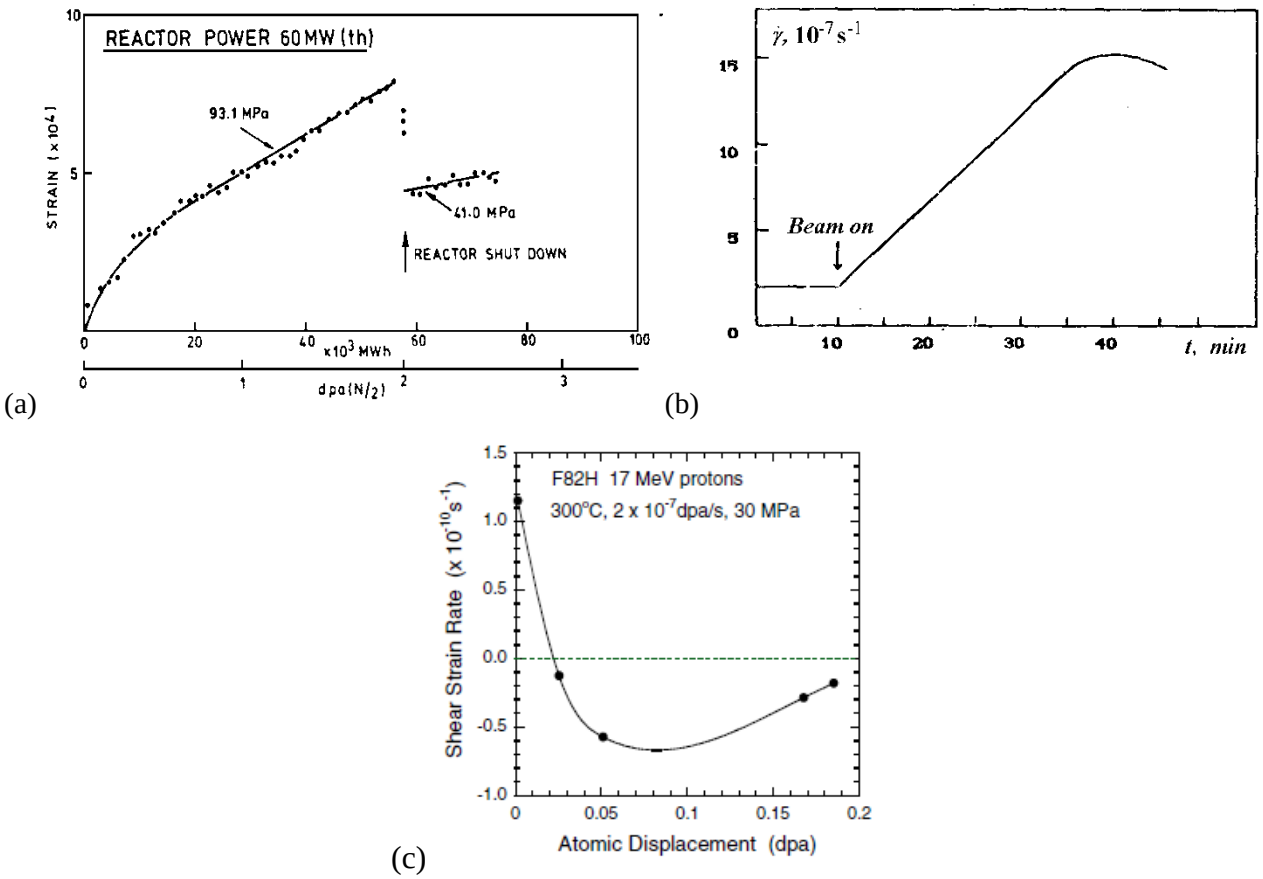

Fig 2.1. (a) An example of transient creep stage: tensile creep of En58B in DFR (from [122]). (b) The initial stage of creep in a twisted Al wire irradiated with 2MeV electrons at a rate of 10^{13} $e^-/(cm^2\ s)$ [26]. (c) An example of 'negative' initial irradiation creep in F82H steel thin wire loaded in torsion (from [123]).

After the quick initial increase, the creep rate gradually falls down to a practically constant value. This creep rate stabilisation takes tens to hundreds of hours in fast neutron reactors [124, 131-136] and tens of hours for charged particle irradiation [43,48,49,51,55,62,126,133,137], equivalent to doses of 0,01-1 dpa. The dependence of the transient strain ε on the irradiation dose $\varphi = Gt$ is approximated in the literature with various relations, e.g. $\varepsilon \propto (1 - \exp(-A\varphi))$ [8,27,36, 37,69,71,138,139] or $\varepsilon \propto \ln(1+A\varphi)$ [41,44], where A is an empirical constant. Theoretical models

are usually in favour of power laws, $\varepsilon \propto \varphi^m$ with $m < 1$ (for example m = 0,46 [140], m = 0.61 [141] or m = 2/3 [142,143]).

During the transient creep stage one usually observes a pronounced evolution of the dislocation microstructure. Prior to the onset of irradiation a metallic sample contains usually a network of weakly nonlinear dislocations, the density of which depends on preliminary thermal and mechanical processing and varies from 10^{11}-10^{12} m^{-2} (in annealed materials) up to ~10^{15}-10^{16} m^{-2} (in strongly cold-worked materials). Usually dislocations are distributed in space rather non-uniformly, a large portion of dislocations being collected in subgrain boundaries and dislocation walls. When the material was loaded prior to the onset of irradiation (to saturate the thermal creep component), dislocation pile-ups constitute a typical feature of material microstructure [144-146].

Practically immediately after the beginning of irradiation interstitial dislocation loops (of Frank type in fcc metals such as austenitic steels) are nucleated in the material [26,43,144,145,147-154]. Their nucleation is the direct consequence of point defect generation in the material by irradiation. The mobility of interstitials in metals is much higher than that of vacancies and remains appreciable down to room temperature (typically, the single interstitial migration barriers are of the order of E_{mI} ~ 0.1-0.3 eV, while those for a vacancy are E_{mV} ~ 0.6-1.3 eV [155]). Hence, for some time after the beginning of irradiation vacancies can be considered as practically immobile, whereas interstitials efficiently diffuse, recombine with vacancies, create interstitial clusters and annihilate at network dislocations. The interstitial clustering, in particular, results in the formation of small interstitial complexes, which are very stable (a typical binding energy of a di-interstitial is of the order of 1 eV [156,157], while the energy of the third interstitial binding to a di-interstitial can be even higher, e.g. ~ 1.5 eV [157]) and constitute the nuclei of interstitial loops. The efficiency of loop nucleation is sensitive to the competition for freely-mobile interstitials between dislocations and newly formed loops, so that the higher initial dislocation network density in cold-worked metals can be expected to somewhat suppress loop nucleation, as compared to annealed samples. Nonetheless, dislocation loop formation following the onset of irradiation is a common feature of dislocation kinetics in both annealed and cold worked materials [158].

Intensive loop nucleation is observed for a limited time (definitely less than 10^{-2}-1 dpa [37, 76,151,154,159-161]). Then the density of loops either saturates, or increases slowly, for example as a consequence of direct in-cascade loop nucleation. The duration of the intensive loop nucleation stage is limited for at least two reasons. First of all, when sufficiently large number density of dislocation loops is formed, the newly created interstitials are more frequently absorbed by these loops (and, naturally, by the network dislocations) than they meet each other. Secondly, the

concentration of vacancies after some time of irradiation increases so much that, despite their low mobility, they become absorbed at point defect sinks approximately at the same rate as the interstitials. As a result, after a certain irradiation dose the further nucleation of interstitial loops is suppressed [154,153,160-162]. According to theoretical estimates, the main part of dislocation density in interstitial loops in conditions relevant for nuclear reactors (temperatures of 200-600^{o}C and dose rates ~ 10^{-7} dpa/s) is accumulated within the time between 5 10^{-7} dpa [163,164] and 10^{-3} dpa [165].

After the termination of the loop nucleation stage, the ensemble of dislocation loops grows until they are built into the dislocation network as a result of intersection with other dislocations [152, 153,160] or are absorbed by grain boundaries. If the material grains are sufficiently large and the initial dislocation density is sufficiently low, in fcc metals such as austenitic steels the faulted Frank dislocation loops can reach a size where it is energetically favourable for them to transform into polyhedral perfect loops [144,145, 166-169]. A non-hydrostatic external load can influence the direction of unfaulting reaction. As a result, the asymmetric unfaulting of loops can lead to anisotropic distribution of loops over orientations [169], which, as shown in sect. 3, directly affects the creep rate at the transient stage.

The growth kinetics of large perfect loops is similar to that of network dislocations. The segments of dislocation line in a perfect loop tend to become straight and their efficiency for point defect absorption can feel the details of the dislocation core microstructure (kinks and jogs on the dislocation line). In contrast, the edge of the extra-plane in a small loop is strongly curved and always provides sufficient place for easy absorption of point defects. Accordingly, the growth of perfect loops is expected to occur more slowly than that of Frank loops (as is indeed observed experimentally [170]).

The growth of irradiation induced dislocation loops and their embedding in the network result in the increase of the overall dislocation density. At the same time, the irradiation-enhanced mobility of network dislocations results in their accelerated annealing, especially in dislocation walls, where their density is much higher than the average in the bulk. Competition between these two oppositely directed processes results in the complete dislocation structure transformation from that typical to thermal creep (with utterly spatially non-uniform dislocation distribution) to a uniform dislocation network with dislocation density at the level of 3-6×10^{14} m^{-2} [148,171-177]. The final dynamic equilibrium dislocation structure is practically insensitive to the dislocation density level in a sample prior to irradiation [173,178,179], see Fig. 2.2. The doses necessary to reach the steady state dislocation density are < 10-20 dpa [148,171-177], sometimes even < 1 dpa [47,149, 180]. Since

irradiation creep is the manifestation of dislocation movement in the material, **it is reasonable to relate the establishment of the dynamic equilibrium dislocation density with the onset of the steady-state irradiation creep stage**. Indeed, simulation experiments show [47,181], that the formation of the dislocation structure relevant for the subsequent steady-state stage of irradiation creep is practically finished by the end of the transient stage.

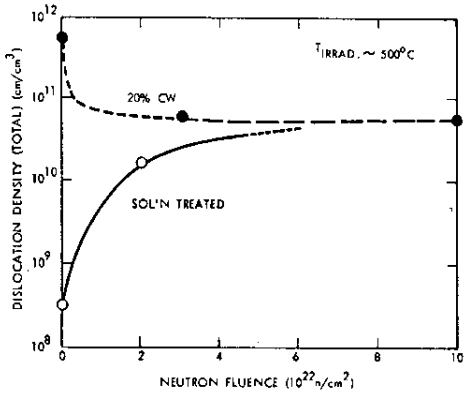

Fig. 2.2. The variation of the dislocation density during neutron irradiation in type AISI 316 SS [173].

The considerations above imply that the transient stage of irradiation creep is a macroscopic manifestation of the movement of network dislocations and the growth of interstitial dislocation loops. Strictly speaking, under certain irradiation conditions (e.g. during the cascade-producing irradiation with fast neutrons and high-energy heavy ions) one can expect also the formation of small (< 1 nm) vacancy loops generated athermally in collision cascades [163]. However, vacancy loops are of secondary importance for irradiation creep. First of all, the dose dependence of irradiation creep is practically identical for all kinds of irradiation, whereas cascade vacancy loops are not formed during irradiation with light charged particles and fast electrons. Secondly, vacancy loops in most of the reactor structural materials (except for zirconium and its alloys [182]) usually quickly dissolve under irradiation and, after the establishment of the steady-state loop size distribution, the role of vacancy loops is reduced to qualitatively unimportant (though to a certain degree affecting quantitative estimates) renormalization of point defect generation rate [183-186]. The account of the vacancy loop contribution to the creep transients [187,188] has only theoretical interest, because these loops can be responsible for only an insignificant part of the total material strain at the transient stage. Analytical estimates indicate that their contribution does not exceed 0.1% [187,189].

The weak sensitivity of the established dislocation density to that present before irradiation implies that the steady-state creep stage should be only weakly sensitive to the differences in the preliminary thermal-mechanical treatment of the irradiated material, which is usually indeed the case [8,40,130,190-193]. In contrast, at the transient stage the effect of the thermal-mechanical treatment can be quite noticeable and results from the domination of one or another competing process that leads to the establishment of the steady-state dislocation density. In annealed materials the transient strain is mainly due to the growth of dislocation loops, whereas in cold-worked materials a contribution from the dislocation network annealing might be of importance. It is usually found that at transient stage cold-worked samples deform faster [8,10,38,39,40, 140,19] and accumulate higher total strain [8,38,40,195] than those annealed. The trend in the duration of the transient stage is less clear, since both increase of transient stage duration with increased cold-work level [45,195] and complete absence of transient stage were reported in cold-worked samples [190].

2.1.2 Steady-state creep (stage II)

After the termination of the transient stage the irradiation creep rate becomes approximately constant, as exemplified in Fig. 2.3. The dislocation structure at this stage consists of network dislocations and large dislocation loops. The total dislocation density remains at this stage approximately constant.

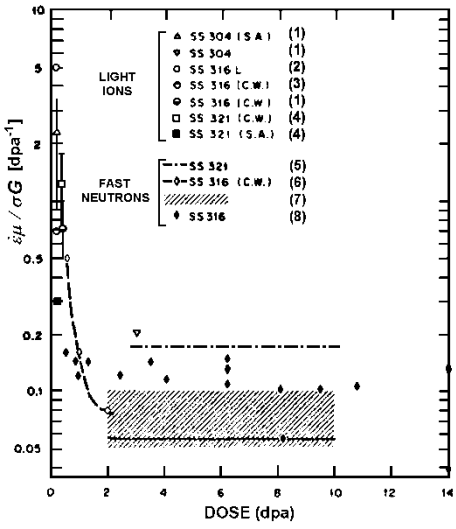

Fig. 2.3. Normalized irradiation creep rate, $\dot{\varepsilon}\mu/\sigma G$, versus dose for stainless steels irradiated with light ions and neutrons (from [113]). References: (1) - [133]; (2) - [114,196]; (3) - [137]; (4) - [45]; (5) - [75]; (6) - [139]; (7) - [40]; (8) - [197].

The independence of the creep rate of the irradiation dose makes this stage the most suitable for studying irradiation creep dependence on various experimental parameters, for comparing results of various experiments and for verification of theoretical modeling predictions.

Many experiments [23,41,44,53,63,75,134,137,155,195,198-203] indicate that in the temperature range of 0.3-0.5 T_m **the steady-state irradiation creep strain depends linearly not only on the dose, but also on the point defect generation rate *G*** (Fig. 2.4). The non-linear (e.g. square root [75,122,127,206-208]) dependence of creep strain on the irradiation flux is often reported for lower temperatures and is typically ascribed to enhanced efficiency of point defect recombination. However, a re-evaluation [17] of some of these data indicates that the non-linearity in *G* can equally well result from misinterpretation of experimental data.

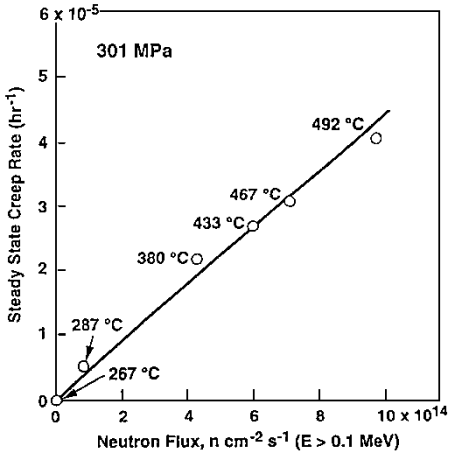

Fig. 2.4. Flux dependence of the secondary creep rates observed in annealed type 09KH16N15M3B SS irradiated in the BR-10 fast reactor (from [204], based on data from [205]).

Having in mind the linear dependence of the irradiation creep strain ε on the irradiation dose, it is convenient to define the so-called irradiation creep modulus, *B*, i.e. the creep strain per unit dose and unit stress,

$$B = \frac{\varepsilon}{\sigma G t}$$

As shown below in section 2.2, at relatively low external stresses the creep rate is directly proportional to the applied stress σ and thus the creep modulus is practically independent of either irradiation or loading conditions. Therefore, the creep modulus is a good measure of the irradiation creep sensitivity to material parameters.

It turns out that the irradiation creep modulus in various metals lays, with rare exceptions, in a rather narrow range (see Table 2.1). Interestingly, the strengthening of ferritic-martensitic steels with high densities of nanometric oxide particles has practically no effect on irradiation creep [88, 90,91,93], so ODS steels are sited together with the normal steels of this class. Examples of the weak variability of the creep modulus for the case of stainless steels are shown in Figs. 2.3 and 2.5.

It can be also noticed that the creep modulus in the accelerator experiments is typically an order of magnitude higher than that measured for the same material in nuclear reactors. This can be, to some extent, an artifact related to the uncertainties of the dpa calculations because, as discussed in relation to eq. (2.2), the efficiency of defect creation depends on the particular irradiation conditions, which is seldom taken into account in the experimental estimates of the creep modulus.

Table 2.1 The typical irradiation creep modulus values for in-reactor irradiations (B_n) and simulation experiments (B_i)

Material	B_n, 10^{-6} $(dpa \times MPa)^{-1}$	B_i, 10^{-6} $(dpa \times MPa)^{-1}$	Temperature range, ^oC	References*)
Austenitic stainless steels	1 – 10	10 – 50	150 – 550	
Ferritic-martensitic steels (including ODS steels)	0.1 – 1	5-10	300 – 500	
Zirconium (pure or Nb doped)	10 – 50	-	300	
Zircaloy-2	100 – 500	10^3	300	
Nickel and high-nickel alloys	1 – 10	20 – 200	200 – 550	
V-4Cr-4Ti	2-5		400-600	[13]
Titanium	2 – 15	-	300 – 450	[50,7]
Aluminum	10^6 – 10^7	-	60 - 250	[20,23,25]
Copper	-	100	200 - 300	[15,31,65]
Silver	-	300 - 500	150 - 300	[31,65]

*) References are given only for materials, which are not studied extensively.

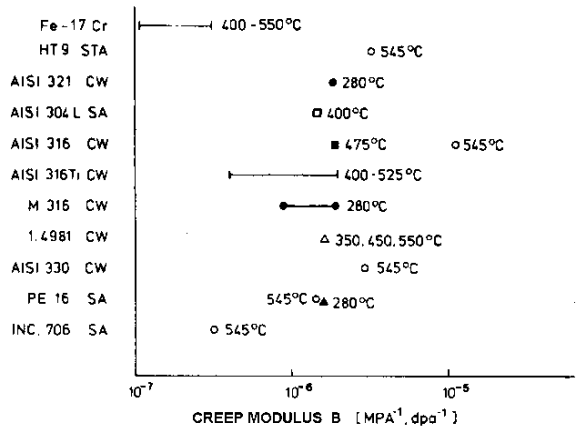

Fig. 2.5. Irradiation creep modulus for several austenitic stainless steels [209]. The data are from: ○ - [210], ● - [122], □ - [211], ■ - [197], Δ - [212], σ - [206], |----| - [213], |-- · --| - [214].

2.1.3 Accelerated creep stage (stage III)

At sufficiently large doses (from 3 up to 30 dpa [40,206,211,215-219]) an increase of irradiation creep rate with irradiation dose can be sometimes observed, e.g. Fig. 2.6(a). Usually, however, the creep rate does not grow indefinitely, but saturates at a new level, exceeding that of secondary

creep, Fig 2.6(b). For this reason, one should be cautious with the interpretation of the measured creep data at the fluences exceeding tens of dpas. The linear dependence of the creep strain on dose in this case may be misleading and distort the creep modulus due to the neglecting of the mechanisms (e.g. swelling) that might lead to the creep acceleration.

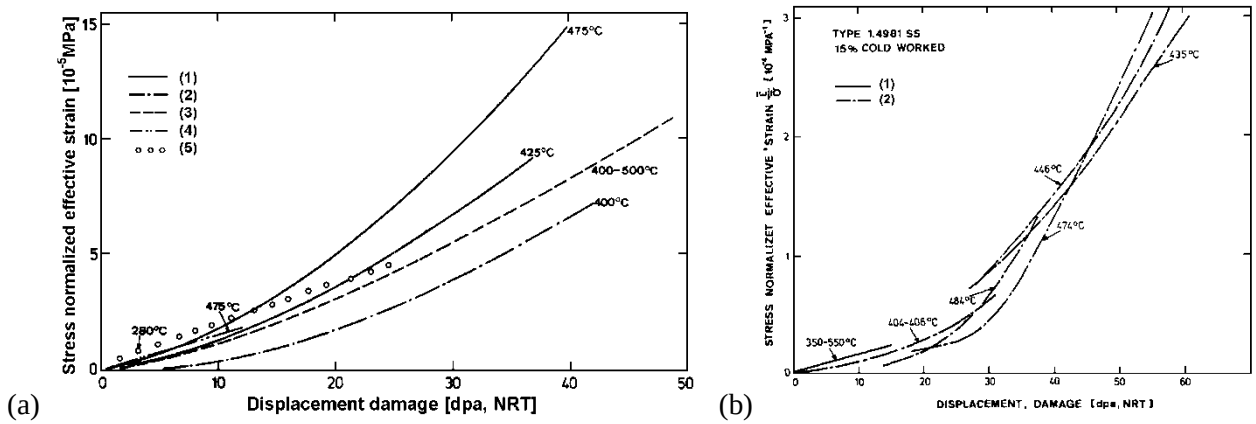

Fig. 2.6. (a) Dose dependence of the stress-normalized creep deformation for type AISI 316 SS. (b) Dose dependence of the stress-normalized creep deformation for 15% CW type 1.4981 (from [209]; the data are from: (a1) - [220]; (a2) - [221]; (a3) - [213]; (a4) - [197]; (a5) - [122], (b1) -[212], (b2)-[222])

The dose dependence of irradiation creep in the third stage is described in the literature in two ways. Sometimes the creep strain is expressed directly in terms of irradiation dose, using both continuously increasing relations like $\varepsilon \propto \varphi^n$ ($n > 1$) [223] and relations accounting for the creep rate saturation (for example for steel 316 they propose $\varepsilon \propto A\varphi + B \ln[\mathrm{ch}(\varphi/\varphi_0)]$, where A and B are some constants and $\varphi_0 \approx 50$ dpa [219]). Alternatively, there is a common trend to ascribe the acceleration of irradiation creep to the effect of swelling. Evidences in favour of such a correlation are

- the correlation of the third stage onset with an appreciable swelling [215,216,224,225]; Fig. 2.7;
- the similarity in the temperature dependencies of irradiation creep and swelling [176,219,226-229]; Fig. 2.8;
- the similar reaction to material microchemistry (in particular, the solutes that reduce swelling in austenitic steel also reduce the creep strain under irradiation [128,230], Fig. 2.9);
- the experimental observation that, when voids have been created by preliminary irradiation, the irradiation creep quickly reaches the third stage, going through the first two stages much faster than usual [76,179,217,231].

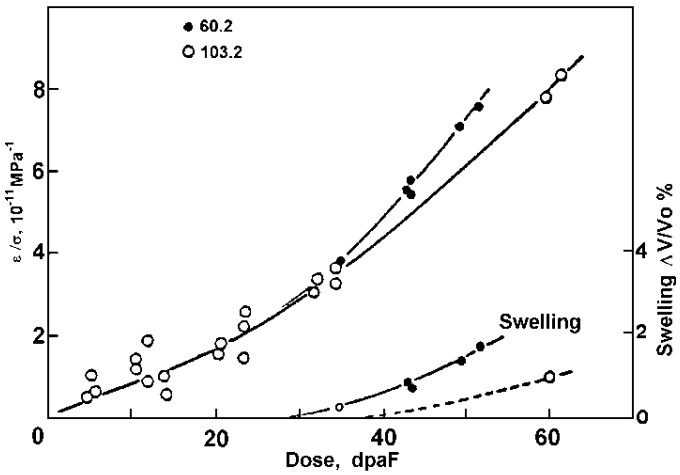

Fig. 2.7. Stress-normalized creep deformation for two sets of 20% CW type 316 SS samples (from [209])

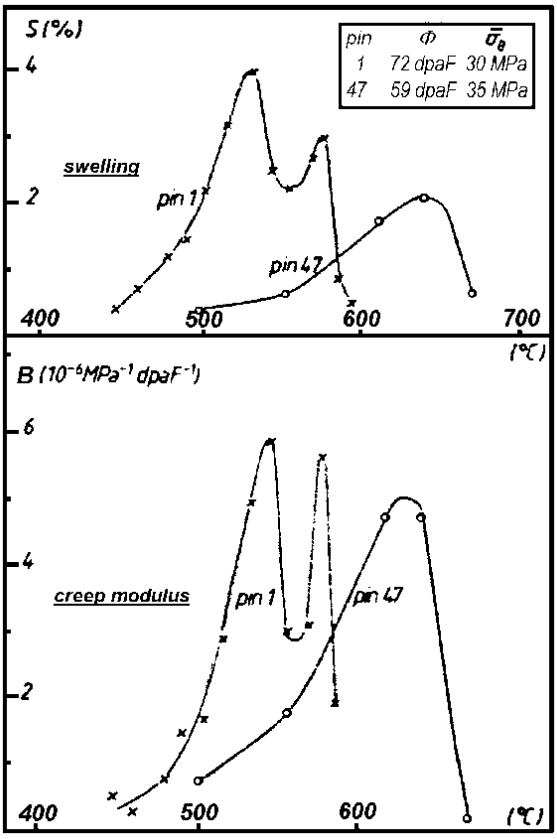

Fig. 2.8. An example of the one-to-one correlation of temperature dependence between irradiation creep and swelling (from [226]).

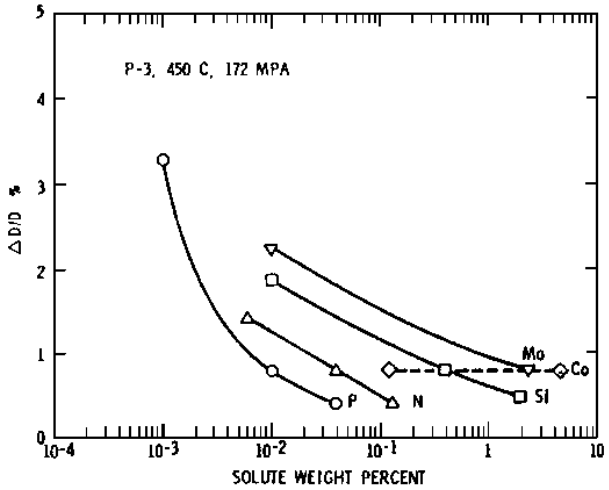

Fig. 2.9. Effect of minor chemical additions on pressurized tube diameter change in type AISI 316 SS [230].

Correspondingly, the dose dependence of irradiation creep rate $\dot{\varepsilon}$ at the third stage is described not in terms of the dose itself, but in terms of either the swelling value, S, or the instantaneous swelling rate, $\dot{S}$. Most frequently, the correlation of the irradiation creep rate to the swelling rate is used, which is expected from theoretical considerations [174,232-239] and provides a nice fit to experimental data [75,76,128,209,210,211,217,218,224,225,226,231,240],

$$\dot{\varepsilon} = BG\sigma + D\sigma\dot{S} \tag{2.2}$$

where B is the steady-state creep modulus and D is a numerical factor that falls in a range $D \sim 10^{-5}$ – 10^{-2} MPa^{-1} for a variety of steels. Alternatively, one can use the dependence of $\dot{\varepsilon}$ on the swelling itself [174,197,223, 241,242], such as

$$\dot{\varepsilon} = BG\sigma + D_1\sigma S^{\lambda}, \tag{2.3}$$

where D_1 and λ are numerical factors. Theoretical models give usually λ = 0.5, while some experimental fits for λ are $\lambda \approx 0.77$ [223] or $\lambda \approx 1.2$ [197] and $D_1 \approx 10^{-4}/G$ MPa^{-1} [197,223]. Relations (2.3)–(2.4) reflect the experimentally observed fact of the "threshold" influence of swelling on irradiation creep, namely, that the swelling-induced increase of the irradiation creep rate becomes noticeable only when either swelling or swelling rate exceed some critical value ($S \sim$ 1.5 - 5% [224,243], or $\dot{S} \sim$ 0,01 %/dpa [209,217]).

In spite of the abundant experimental data in support of equation (2.3), the correlation between the irradiation creep and swelling should be considered with certain caution [244]. Indeed, a typical irradiation creep experiment involves measurement of the overall relative change $\Delta L/L$ of some

linear parameter L (length of a tensile sample, tube diameter, etc.), which contains contributions from the both the volume conserving deformation (i.e. the true irradiation creep strain, ε) and the deformation caused by the swelling, S, i.e.

$$\Delta L / L = \varepsilon + \frac{1}{3} S, \tag{2.4}$$

where isotropic dislocation distribution over orientations is implicitly assumed (dislocation distribution anisotropy can additionally affect the factor before S, see sect. 3.2.1.3). Accordingly, in order to extract the creep-related deformation from the overall length change, one should measure at the same time the accumulated swelling. This means, however, the destructive analysis of samples for each data point, which is very expensive and technically inconvenient.

To simplify matters, one usually estimates the creep contribution to the overall strain, using in eq. (2.4) swelling values S_0 taken from independent experiments on stress-free samples. It is known, however, that the external stress accelerates swelling according to the relation:

$$S = S_0 (1 + D^S(T) \sigma_H), \tag{2.5}$$

where σ_H is the hydrostatic component of stress and D^S is a numerical factor (possibly temperature-dependent). E.g. for steels $D^S \approx 2\text{-}5\times10^{-3}$ MPa^{-1} [98,218,245-247] and for nickel $D^S \approx 6\times10^{-2}$ MPa^{-1} [248]. From the microstructural point of view, the swelling acceleration is usually related to the effects of stress on void nucleation, e.g. the reduction of the void nucleation time lag [3,178,249] or the increase of the void number density [250]. As can be easily seen, $D \sim D^S/3$ and thus it can not be excluded that the swelling rate dependent contribution in (2.3) is largely an artifact, related to the neglect of swelling enhancement by stress.

Indeed, the estimates of irradiation creep rate with account of stress dependence of swelling have shown (first for stainless steel 316 irradiated by fast neutrons [244,251] and later on for some other steels [99,193,252]), that at some swelling levels the irradiation creep rate falls well below the values typical for the steady-state stage, maybe even to zero (Fig. 2.10). Hence at the later part of the third creep stage, corresponding to high enough swelling levels, all the observable strain acceleration may be due to the influence of external loading on swelling.

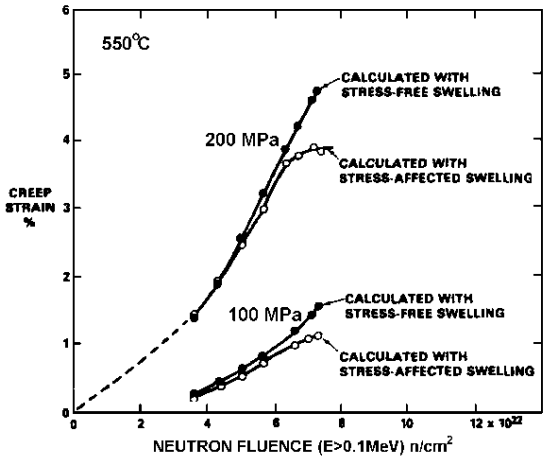

Fig. 2.10. Calculated creep strain for two pressurized pins of type AISI 316 SS, showing how the use of stress-free swelling camouflages the onset of the saturation stage of creep [253].

Having in mind the observed correlation between the creep and swelling rates, it is tempting to conclude that the irradiation creep acceleration is always the direct consequence of swelling. This statement is, however, not evident, because the relation between creep and swelling is not unequivocal. There exist results, indicating the lack of proportionality between irradiation creep and swelling [122,254,255], or even directly contradicting to such correlation. For example, no irradiation creep rate modification was observed in samples irradiated up to high doses (~40-60 dpa) [256], where the swelling is quite pronounced, and, on the contrary, the third stage of creep was observed in martensitic steel 1.4914 [257] and in PCA (Primary Candidate Alloy) [255] with practically no swelling.

Not denying the correlation between irradiation creep and swelling, it seems more reasonable to conclude that both the irradiation creep acceleration and the development of swelling are independent consequences of microstructural and microchemical changes in the irradiated material. In steels these changes can be related to phase transformations and matrix depletion with some impurities, precipitating from solid solution into secondary phase particles [3,176,253,25].

Summing up section 2.1, one can conclude that **the comparison of the material microstructure development during irradiation with the dose dependence of irradiation creep indicates, that the following microstructural components are primarily responsible for the observed irradiation creep behaviour: network dislocations and growing dislocation loops at the transient stage, network dislocations at the steady-state creep stage and network dislocations plus voids (or, where relevant, helium bubbles) at the accelerated creep stage**.

2.2 Stress dependence of irradiation creep

2.2.1 Typical loading schemes

The irradiation creep is studied using both direct loading techniques (that is deformation under a constant external load) and indirect methods (stress relaxation [24,68,50,70,181,217,259-265] or constant strain rate deformation [72]). The discussion of experimental advantages and drawbacks of the majority of these methods can be found in the review [75]. Although the indirect methods are usually considerably simpler for practical realization, their results allow only qualitative conclusions and cannot be interpreted without *a priori* assumptions. For instance, the numerical estimates of the creep rate during stress relaxation are possible only if one assumes the direct proportionality between the creep strain and the applied stress [266]. Therefore, the direct methods are preferable when one is interested in the investigation of the creep rate dependence on the mode and the magnitude of external loading.

Three basic kinds of direct loading schemes are used in irradiation creep experiments: (i) uniaxial tension of rods (in the case of in-reactor irradiation) and thin films or wires (in simulation experiments on charged particle accelerators); (ii) nearly bi-axial loading of tubular samples – either fuel pins themselves, or specially prepared hermetically sealed cylindrical capsules with a constant internal pressure of inert gas; and (iii) nearly pure shear loading (stretching of thin wire springs or torsion of wires, tubes or rods). Quite different stress and strain parameters are measured in these experiments. Namely, in the uniaxial tests the stress σ_1 and strain ε_1 in the loading direction are measured. In the case of internally loaded tubes one considers usually the hoop stress and strain, σ_θ and ε_θ, although in some experiments longitudinal strains are measured, providing useful information about the concurrent swelling. Finally, the shear experiments involve shear stress τ and shear strain γ.

In order to compare the results of experiments applying different loading schemes, it is a common practice to reduce the actual stress and strain to the so-called equivalent stress σ and equivalent strain ε. Having in mind that the numerical comparisons for different experiments are reasonable mainly in the strain range, where the irradiation creep rate is linear in stress, one can use the so-called Soderberg relations [267]

$$\frac{\varepsilon}{\sigma} = \frac{\varepsilon_1}{\sigma_1} = \frac{4\varepsilon_\theta}{3\sigma_\theta} = \frac{\gamma}{3\tau} \qquad (2.6)$$

Equation (2.6) has an important implication for the analytical modeling of irradiation creep. Since the results obtained using different loading schemes can be straightforwardly converted to one another, it is common practice to consider in analytical models only the simplest case of uniaxial loading.

2.2.2 Creep dependence on stress

The experimental dependence of irradiation creep rate on the applied stress is usually described in terms of a power law, $\dot{\varepsilon} \propto \sigma^n$, where n can vary depending on the stress range considered. Generally it is possible to allocate up to three ranges of stress level with different values of strain exponent [268], separated by critical values σ* and σ**. At low stress levels (σ < σ*) n = 1 and this linear creep rate dependence on stress seems to be a universal law for quite different materials under different irradiation conditions and loading schemes (see Fig. 2.11).

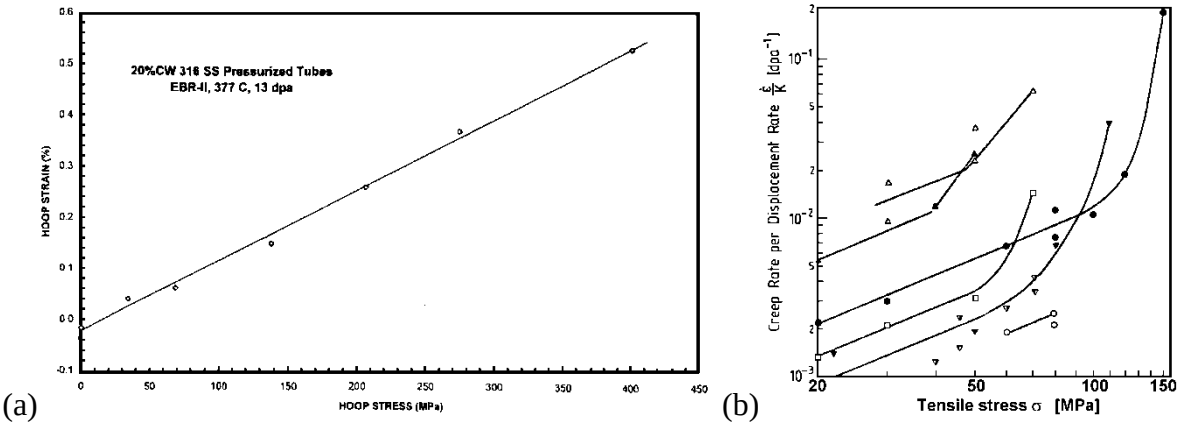

Fig. 2.11. (a) Hoop strain versus hoop stress data for the EBR-II pressurized tube test at 377°C and 13 dpa (from [269]). (b) Creep rates as a function of tensile stress in proton-irradiated high purity metals at various temperatures. Nickel: (○) 200°C, (●) 300°C; copper (□) 150 °C, (■) 200 °C; silver: (Δ) 97 °C, (♦) 150 °C; platinum: (▽) 220 °C, (▽) 240 °C, (◆) 300 °C (from [31]).

On the contrary, at high stresses (σ > σ**) the stress exponents are also high; one can observe n = 3 [53,270], 4 [53,271], 5 [257] and even 10 [261]. It is reasonable to assume that in this case one deals with the plastic flow of material because the values of σ** correlate well with the yield stress, e.g. with $\sigma_{0.2}$, as shown in Fig 2.12. For the case considered in this figure, a correlation σ** = $1.3\sigma_{0.2}$ is proposed [31]. The presence of the pre-factor exceeding unity is reasonable, since the yield stress in the figure is that of unirradiated materials, while a more appropriate correlation would be with that of irradiated materials, usually somewhat higher due to radiation hardening.

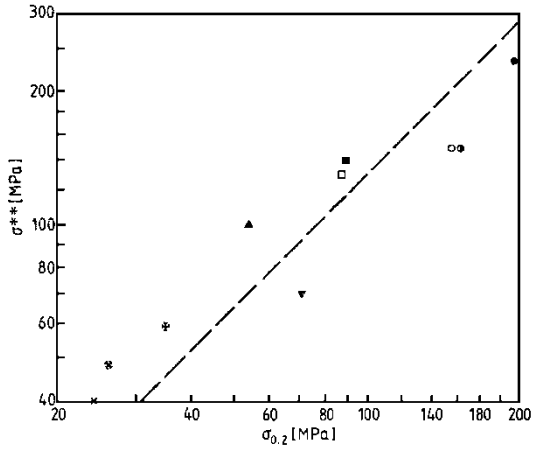

Fig. 2.12. Stress for the onset of strongly non-linear stress dependence of irradiation creep, σ**, as a function of yield stress for pure metals shown in Fig. 2.11(b) (from [31]).

In some materials the linear stress range is followed by one where stress exponents exceed unity, but not too much. E.g. one can observe values of $n \sim 1.5$ [40,123,133,210,231,272-276] or $n = 2$ [43,59,65,114,151,196,198,200,277,278], see Fig. 2.13, even though more common is the case where this non-linearity is not observed at all (see e.g. [53,64]). These stress exponents are too low for plastic flow or thermal creep and the creep at this stage is usually still considered as caused by irradiation, while the change of the stress exponent is ascribed to the change of the governing microstructural mechanism of irradiation creep (e.g. the transition from pure dislocation climb to the climb-controlled glide, see sect. 3). In any case, the quadratic stress dependence is valid only within a limited stress range ($\sigma^* < \sigma < \sigma^{**}$). The values of σ* in those reactor structural materials where the stress nonlinearity is observed have typically the order of σ**/3 (that is 100-200 MPa) [268], but are sensitive to the studied material and the experimental conditions.

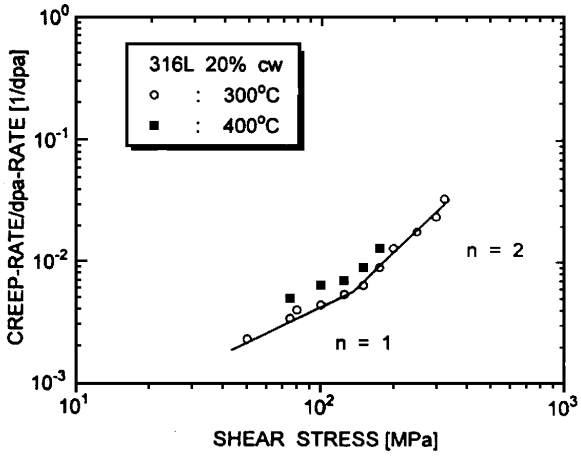

Fig. 2.13. Stress dependence of the irradiation creep rate for 20% cold-worked 316L stainless steel (from [279]).

Sometimes attempts are made to describe the dependence $\dot{\varepsilon}(\sigma)$ by a unique law (for example, $\dot{\varepsilon} \propto \sigma \exp(\frac{\sigma}{\sigma^*})$ [7,131,280-282] or $\dot{\varepsilon} \propto sh(\frac{\sigma}{\sigma^*})$ [283]). However, such laws are hardly anything more than empirical fits, because the change of stress exponent is most probably related to the change of the dominant microstructural mechanisms of creep, each having its own stress dependence.

2.2.3 Microstructure development at different stress levels

The study of dislocation patterns evolving at different stress levels allows the dominating modes of dislocation movement to be specified and thus to be more specific when choosing between plausible basic mechanisms of irradiation creep.

Generally, edge dislocations in metals exhibit two movement modes - glide and climb, whereas screw dislocations can only glide, though the slowest process limiting their sliding speed can be the desorption and absorption of point defects by edge-type jogs [17,100,284]. Below we restrict our consideration only to edge dislocations, since the movement of screw dislocations is expected to contribute mostly to the thermal creep, rather than to the irradiation one [17].

The basic distinction between the two kinds of edge dislocation movement is that the glide is a conservative process, whereas the climb (building-up or eating-out of the dislocation extra-plane) requires matter supply, achieved usually through the diffusion of point defects. In the absence of irradiation and at temperatures below 0.5-0.6 T_m, the concentrations of point defects in metals are so low that practically the only possible mode of dislocation movement during creep is the glide. The thermal equilibrium concentration of vacancies becomes noticeable and contributes to thermal creep (via Nabarro's mechanism [285,286]) only when the temperatures are rather high.

Irradiation produces relatively high supersaturations of point defects in a material. As a result, irradiation sharply accelerates dislocation climb, which both directly contributes to creep and, by facilitating dislocation glide, allows dislocations to overcome glide barriers by climbing to other gliding planes. Accordingly, the dislocation patterns formed in irradiation samples are governed to a large extent by irradiation and temperature, rather than by the applied loads, as is the case with the thermal creep [213,250]. As already mentioned, the generation of interstitials by irradiation results in fast nucleation and growth of interstitial (Frank) loops, which is impossible in the absence of irradiation. Direct transmission electron microscopy (TEM) studies of dislocation structure development in stainless steel 316 [144,151,168] and in nickel [43] during irradiation creep show that the growth of dislocation loops and the annealing of network dislocations occurs soon after the

onset of irradiation (at doses < 1 dpa) and completely destroy the microstructure consisting of subgrain walls, slip bands and dislocation pile-ups, which is characteristic for thermal creep.

Hence, it is only natural to expect that the creep mechanisms under irradiation and without it should be essentially different, at least at those temperatures where irradiation creep exceeds the thermal one. However, which particular kind of dislocation movement, i.e. climb or climb-limited glide, provides the largest contribution to irradiation creep, depends largely on the external loading level. The results of TEM studies of dislocation structure evolving during irradiation creep indicate that, in the stress level range where the creep rate is linear in σ, the domination of dislocation climb is manifest [145,146], whereas at larger stress levels one can identify the features related to the dislocation multiplication and sliding [146], which means that both kinds of dislocation movement occur.

With regards to the analytical modeling of swelling-free irradiation creep, these results mean that in the stress range $\sigma < \sigma^*$ it is sufficient to consider the contribution from dislocation climb (including, in particular, the growth of dislocation loops at the transient creep stage). At stress levels in the range of $\sigma^* < \sigma < \sigma^{**}$ both the dislocation climb and the climb-limited glide should be taken into account. The nonlinear stress dependence of irradiation creep rate in this stress range indicates that the glide-related mechanisms provide the main contribution, because it is hard to explain the stress dependence non-linearity in the framework of pure climb mechanisms.

The third stage of irradiation creep is yet another regime, where climb-limited glide of dislocations is important. The evolution of voids generally accelerates dislocation climb (irrespective to the effect of stress) and simplifies the overcoming of glide barriers. On the contrary, the role of purely climb-related mechanisms decreases with the increase of swelling [116,162,183,287].

Finally, at very high stresses ($\sigma > \sigma^{**}$) the main part in the material deformation is played by dislocation glide, controlled not only by climb over pinning centers, but by dislocation multiplication and mutual annihilation, as typical for plastic flow. Therefore, it is natural to expect [1,45,288] that at very high stresses the in-reactor material flow is similar to that of unirradiated control samples, as was indeed experimentally observed [6,45,53,64,191,262,280, 289,290].

2.4 Temperature dependence of irradiation creep

Irradiation creep is observed not only in a limited range of external loads, but also in a limited temperature range, where the maximum temperature usually does not exceed ~ $0{,}5T_m$. At higher

temperatures the irradiation component of creep rate is noticeably less than the thermal one, which grows exponentially with temperature as a result of both the increase of thermal concentration of vacancies and the acceleration of thermally activated processes of mass transfer. **At high temperatures the creep activation energy are practically identical under irradiation and without it and are close to the self-diffusion energy via vacancy mechanism** [277,291].

The major body of the available data concerning irradiation creep falls within the temperature range 0,25-0,5 T_m, which is relevant to operational conditions of structural materials in fission and currently designed fusion reactors. In this temperature range **the irradiation creep dependence on temperature is rather weak**. Usually, in experiments with a limited number of temperature points no pronounced temperature dependence at the typical working temperatures of nuclear reactors is noticed [1,15,16 89 127,129,130,190,215,291,292], though some increase [13,22,2529,63,114, 197,204,208,226,293-295] or decrease [50,296-299] of irradiation creep with the increase of temperature is reported as well. Several rather detailed (even though not numerous) studies of the temperature dependence of creep in irradiated materials show that at lower temperatures a weak monotonous increase of $\dot{\varepsilon}$ with temperature is observed, whereas at temperatures closer to the transition from irradiation to thermal creep a depression of creep rate takes place, leading to a characteristic "hump" in the temperature dependence [66,122,213,226,255,272,273,293,300-301], see Fig. 2.14. The "hump" like temperature dependence is more typical for pre-irradiation cold-worked materials [213,226,255,300], as well as for ferritic-type steels with inherently high dislocation density [272,273,293]. Such specific form of the temperature dependence of irradiation creep rate is one of the important criteria for the validation of the irradiation creep theory predictions.

The "hump" on the temperature dependence of irradiation creep is usually located in the same temperature range where the "bell-shaped" temperature dependence of swelling is observed. This fact is often considered as a proof of the direct correlation between swelling and irradiation creep [176]. This interpretation should, however, be taken with caution because the "hump" in the irradiation creep is observed also when no swelling is experimentally detected [213] or the doses are too low for noticeable swelling (< 3 dpa) [300]. Moreover, the responses of creep and swelling to a progressive temperature decrease are not correlated [302]. Finally, in a comparative study of SS 316 tubes in annealed and cold-worked states [213], the normal "bell-shaped" dependence of swelling was noticed in both types of tubes, whereas the "hump" on the temperature dependence of irradiation creep was observed only in cold-worked samples.

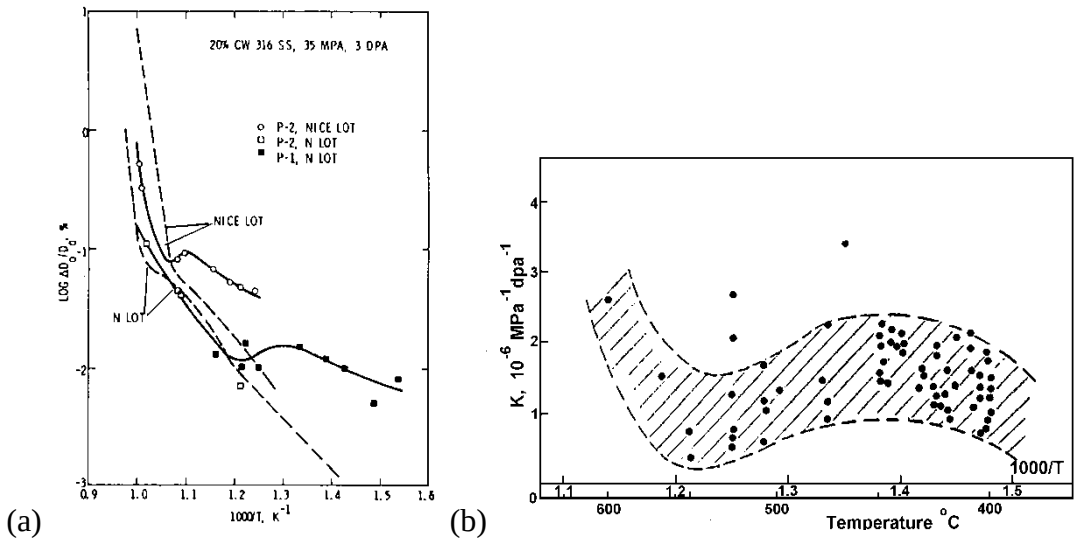

Fig.2.14. (a) The temperature dependence of irradiation creep in type AISI 316 CW [300]; (b) The creep modulus of 20% CW type 316 SS as a function of inverse irradiation temperature [213].

The results of irradiation creep measurements in copper [33] indicate, however, that it is quite reasonable to ascribe the noticeable temperature dependence of irradiation creep rate to the dominance of dislocation glide. Indeed, as can be seen in Fig. 2.15, the variation of the creep rate inversely reflects the changes in the material yield stress, which is quite natural for the climb-controlled-glide mechanism of irradiation creep. Moreover, the increase of the copper purity completely removes the "pit" in the irradiation creep curve (curve 3 in Fig 2.15).

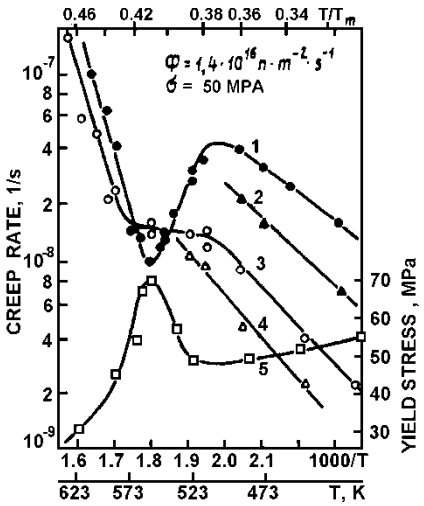

Fig. 2.15. The temperature dependence of the reactor (1,2) and the thermal (3, 4) copper (99.95%) creep rate and of the yield stress (5): the grain size are 35 (1, 3) and 50 μm (2, 4). (from [33]).

At low temperatures (< 0,25 T_m) the irradiation creep was rarely addressed [36,37,71,299] and is investigated poorly, see Table 2.2. Nonetheless, it is established, that even at temperatures of some tens of Kelvin irradiation accelerates creep and the values of the creep rate are comparable to those observed at higher temperatures. In the temperature range of 0,2-0,25 T_m the irradiation creep rate has the same order of magnitude as at higher temperature and even tends to be faster than at higher temperatures [71].

Table 2.2

Some Low-Temperature Creep Experiments

Temperature	**Material**	**Creep modulus, 10^{-6}/(Mpa ×dpa)**	**Reference**
20 K	W	Irradiation increases creep rate	[37]
20 K	Mo	2	[71]
36 K		7	
20 K	Mo	2	[36]
60°C	Steel HT-9	6.3	[299]
	Alloy Fe-15%Cr	10	

3. Theoretical models of irradiation creep

3.1 Brief introduction to irradiation creep theory

The plastic deformation of metals is, on the microscopic scale, the result of dislocation motion. Let us recall, therefore, how the rate of macroscopic deformation is related to the dislocation motion parameters. As mentioned in section 2, only edge dislocations (in the form of either network, or loops) will be considered.

In a general case the strain of a material is described by a second-order tensor, ε_{ij} (where the subscripts i,j = 1,2,3 denote Cartesian coordinates), which can be expressed in terms of dislocation velocities $\boldsymbol{V}$ as [303]

$$\dot{\varepsilon}_{ij} = \Omega^{-1} e_{imn} \int V_m t_n b_j dl, \tag{2.7}$$

where $\boldsymbol{t}$ is a unit vector along the dislocation line, $\boldsymbol{b}$ is the Burgers vector of the dislocation, Ω is the sample volume, e_{imn} is the anti-symmetric Kronecker's tensor and integration is along all edge dislocation lines in the material. Here and below a point over a symbol means time derivative and the Einstein summation rule over repeated subscripts is implied.

In order to get some useful information from this equation, it is necessary to introduce some reasonable simplifications concerning the nature of the dislocation structure. Let us assume, first of all, that network dislocations are straight lines, while dislocation loops are perfectly circular. Since contributions to the strain from network dislocations and from loops are additive, let us discuss them separately, starting with the contribution from network dislocations.

It is usually safe to assume that a straight dislocation moves as a whole with the same average velocity which, however, can depend on the dislocation orientation in the material. Usually the number of possible dislocation orientations in a crystal is limited, let us say equal to some K. Then the dislocation network contribution to the total creep rate can be reduced to

$$\dot{\varepsilon}_{ij}^{D} = e_{imn} \rho \left\langle V_m t_n b_j \right\rangle, \tag{2.8}$$

where the angular brackets for an arbitrary function F^k of dislocation orientation k ($1 < k < K$) mean the averaging over dislocation orientations,

$$\left\langle F \right\rangle = \sum_{k=1}^{K} f^k F^k, \tag{2.9}$$

with the weight $f^k = \rho^k/\rho$, where ρ^k is the density of dislocations with orientation k and ρ - the total network dislocation density in the sample.

Due to symmetry reasons, the dislocation velocity is normal to the dislocation line direction ***t***. Having in mind that the Burgers vector of an edge dislocation is also normal to ***t***, we can write down ***V*** as a sum of two vectors:

$$\mathbf{V}^k = -V_c^k \mathbf{n}^k + V_g^k \hat{\mathbf{b}}^k, \qquad (2.10)$$

where $\hat{\mathbf{b}}^k = \mathbf{b}^k / b$, $\mathbf{n}^k = [\hat{\mathbf{b}}^k \times \mathbf{t}^k]$, b is the absolute value of dislocation Burgers vector (assumed for simplicity to be independent of dislocation orientation), V_g^k is the velocity of dislocation parallel to the dislocation Burgers vector and V_c^k is velocity of dislocation in the direction of its extra plane. The movement in the direction of the Burgers vector (called slide or glide) involves only the shift of the dislocation extra-plane and occurs under the action of local shear stresses. On the contrary, the movement in the direction normal to the Burgers vector (climb) involves the dissolution or build-up of the extra plane. The signs before the terms in the r.h.s. of eq. (2.10) are chosen so that $V_c > 0$, when the dislocation climbs by extra plane build-up, while $V_g > 0$ when the dislocation glides in the direction of the Burgers vector.

Substituting (2.10) into (2.8), one obtains (cf. [304,305]):

$$\dot{\varepsilon}_{ij}^D = \rho b \left\langle \hat{b}_i \hat{b}_j V_c \right\rangle + \frac{1}{2} \rho b \left\langle (\hat{b}_i n_j + n_i \hat{b}_j) V_g \right\rangle. \qquad (2.11)$$

According to eq. (2.11), one can consider contributions to creep rate from dislocation climb and glide as formally additive. This does not mean, however, that climb and glide of dislocations occur completely independently. On the contrary, when the external strains are below the yield stress, the average dislocation glide velocity in real materials is much less compared to the glide velocity in a perfect crystal. This is because the glide is hindered by various barriers (point defects, impurity atoms, secondary phases, other dislocations, etc.). The barriers can be overcome either thermofluctuatively or by climb of the pinned dislocation segments to another glide planes, where the barrier is no more operative. The temperatures relevant for the dominance of irradiation creep are usually too low for overcoming barriers by thermal fluctuations, so dislocation climb limits the average glide velocity. Quantitative discussion of the climb-limited glide is given below in sect. 3.2.2.

In contrast to network dislocations, interstitial loops can glide only under the action of shear stress gradients [284], which are seldom created in the irradiation creep experiments and, even if present,

are not big enough to force the glide of loops of sizes of several tens to hundreds nanometers, which are of interest for the transient creep stage. Hence, the glide mode of dislocation loop movement is little relevant for irradiation creep. Strictly speaking, another movement mechanism is possible for very small (< 1 nm) perfect interstitial loops, as observed in Molecular Dynamics (MD) computer simulations for copper [306] and α-iron [307,308]. This mechanism is very similar to glide, since it is one-dimensional and involves no absorption or desorption of point defects. However, in contrast to glide, this movement occurs in a stochastic manner, even without external stresses. Because such small dislocation loops can form directly in collision cascades (see e.g. [306,309-311], they contribute to irradiation creep in the case of cascade forming irradiation, which serves as a source of dislocation loops operating during the whole experiment time. However, here we do not consider this mechanism because up to now no discussion of the contribution of one-dimensionally moving small dislocation loops to irradiation creep are reported in the literature. Therefore, only the growth of dislocation loops due to point defect absorption is considered below.

Let us assume that, similarly to the case of network dislocations, the number of possible loop orientations in the material is finite and equal to M. In agreement with experimental data, one can assume that practically immediately after the onset of irradiation the volume number densities of loops attain the values, N_L^m ($1 < m < M$), and do not change until the loops become very large and incorporate into the dislocation network. Let us introduce for the loops with orientation m the distribution function $f^m(R,t)$ over radii R at time t, such that

$$\int f^m(R,t)dR = N_L^m / N_L ,$$

where N_L is the total volume density of loops. The growing loop contribution to the creep rate will then be given by

$$\dot{\varepsilon}_{ij}^L = 2\pi b \sum_{m=1}^{M} \hat{b}_i \hat{b}_j \int_0^{R_{\max}} V^m(R) f^m(R,t) R dR, \qquad (2.12)$$

where V^m is the loop growth rate. To simplify matters, one can assume that at the transient irradiation creep stage all loops of the same orientation have the same radius R^m. Then the component of irradiation creep rate due to dislocation loops, $\dot{\varepsilon}_{ij}^L$, can be written down as

$$\dot{\varepsilon}_{ij}^L = 2\pi N_L b \left\langle \hat{b}_i \hat{b}_j R V_L \right\rangle, \qquad (2.13)$$

where the orientational average is performed as in the relation (2.9), but with the weight of f_L^m.

It is seen from eqs. (2.11) and (2.13) that processes of two kinds give rise to creep, namely those related to dislocation movement and those related to the evolution of the dislocation structure itself, which involves both the total dislocation density variation and the redistribution of dislocations over orientations.

From the theoretical point of view, it is convenient to concentrate first on the dislocation movement mechanisms, assuming that the dislocation structure is stabilized and involves predominantly network dislocations. As shown in sect. 2.1, this situation corresponds to the secondary creep stage. When the basic mechanisms leading to dislocation movement anisotropy are established, we will proceed to the effects of microstructure development, as appropriate for primary creep and for swelling-promoted creep.

3.2 Steady-state irradiation creep

At the steady-state stage the rate of irradiation creep is given by equation (2.11) and contains two terms, one of which is due to dislocation climb and another to dislocation glide. Let us consider these terms separately, starting from the climb mode of dislocation motion.

3.2.1 Creep mechanisms based on stress-induced dislocation climb

3.2.1.1 Dislocation climb rate

As follows from (2.11), the dislocation climb contribution to the creep rate is determined by the climb velocity V_c^k, which can be expressed in terms of point defect currents per unit dislocation length, J_α ($\alpha = v$ for vacancies and i for interstitials) as

$$V_c^k = b^{-1}(J_i - J_v). \qquad (2.14)$$

In order to calculate the point defect currents to dislocations, one has to solve an appropriate diffusion problem for point defects in the matrix, assuming that the thermal equilibrium concentrations of point defects, $C_{\alpha d}^k$,are maintained at the jogs on the dislocation lines, where the point defect absorption occurs. Note that in externally loaded material this equilibrium concentration can depend on dislocation orientation with respect to the stress orientation, as indicated by a superscript k.

An exact solution of such a diffusion problem in multiply-connected regions between point defect sinks is usually hopeless. On the other hand, macroscopic parameters, such as the creep rate, should not be very sensitive to the details of individual dislocation motion and are determined by the "average" rate of dislocation climb. The usual approach applied in this case involves the use of the

rate theory [312,313]. According to this approach, all point defect sinks (network dislocations in our case) are “smeared” over the material volume and the matrix is considered as a uniform "lossy" continuum (or, alternatively, "effective medium"). Correspondingly, one can assume that some "average" (in the sense of statistical averaging over the sink ensemble [313]) concentrations of point defects, C_α ($\alpha = i,v$), are established in the material, as a result of a balance between point defect generation by irradiation and point defect loss either at sinks or due to mutual recombination,

$$G - \rho\langle J_\alpha \rangle - \sigma_R (D_i + D_v) C_i C_v = 0. \tag{2.15}$$

where G is the point defect generation rate, D_α is the diffusion coefficients for α-type point defects and σ_R is the recombination factor. From common sense reasoning (justified by strict analytical consideration [313]), one can expect that the point defect current to a dislocation should be proportional, first of all, to the difference between the average point defect concentration in the matrix C_α and the equilibrium concentration near the dislocation, $C_{\alpha 0}^k$, and, second, to the point defect mobility, as specified by diffusion coefficient D_α,

$$J_\alpha^k = Z_\alpha^k D_\alpha (C_\alpha - C_{\alpha 0}^k), \tag{2.16}$$

where Z_α^k are the proportionality factors (so-called "bias factors"), which are determined by the sink geometry, orientation in space and the efficiency of sink elastic interaction with point defects.

Solving the set of equations (2.15) and (2.16), one can re-write the dislocation velocity (eq. (2.14)) as

$$V_c^k = V_{cT}^k + V_{cI}^k, \tag{2.17}$$

where V_{cT} is the thermal climb rate, related to the dependence of the equilibrium vacancy concentration on dislocation orientation (contribution due to interstitial is usually omitted due to extremely low interstitial solubility in metals),

$$V_{cT}^k = \frac{Z_v^k D}{b}\left(C_{v0}^k - \frac{< Z_v C_{v0} >}{< Z_v >} \right), \tag{2.18}$$

and V_{cI} is the climb rate due to the effect of irradiation,

$$V_{cI}^k = \left(\frac{Z_i^k - < Z_i >}{< Z_i >} - \frac{Z_v^k - < Z_v >}{< Z_v >} \right) \frac{G}{b\rho} \Phi\left(\frac{G}{G_R} \right), \tag{2.19}$$

where

$$G_R = < Z_i >< Z_v > \frac{D_i D_v \rho^2}{4\sigma_R (D_i + D_v)}$$

and the functional form of function Φ is

$$\Phi(x) = \frac{2}{1+\sqrt{1+x}}.$$

In writing down the equations we omitted the terms proportional to the equilibrium vacancy concentration in the argument of Φ, because it is negligible in the region of low temperatures, where the deviation of Φ from unity is noticeable.

Thus the dislocation climb rate includes two contributions, one of which is not related to irradiation and is not considered any more. So only equation (2.19) is discussed below. **The most important feature of equation (2.19) is the dependence of the climb rate on dislocation bias factors Z_α for vacancies and interstitials**. Indeed, it is seen that **irradiation leads to dislocation climb acceleration only provided that the external load leads in some way to a "double" asymmetry of point defect absorption by dislocations**. First of all, the dislocation bias factors should depend on dislocation orientation with respect to external loads and, secondly, this dependence should be different for vacancies and interstitials. Let us consider what models have been proposed for the explanation of influence of external loading on the orientational dependence of bias factors Z_α. Having in mind relation (2.7), we restrict to a simple case of uniaxial loading by stress σ.

3.2.1.2 Mechanisms of stress-induced anisotropy of dislocation bias factors

Up to now, **only three mechanisms of dislocation bias factor modification by external stress, answering the necessary requirements, have been suggested** in the literature. They can be generally referred to as **Stress-Induced Preferred Absorption (SIPA)**, though initially this name referred to only one of them, that based on the stress-induced elastic modulus anisotropy of point defect interaction with dislocations [162,304,314-316]. The other two mechanisms consider the **effect of anisotropic external stresses on the point defect mobility** [317-323] **and on the efficiency of point defect accumulation in dislocation cores** [324-327]. Let us discuss them in more detail.

3.2.1.2.1 Stress-modified modulus interaction of point defects with dislocations

Historically, this was the first mechanism suggested in the literature. It treats point defects as spherical inclusions (isotropic centers of a dilatation) with elastic constants, distinct from those of the surrounding matrix. This is a reasonable approximation for vacancies, but for self-interstitial

atoms, which in metals usually have a dumbbell (or even crowdion) configuration, the applicability of such model is not obvious. However for isotropic (or cubic) materials one can expect that the model can still be acceptable, if one takes an average over possible dumbbell orientations. The idea of the mechanism is that **the external loading "polarizes" point defects**, see Fig. 3.1. As a result, dislocations of different orientations with respect to the applied stress become non-equivalent in terms of the strength of their elastic interaction with polarized point defects.

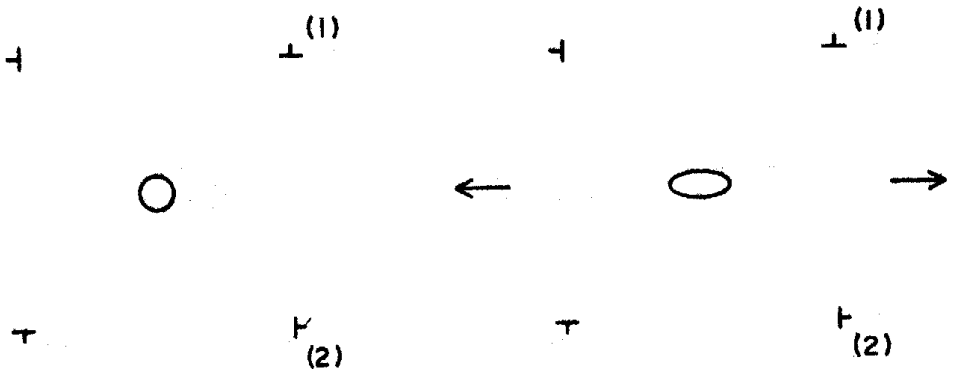

Fig. 3.1. A schematic representation of the stress induced bias in the point defect-dislocation interaction (from [162]).

The energy of interaction of a polarized point defect with a *k*-type dislocation with, U_α^k, looks like [316]:

$$U_\alpha^k = k_B T \frac{R_\alpha^k}{r} \sin\theta, \tag{2.20}$$

where k_B is the Boltzmann factor, T is the absolute temperature, r and θ are the polar coordinates related to the dislocation, and R_α^k is the characteristic radius of dislocation interaction with point defects,

$$R_\alpha^k = \frac{\mu\omega b}{\pi k_B T}\left(e_\alpha^0 + p_\alpha^K \frac{\sigma}{E} + p_\alpha^\mu q^k \frac{\sigma}{\mu}\right), \tag{2.21}$$

Here E and μ are, respectively, the Young modulus and the shear modulus of material, ω is the atomic volume, e_α^0 is the effective dilatation of a point defect, p_α^K and p_α^μ are the factors, expressed, respectively, in terms of either the bulk moduli (K, K_α) and shear moduli (μ, μ_α) of the matrix and the point defects of type α [316], or in terms of elastic polarizabilities of point defects P_α^K and P_α^μ [328]. The dependence of the interaction energy on the dislocation orientation is given by the factor q^k [329]:

$$q^k = 3\nu(\mathbf{t}^k\mathbf{s})^2 + 3(\hat{\mathbf{b}}^k\mathbf{s})^2 - (1+\nu), \qquad (2.22)$$

where ***s*** is the unit vector in the direction of applied load. As follows from relation (2.21), the anisotropy of dislocation interaction energy with point defects is due to the differences of shear moduli of point defects and the matrix.

Computer simulation of vacancy formation in α-Fe under the combined action of the external and dislocation stress fields [330] indicated no dependence of the vacancy formation energy on the stress direction. On the contrary, the dumbbell interstitial atoms, that easily rotate on-site under the action of shear loads [331], are expected to be quite sensitive to stress orientation. For the order of magnitude estimates one can usually assume $p^{\mu}_i \approx 0.5$ and $p^{\mu}_v = 0$ [315]. The estimate of p^{μ}_i and p^{μ}_v using the values for point defect polarizabilities in Al [332] also indicate that $p^{\mu}_i >> p^{\mu}_v$, though the values of p^{μ}_i are predicted to be an order of magnitude higher.

The estimates of R_α^k show that at the experimentally relevant temperatures there holds the relation $r_0 \ll R_\alpha^k \ll R_d$, where r_0 is the radius of a dislocation core and $R_d \approx (\pi\rho)^{-1/2}$ is the average distance between dislocations. In such an approximation, the following expression for Z_a holds [333]:

$$Z_\alpha^k = \frac{2\pi}{\ln(2R_d / R_\alpha^k)} \approx Z_\alpha^0\left(1 + \frac{Z_\alpha^0 p_\alpha^\mu}{2\pi e_\alpha^0} q^k \frac{\sigma}{\mu}\right), \qquad (2.23)$$

where Z_α^0 is the bias factor value in a stress-free matrix. As can be seen, Z_α^k depends, indeed, on both the type of point defect involved and the dislocation orientation, via q^k.

3.2.1.2.2 Stress-induced anisotropy of point defect diffusion

The physical reason for the bias factor anisotropy is the modification of the energy barriers for point defect diffusion in the loading direction and perpendicularly to it. In such situation the diffusion is described not by a scalar diffusion coefficient, as it was in the isotropic material, but by a tensor of diffusion coefficients $D_{\alpha,ij}$. The general form of a diffusion tensor in a crystal lattice can be presented as [334]:

$$D_{\alpha,ij} = \nu_\alpha \sum_{\mathbf{h}} \lambda_{\mathbf{h}} h_i h_j \exp\left(-\frac{E_\alpha^h}{k_B T}\right), \qquad (2.24)$$

where ν_α is the vibration frequency of point defects in the lattice, h_i is the i-th component of a vector **h**, connecting an equilibrium point defect position with one of the neighbour equilibrium positions, $E_\alpha^{\boldsymbol{h}}$ is the energy barrier of diffusional jump in the direction ***h***, $\lambda_{\boldsymbol{h}}$ the factor that takes into account a possibility of the dumbbell diffusion mechanism (for interstitial atoms), and

summation in (2.24) is performed over all nearest neighbour sites to which the point defect can jump. If the material is under the action of elastic deformations $e_{ij}(\boldsymbol{r})$, the energy $E_\alpha^{\boldsymbol{h}}$ can be written down as:

$$E_\alpha^h = E_\alpha^m - P_{\alpha,kl}^s(\mathbf{h})e_{kl} - \frac{1}{2}Q_{\alpha,klmn}^s(\mathbf{h})e_{kl}e_{mn}, \qquad (2.25)$$

where $P^s{}_{\alpha,kl}$ and $Q^s{}_{\alpha,klmn}$ are, respectively, the force tensor and the elastic polarizability tensor in a saddle point of a diffusional jump. Both these tensors depend, generally speaking, on the direction of the jump. According to relation (2.25), the diffusion coefficient dependence on the external loading and the dislocation orientation can originate from two sources.

First of all, the strains e_{kl} in equation (2.25) are a sum of external strains ε^o_{ij} and the strains created by a nearby dislocation ε^d_{ij}. Although these two strains enter additively in the second term in (2.25), their effect on the diffusivity is not additive, because in the vicinity of a dislocation core $P^s{}_{\alpha,kl}\varepsilon^d_{kl} \geq k_BT$ and hence the exponentials in (2.24) can not be straightforwardly expanded in the powers of total deformation [334]. As shown below, the resulting corrections to dislocation bias factors turn out to be dependent on both the point defect type and the dislocation orientation with respect to stress.

Secondly, the last term in the r.h.s. of equation (2.25) depends on products of the type $\varepsilon^o_{kl}\varepsilon^d_{mn}$, which include interference terms that depend simultaneously on the external loading and the orientation of a dislocation. The account of such terms results, correspondingly, in corrections to the diffusion coefficients and to the dislocation bias factors, which satisfy the "double anisotropy" requirement and can contribute to irradiation creep [335]. Having in mind, however, that this mechanism is of the second order in strains, it is possible to neglect it as compared to the first-order one.

If the external stress is sufficiently low ($\sigma\omega/k_BT$ « 1) and the crystalline lattice is cubic, the bias factors can be presented as [334]

$$Z_\alpha^k = Z_\alpha^0\left(1 - \frac{(1+\nu)}{2(1-2\nu)}e_\alpha^s q^k \frac{\sigma\omega}{k_BT}\right), \qquad (2.26)$$

where ν is the Poisson ratio of the material, ω the atomic volume, $e^s{}_\alpha$ the point defect dilatation in the saddle point of diffusion jump, $Z^0{}_\alpha$ the bias factor of the unloaded dislocation, and the orientation factor q^k is defined by the relative orientations of the unit vector of dislocation

orientation, $\boldsymbol{t}^k$, the unit vector $\boldsymbol{s}$ in the direction of applied stress and the basis vectors $\boldsymbol{e}_p$ (p = 1,2,3) of the crystalline lattice,

$$q^k = d_\alpha^{(2)}(\mathbf{st}^k)^2 + d_\alpha^{(3)}\sum_{p=1}^{3}(\mathbf{se}_p)^2(\mathbf{t}^k\mathbf{e}_p)^2, \qquad (2.27)$$

where d_α $^{(2)}$ and d_α $^{(3)}$ are the factors determined by point defect force tensors in saddle points of diffusional jump (that is, are defined exclusively by material properties). Numerical values for $d^{(2)}$ and $d^{(3)}$, estimated using computer simulation values for copper and iron, are summarized in Table 3.1.

Table 3.1 - Numerical estimates of $d^{(s)}$ for copper and α-iron [334]

	Copper *		**α-Iron**	
	v	*i*	*v*	*i*
$d^{(2)}$	-0.62(-0.35)	0.20(0.13)	0.88	0.60
$d^{(3)}$	-1.51(-0.85)	-0.24(-0.16)	-0.88	-0.60

*)The values in parentheses are estimated with the data from [336], all other values use the data from [337]

3.2.1.2.3 Stress-modified efficiency of point defect absorption by dislocations

Both preceding models implicitly assume that dislocations absorb any point defect that jumps into its core. Actually, straight edge dislocations laying along low-index crystallographic directions have atomically smooth edges of extra-planes, divided by separate jogs and kinks, and the lengths of smooth segments considerably exceed the interatomic distance *a* [284]. **A point defect entering the dislocation core on a smooth segment does not lose its individuality** [338] **and can diffuse along the extra-plane edge. Eventually, the defect either jumps out of the core back into the volume of material, or is absorbed at a dislocation jog, thus contributing to the climb of the dislocation** (the direct electron microscopy observation of not conservative movement of dislocation jogs was carried out e.g. in [339]).

Even when the concentration C_j of jogs on a dislocation is rather low ($aC_j << 1$), the dislocation can act as a perfect sink for point defects, provided $\lambda_\alpha C_j \geq 1$, where λ_α is the average distance traveled by a point defect in the dislocation core. However, in the opposite limiting case ($\lambda_\alpha C_j << 1$) the dislocation can be considered rather as a discrete chain of jogs capturing point defects only from the neighbouring pieces of dislocation line of length λ_α. Correspondingly, the effective absorbing length of a dislocation and, hence its sink strength for point defects becomes proportional to $\lambda_\alpha C_j$ [324,340]. In this case the dislocation bias factors can be written down as [325]

$$Z_\alpha^k = \beta_\alpha^k \lambda_\alpha^k C_j^k, \tag{2.28}$$

where β_α^k is the coefficient that depends on C_j^k and on the effective radius of elastic interaction of point defects with dislocation, R_α^k, as given by equation (2.21). The "discrete" structure of dislocation as a sink for point defects allows the bias factors to be modified by an external load via its influence on the defect diffusion in dislocation core and the linear density of jogs.

The relation specifying the average jog concentration on dislocation is not very certain, though the lowest bound for C_j is given by the thermal concentration of jogs C_j^{th}, defined as

$$C_j^{th} = a \exp\left(-\frac{E_j}{k_B T}\right), \tag{2.29}$$

where E_j is the energy of jog formation on dislocation line. Experimental estimates of E_j are scarce (e.g. E_j = 0.3-0.4 eV for undissociated dislocations in copper and aluminum, and E_j ~ 4 eV for dissociated dislocations in copper [341]). A rough estimate of E_j can be done according to the relation $E_j \approx 0.1\mu\omega$ [284]. For Al it gives $E_j \approx 0.4$ eV, which is in good agreement with the above-mentioned experimental values.

The **dependence of jog concentration on the external load can result from variations of the energy barrier that must be overcome for the nucleation of new jog pairs** on a straight segment of extra-plane edge [325]. Indeed, new jogs are nucleated in pairs when a cluster of Λ atoms is added to extraplane or a row of Λ vacancies "eats out" the extra-plane ($\Lambda \approx$ 2-3). Formation of such clusters on a dislocation with orientation k in the field of external loads σ_{ij} requires an additional work $\delta A^k = -\Lambda\sigma_{nn}\omega$ or $\delta A^k = -\Lambda\sigma_{nn}\omega$, respectively, where $\sigma_{nn} = \hat{b}_i^k \hat{b}_j^k \sigma_{ij}$ is the stress acting normal to the dislocation extra-plane. When a dislocation climbs, absorbing predominantly point defects of one certain type, only the jog pairs formed by these point defects will survive. Therefore, the external load changes jog concentration proportional to $\exp(-\Lambda\sigma_{nn}\omega/k_B T)$, if dislocation preferentially absorbs vacancies and $\propto \exp(\Lambda\sigma_{nn}\omega/k_B T)$ in the opposite case.

The mean free path of a point defect in the dislocation core, λ_α, is given by the relation [325]

$$\lambda_\alpha^k = a \exp\left(\frac{\Delta Q_\alpha^k}{k_B T}\right), \tag{2.30}$$

where $\Delta Q_\alpha = (E_{b\alpha} + E_{m\alpha} - E^d_{m\alpha})/2$, $E_{m\alpha}$ and $E^d_{m\alpha}$ are migration barriers of point defects in the bulk and in the dislocation core, and $E_{b\alpha}$ is the energy of their binding to dislocations.

The external load can change the values of both formation and migration energies of point defects in dislocation core, $E^d_{f\alpha}$ and $E^d_{m\alpha}$ [342]. So let us expand the energy $Q_\alpha^{dk} = E^{dk}_{f\alpha} + E^{dk}_{m\alpha}$ to the first order in external strains ε^o_{ij}, i.e. $Q_\alpha^{dk} = Q_\alpha^d (1+P^{dk}_{\alpha,ij}\varepsilon^o_{ij})$, where $P^{dk}_{\alpha,ij}$ is the force tensor of a point defect in the saddle point of diffusion jump along the core of a dislocation of orientation k. Assuming that the relaxation volume of a point defect, $\Delta V_\alpha^d = \mathrm{Tr}\, P^{dk}_{\alpha,ij}/K$, where K is the bulk modulus of the material, is independent of dislocation orientation, and using the Hook's law for ε^o_{ij}, the orientational dependence of λ_α can be represented as

$$\lambda_\alpha^k \propto \exp\left\{\frac{1+\nu}{6(1-2\nu)}\frac{p^k_{\alpha,ij}\sigma_{ij}\Delta V^d_\alpha}{k_B T}\right\}, \tag{2.31}$$

where $p^k_{\alpha,ij} = 3P^{dk}_{\alpha,ij}/\mathrm{Tr}\, P^{dk}_{\alpha,ij}$.

3.2.1.3 Irradiation creep rates due to dislocation climb

The **climb-controlled contribution to the irradiation creep rate**, $\dot\varepsilon^I_{ij}$, is obtained by straightforward substitution of equation (2.19) into the first term in the r.h.s. of equation (2.11):

$$\dot\varepsilon^I_{kl} = \left(\frac{<\hat b_k \hat b_l Z_i>}{<Z_i>} - \frac{<\hat b_k \hat b_l Z_v>}{<Z_v>}\right) G\Phi\left(\frac{G}{G_R}\right). \tag{2.32}$$

Using this relation, it is possible to analyze the dependence of the steady-state irradiation creep on irradiation parameters.

3.2.1.3.1 Irradiation creep dependence on the point defect generation rate

The dependence of in-reactor creep rate on the point defects generation rate G is markedly different for three temperature intervals. In the low-temperature region, where the point defect annealing behaviour is dominated by recombination, $\dot\varepsilon^I_{ij} \propto \sqrt{G}$ (cf. [75,122,206]). At intermediate temperatures the creep rate is described by the usual linear law $\dot\varepsilon^I_{ij} \propto G$. Finally, in the high-temperature region the irradiation creep is negligible as compared to the thermal component of creep. It should be emphasized that such qualitative behaviour is due to point defect annihilation regimes, rather than to a particular kind of SIPA mechanism However, the transition temperatures T^* and T^{**} between the three temperature regions can be sensitive to details of point defect capture by sinks. The estimates of T^* and T^{**} are given below in subsection 3.2.1.3.4.

3.2.1.3.2 Irradiation creep dependence on the load intensity

As already discussed, it is assumed that the studied material is under the action of a uniaxial stress σ applied along the axis 1 of the Cartesian system of coordinates. As long as the stress σ is sufficiently small, the bias factors Z_α can be expanded to the first order in σ (or, more conveniently, in a dimensionless parameter σ/μ):

$$Z_\alpha^k = Z_\alpha^0\left(1+\delta_\alpha^k\frac{\sigma}{\mu}\right), \tag{2.33}$$

where $Z_\alpha{}^0$ is the stress-free value of corresponding bias factor and δ_α^k is the first derivative of Z_α with respect to the normalised stress (σ/μ). Substitution of (2.33) into (2.32) gives

$$\dot{\varepsilon}_{kl}^{DC} = B_{kl}\frac{\sigma}{\mu}G\Phi\left(\frac{G}{G_R}\right), \tag{2.34}$$

where $\boldsymbol{B_{kl}}$ **is the creep compliance (a tensor analog of the creep modulus)**, defined as

$$B_{kl} = \left\langle \hat{b}_k\hat{b}_l(\delta_i-\delta_v-<\delta_i-\delta_v>)\right\rangle. \tag{2.35}$$

Relation (2.34) demonstrates that the in-reactor creep rate at comparatively small stresses is linear in σ. This stress dependence has universal character, irrespective of the mechanism ensuring anisotropy of point defect absorption by dislocations. On the other hand, the applicability range of the linear relation (that is, the maximum stress σ^* until which relation (2.35) holds) depends on the particular mechanism.

When the bias factor anisotropy is due to the stress effects of elastic interaction of point defects with dislocations, σ^* is of the order of the shear modulus of the material, μ. Because such loading stresses cannot be reached in creep experiments, the linear dependence of the creep rate on stress can be expected at any relevant stress. On the other hand, when the bias factor modification is due to the stress effect on point defect energetics (diffusion barriers, energies of jog nucleation on dislocations, etc.), the critical stress σ^* is of the order of $\sigma^* \sim k_BT/\omega$, which gives values of about several hundreds MPa at typical reactor temperatures of 300-600°C. It is interesting to note, that these values are of the same order of magnitude as the yield stress of irradiated metals, which naturally promotes a question, whether such mechanisms can be responsible for the observed non-linearity of irradiation creep at $\sigma > \sigma^*$. It is easy to show, however, that this is not the case.

Indeed, let us assume that at large stresses the bias factors are described by a relation of the type $Z_\alpha^k \propto \exp(\Lambda_\alpha^k \sigma\omega / k_B T)$, where the value of Λ_α^k is determined by a particular mechanism. Then the basic contribution to all orientational averages of Z_α, entering (2.32), will be given by dislocations with that orientation κ, for which Λ_α^κ is the biggest positive number. But then $\left\langle \hat{b}_k \hat{b}_l Z_\alpha \right\rangle / \left\langle Z_\alpha \right\rangle \to \hat{b}_k^\kappa \hat{b}_l^\kappa$ and does not depend on stress at all. Then equation (2.32) predicts that **the irradiation creep rate determined by dislocation climb should vanish at high stresses**. The physical reason for this conclusion is transparent. **At too high stresses both vacancies and interstitial atoms created by irradiation are predominantly captured by dislocations with the same preferred orientation, so the net dislocation climb vanishes**.

Summing up, the experimentally observed non-linearity of in-reactor creep rate cannot be described in terms of the models based on dislocation climb and requires the account of alternative mechanisms (e.g. considering dislocation sliding). Therefore the remaining part of the current section deals with the region of linear dependence of irradiation creep rate on stress.

3.2.1.3.3 The irradiation creep compliance

The **value of the irradiation creep compliance B_{kl} is determined by the specific mechanism resulting in the anisotropy of bias factors Z_α.**

For example, **for the case of *stress-induced elastic modulus anisotropy* mechanism** one has

$$B_{kl} = S_{kl}^{EMA}\left(\frac{Z_i^0 p_i^\mu}{2\pi e_i^0} - \frac{Z_v^0 p_v^\mu}{2\pi e_v^0} \right), \qquad (2.36)$$

where S_{kl}^{EMA} is the structure factor, determined by the distribution of dislocation orientations with respect to the applied load,

$$S_{kl}^{EMA} = 3\nu \left\langle \hat{b}_k \hat{b}_l \left((\mathbf{ts})^2 - <(\mathbf{ts})^2> \right) \right\rangle + 3 \left\langle \hat{b}_k \hat{b}_l \left((\hat{\mathbf{bs}})^2 - <(\hat{\mathbf{bs}})^2> \right) \right\rangle .$$

Using the estimates $p^\mu_i \approx 0.5$, $p^\mu_v = 0$, $Z^0_i \approx 3$, $e^0_i \approx 1.5$, we get

$$B_{kl} \sim S_{kl}^{EMA},$$

that is the creep compliance is of the order of unity. This prediction is very similar to the estimates commonly reported for the in-reactor creep modulus in experimental publications, which was considered for some time as a justification for this mechanism. However, later on it became clear that the point defect generation rate by fast neutrons is overestimated by nearly an order of magnitude, when estimated using the common standards, and thus the analytical prediction of the

creep compliance value should be at least an order of magnitude higher in order to fit experimental observations. This cannot be achieved by varying parameters entering (2.36) within reasonable limits. Together with the above mentioned inconsistency in the prediction of limiting stress σ^*, this **rules out stress-induced elastic modulus anisotropy as a relevant mechanism of irradiation creep**.

In the case of *stress-induced diffusion anisotropy* the stress-induced modification of dislocation bias depends on the dislocation orientation with respect not only to the stress, but to the crystal lattice as well. In a monocrystal, the creep compliance has the form [334]

$$B_{kl} = \frac{3K\omega}{4k_B T}\left[\left(e_i^s d_i^{(2)} - e_v^s d_v^{(2)}\right) S_{kl}^{(2)} + \left(e_i^s d_i^{(3)} - e_v^s d_v^{(3)}\right) S_{kl}^{(3)}\right], \tag{2.37}$$

where $S_{kl}^{(2)}$ and $S_{kl}^{(3)}$ are structure factors, defined as

$$S_{kl}^{(2)} = \left\langle \hat{b}_k \hat{b}_l \right\rangle \left\langle (\mathbf{ts})^2 \right\rangle - \left\langle \hat{b}_k \hat{b}_l (\mathbf{ts})^2 \right\rangle \tag{2.38}$$

and

$$S_{kl}^{(3)} = \sum_{p=1}^{3} (\mathbf{e}_p \mathbf{s})^2 \left\{ \left\langle \hat{b}_k \hat{b}_l \right\rangle \left\langle (\mathbf{e}_p \mathbf{t})^2 \right\rangle - \left\langle \hat{b}_k \hat{b}_l (\mathbf{e}_p \mathbf{t})^2 \right\rangle \right\}, \tag{2.39}$$

while other variables are the same as in section 3.2.1.2.2. An estimate of the creep compliance in steel at T = 300 ^{o}C using the point defect polarization data from [337] (see also Table 3.1) gives, ,

$$B_{kl}^{DA} \approx 20 S_{kl}^{(2)} + 7 S_{kl}^{(3)},$$

for copper and,

$$B_{kl}^{DA} \approx 70 (S_{kl}^{(2)} - S_{kl}^{(3)}).$$

for α-iron. In the latter case the identical coefficients before structure factors constitute a general feature of bcc metals, where $d_\alpha^{(2)}$ = - $d_\alpha^{(3)}$ due to the specific point defect symmetry in the saddle points of diffusion jumps [343].

One of the most interesting features of equation (2.39) is the prediction of the creep compliance dependence on load orientation with respect to the crystal axes, the effect being most pronounced in bcc materials [323]. This dependence provides a direct way for the experimental validity check of the elastodiffusion mechanism of irradiation creep. Moreover, the experimentally obtained values of creep compliance can be used to estimate the parameters of anisotropic point defect diffusion in particular materials. Yet, to our knowledge, nobody tried to use this possibility up to now.

In polycrystalline materials the expression for creep compliance should be additionally averaged over different grain orientations (that is - over $\boldsymbol{e}_p$ in (2.39)). Assuming the isotropy of grain orientations, one gets

$$S_{kl}^{(3)} = \frac{2}{5} S_{kl}^{(2)}$$

so that the dependence on the stress orientation with respect to lattice orientation is completely lost.

Since at temperatures up to 1000°C the relation $\mu\omega/k_BT$ » 1 holds, **the value of creep compliance for the elastodiffusion mechanism correlates reasonably well with experimental predictions, making it the most probable mechanisms for SIPA-type irradiation creep** [322,323].

Finally, **in the framework of mechanism based on the *stress effect on point defect absorption by dislocations*** the bias factors Z_α are given by eq. (2.28). In linear approximation in σ, each of three multipliers in the right hand part of eq. (2.28) depend on the dislocation orientation with respect to loading direction. However, the contribution to the creep compliance from C_j vanishes because this parameter is independent of the point defect type. The stress enhanced jog nucleation affects the creep compliance only through the dependence of the factors β_α^k on the jog concentration [325]

$$B_{kl} = S_{kl}^{EJN} \frac{\beta_i^2 \beta_v^2}{2(4\pi)^4} \ln\left(\frac{e_i^0}{|e_v^0|}\right) \frac{\Lambda \mu\omega}{k_B T}, \qquad (2.40)$$

where $S_{kl}^{EJN} = <\hat{b}_k \hat{b}_l (\zeta_j (\mathbf{bs})^2 - <\zeta_j (\mathbf{bs})^2>)>$, ζ_j = 1 when a dislocation absorbs predominantly interstitials, or ζ_j = -1 in the opposite case. Taking $\beta_i \sim \beta_v \sim 5$ [325], $\Lambda = 2$, $e^0{}_i \approx 1{,}5$, and $|e^0{}_v| = 0.5$, we obtain

$$B_{kl} = 0.03 S_{kl}^{EJN} \frac{\mu\omega}{k_B T}.$$

The contribution to creep compliance from the orientational anisotropy of pipe diffusion of point defects along dislocation cores, eq. (2.31), equals to

$$B_{kl} = (e_i^d S_{i,kl}^{PDA} - e_v^d S_{v,kl}^{PDA}) \frac{K\omega}{12 k_B T}, \qquad (2.41)$$

where $e_\alpha^d = \Delta V_\alpha^d / \omega$, K is the bulk modulus of material, and the structure factors are defined as

$$S_{\alpha,kl}^{PDA} = \left\langle \hat{b}_k \hat{b}_l (p_{\alpha,11}^d - < p_{\alpha,11}^d >) \right\rangle. \qquad (2.42)$$

Here $p^d_{\alpha,11}$ is the component of polarization tensor in the coordinate system with the axis 1 coinciding with the load direction. Information about polarization tensors of point defects in dislocation core is practically lacking in the literature. A very rough estimate of

$$B_{kl} = 0.03\frac{\mu\omega}{k_B T}.$$

can be obtained using the results for the effect of external load on vacancy diffusion along dislocations of the type a<100>{001} in α-Fe [344] and assuming isotropic distribution of dislocations over orientations. That is, **the contribution to the irradiation creep compliance from the stress effect on point defect absorption by dislocation is expected to be comparable to that from elastodiffusion**.

Finally, it is worth mentioning that, whatever the bias factor anisotropy mechanism, the resulting creep compliance is sensitive (via structure factors) to the dislocation distribution in the material. In order to get a feeling of the importance of the account of dislocation distribution for irradiation creep predictions, let us compare two representative situations: (i) completely isotropic distribution of dislocations over orientations, and (ii) "cubic" distribution of dislocations over orientations with three different dislocation types, namely dislocations which are perpendicular to the loading axis with the Burgers vector along (k = 1) and normally (k = 2) to this axis, and dislocations which lie along the loading axis with the Burgers vector normal to this axis (k = 3). The values for the structure factor component S_{nn} that corresponds to creep along the loading axis are summarized for these two dislocation distributions in Table 3.2.

Table 3.2

Structural factors S_{nn} for various mechanisms of point defect absorption by dislocation

Dislocation distribution	Irradiation creep			Thermal creep, $S^T{}_{nn}$
	Elastic modulus modification, $S^{EMA}{}_{nn}$	Bulk diffusion anisotropy, $S^{(2)}{}_{nn}$	Dislocation core diffusion anisotropy, * $S^{PDA}{}_{\alpha,nn}$	
Fully isotropic	$\frac{2(2-\nu)}{15}$	$-\frac{2}{45}$	$\frac{2}{15}(p^d_{\alpha,11}-1)$	$\frac{4}{45}$
Cubic	$3f_1(1\text{-}f_1\text{-}\nu f_3)$	$-f_1 f_3$	$f_1\{f_2(p^d_{\alpha,11}-p^d_{\alpha,22})+$ $f_3(p^d_{\alpha,11}-p^d_{\alpha,33})\}$	$f_1(1\text{-}f_1)$

* Contribution from one type of point defects

One can see that in the case of "cubic" distribution of dislocations over orientations the maximum value of creep rate along the loading axis is reached at noticeably anisotropic distribution of dislocations over orientations. It is interesting that an anisotropic dislocation distribution (with $f_1 > f_2, f_3$) is very typical for the dislocation density evolution at the transient stage of irradiation creep [170]. If pronounced, such anisotropy can noticeably decrease the structure factor as compared to the dislocation equi-partition over orientations.

3.2.1.3.4 Irradiation creep dependence on the irradiation temperature

In this section we restrict ourselves to the isotropic distribution of dislocations over orientations and consider only the component of strain rate along the loading axis. $\dot{\varepsilon}^I_{11}$. We also assume that the temperatures are always below the critical value T^{**}, above which the thermal creep dominates.

In the temperature region of interest, the temperature dependence of irradiation creep rate is largely determined by the function Φ entering equation (2.34). One generally meets two temperature ranges, separated by a certain temperature T^*. At temperatures $T > T^*$, where point defects are mostly absorbed by dislocations, $\Phi \approx 1$ and the temperature dependence of irradiation creep is that of the creep compliance, i.e. relatively weak. On the contrary, at low temperatures ($T < T^*$) the basic mode of point defect annealing is their mutual recombination and the temperature dependence is dominated by an exponential term,

$$\dot{\varepsilon}^I_{11} \propto \exp\left(-\frac{E_{mv}}{2k_B T}\right). \qquad (2.43)$$

The transition temperature T^* can be defined from the condition $G \sim G_R$, which gives

$$k_B T^* \approx E_{mv} \ln^{-1}\left[\frac{Z_i^0 Z_v^0 D_{v0} \rho^2 a^2}{4\sigma_R G}\right]. \qquad (2.44)$$

An estimate of T^* at typical parameter values $D_{v0} = 1$ cm^2/s, $\rho = 3\times10^{10}$ cm^{-2}, $a = 0.2$ nm, $\sigma_R = 5$, $Z_\alpha^0 \approx 3$, $S^R_{11} = S^T_{11}$, and $C^R = 0.1$ gives (assuming in-reactor point defect generation rates of $G \approx 10^{-7}$ dpa/s):

$$k_B T^* \sim E_{mv}/40.$$

The vacancy migration energy normally falls within the range 6.5 - 8 $k_B T_m$ [345], hence the homologous critical temperature is $T^*/T_m \sim 0.16$-0.2.

The range of intermediate temperatures, $T^* < T < T^{**}$ is the most interesting one from the practical point of view. In this range the **temperature dependence of the irradiation creep rate is**

determined entirely by the specific physical mechanism, causing the anisotropy of point defect distribution between differently oriented dislocations. The mechanism of elastic modulus anisotropy predicts no dependence of the irradiation creep rate on temperature, whereas the mechanisms based on the stress-induced anisotropy of point defect migration processes give $\dot{\varepsilon}_{ij}^{DC} \propto T^{-1}$ [323,34]. Unfortunately, in experimental conditions it is hard to reliably discern between these possibilities, because the creep rate variations predicted by different models in the specified temperature interval are relatively weak and can be disguised by the scatter of experimental points.

3.2.2 Creep mechanisms based on climb-controlled dislocation glide

3.2.2.1 Dislocation glide through a system of barriers

Dislocation glide in perfect crystals starts when the resolved shear stress in the dislocation glide plane exceeds a certain threshold value (Peierls barrier [284]) and the glide velocity V_{g0} is extremely fast (of the order of the sound velocity). However, in real metals the average glide velocity of dislocation, V_g, is usually much less than V_{g0}, due to the presence of various obstacles on the dislocation glide plane (impurity atoms, precipitates, voids, dislocation loops, other dislocations, etc.). These obstacles serve as barriers hindering the glide. As a result, **the limiting step in the dislocation glide motion is not the glide itself, but the barrier overcoming**. A dislocation can come over a barrier **either thermofluctuatively, or climbing into a parallel glide plane, where the current barrier is no more operative**. For qualitative understanding of the physical picture it will be sufficient to restrict ourselves to the case where barriers of only one kind are present in the material, because even in a multi-barrier situation only the most strong barrier system limits the average dislocation slide velocity [346,347].

If the average time required for a dislocation to overcome a barrier is τ_b and the average distance glided by a dislocation between consecutive pinning barriers in the glide plane is L_g, then the total time spent by a dislocation in order to shift from one barrier to the next one is $\tau = \tau_b + (L_g/V_{g0})$, while the average glide velocity is

$$V_g = \frac{L_g}{\tau} = \frac{1}{1+\frac{V_{g0}\tau_b}{L_g}} V_{g0}.$$

The average time required for a dislocation to overcome a barrier can usually be defined as

$$\frac{1}{\tau_b} = \nu_{d0} \exp\left(-\frac{U_b}{k_B T}\right) + \frac{|V_c|}{h}, \qquad (2.45)$$

where ν_{d0} is the attempt frequency, U_b is the activation energy to overcome the barrier, V_c is the average climb velocity, and h is the barrier geometrical "height". Strictly speaking, this relation is not the most general one and can be further modified when special effects are to be considered. For example, if the barrier height changes with time (which is the case for e.g. dislocation loops, voids and precipitates), then the dislocation climb velocity in the r.h.s. of (2.45) should be replaced with the difference $|V_c|$ - (dh/dt) [348,349]. On the other hand, especially when the barrier heights are of the order of interatomic distance, the dislocation climb velocity can be limited not by the average value V_c, but by local climb of pinned dislocation segment due to the short-term currents of point defects from nearby cascades of atomic collisions [350-353]. However, these additional corrections can be of importance only in special conditions and are not considered here.

In the absence of irradiation, the glide barriers are mainly overcome by various kinds of thermal fluctuation processes [284], while the climb contribution can be important only when the barriers are too strong and the stresses sufficiently high to provide substantial redistribution of thermal vacancies between differently oriented dislocations. **Irradiation creates in material high supersaturations of point defects and barriers are overcome predominantly by dislocation climbing** into a parallel glide plane. On the other hand, the climb velocities are usually quite low, so that the relation $h/V_c \gg L_g/V_{g0}$ holds. As a result, the average dislocation glide velocity under irradiation is usually limited by climb over barriers and provides the following contribution to the irradiation creep rate (as determined by the second term in the r.h.s. of equation (2.11)):

$$\dot{\varepsilon}^I_{kl} = \frac{1}{2}\rho b \left\langle (\hat{b}_i n_j + n_i \hat{b}_j) |V_c| \frac{L_g}{h} \right\rangle, \qquad (2.46)$$

A relation of this kind was first proposed (without the averaging over dislocation orientations) for the description of thermal creep [354,355], but its derivation did not explicitly specify the mechanism of dislocation climb and so it is equally valid for irradiation creep, provided appropriate parameter values are substituted [356-358].

As follows from relation (2.46), in order to find the irradiation creep rate in the framework of the climb-controlled glide model, it is necessary to know not only the dislocation climb rate, but also the "glide factor", L_g/h, determined by the type and the parameters of that barrier system, which provides the major hindrance for the glide.

3.2.2.1.1 The efficiency of dislocation stopping by barriers

Various components of the defect microstructure of irradiated material are considered in the literature as obstacles for dislocation glide, including those not directly related to irradiation (impurity atoms [347], network dislocations [359], secondary phase precipitates [360,361]) and those arising as a result of irradiation (cascade depleted zones [357,362,363], dislocation loops [41,52,62,234,235], voids [362]). **Each of these barrier types has its own efficiency of dislocation stopping, which is conveniently characterized by the value of a critical shear stress σ_y, necessary for the athermal break-through of a dislocation through the ensemble of barriers**. In fact, σ_y characterizes the maximum stress, at which the given system of barriers can prevent the glide of dislocations. At larger stresses this barrier system becomes inactive.

Let us consider a model where a straight edge dislocation glides under the action of external loading σ_{13} in the direction of axis 1 in a plane normal to axis 3, periodically hanging up at a regular grid of obstacles (see Fig. 3.2). The gliding dislocation is considered as a flexible string with a constant linear tension γ (it is usually accepted that $\gamma \approx \mu b^2/2$ [365]). To simplify the discussion, let us assume that the obstacles form a square lattice in the glide plane and the distance between the neighbour barriers equals L_b.

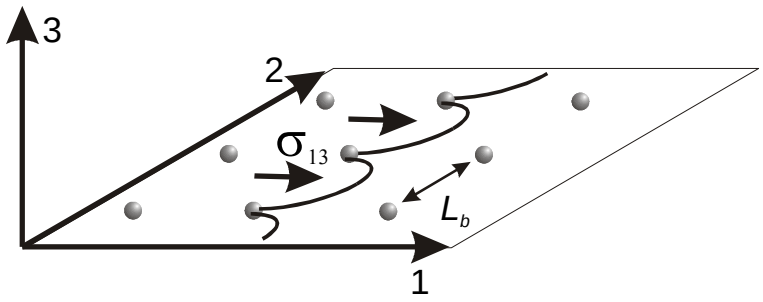

Fig. 3.2. A schematic representation of a dislocation gliding through the array of obstacles.

In such a model the dislocation hangs up at an obstacle, if the following condition is satisfied

$$\sigma_{13} b L_b \le F_b, \qquad (2.47)$$

where F_b is the resistance force of a single obstacle. As the dislocation hangs up at barriers, its free segments bend forward, reaching the curvature radius of $R_c = \gamma/b\sigma_{13} \approx \mu b/2\sigma_{13}$ [366]. Thus the force acting on an obstacle from two adjacent free dislocation segments is equal to $F = 2\gamma\cos(\varphi/2)$, where

φ is an angle between these adjacent dislocation segments. If, by analogy, we introduce a critical angle, φ_b, such that $F_b = 2\gamma\cos(\varphi_b/2)$, the critical stress for dislocation unpinning can be written as

$$\sigma_y = \mu\frac{b}{L_b}\cos(\varphi_b/2). \tag{2.48}$$

A somewhat more complicated situation arises when the barriers form a disordered array, e.g. they are completely randomly (though uniformly) distributed in space. In this case the average distance between barriers at a dislocation, L_s, depends on the applied shear stress as [367-369]:

$$L_s = \chi_s\left(\frac{3\mu b L_b^2}{\sigma_{13}}\right)^{1/3}, \tag{2.49}$$

where L_b is, as before, the average distance between barriers in the dislocation glide plane, and χ_s~1, being only weakly dependent on stress (varying from $\chi_s \approx 0.9$. at $\sigma_{13}\to 0$ to $\chi_s \approx 1{,}2$ at $\sigma_{13}\to\sigma_y$ [369]). Hence,

$$\sigma_y = \frac{1}{\sqrt{3}\chi_s^{3/2}}\frac{\mu b}{L_b}\cos^{3/2}(\varphi_b/2). \tag{2.50}$$

It is interesting to note that this relation correlates qualitatively well with the empirical law received as a result of numerical simulation of dislocation break-through a system of randomly located point-size obstacles [366]:

$$\sigma_y = \frac{4}{5}\frac{\mu b}{L_b}\left[1-\frac{\varphi_b}{4\pi}\right]\cos^{3/2}(\varphi_b/2). \tag{2.51}$$

It is seen that the random arrangement of barriers results in the reduction of the critical stress in comparison with the ordered arrangement for all φ_b and this reduction is the most essential for weak barriers (when $\varphi_b \to \pi$).

The critical angle φ_b differs for different barriers and can serve as an indicator of the relative strength of individual barriers. It is a common practice to separate barriers into three classes [370]:

- weak barriers ($\cos(\varphi_b/2) < 1/4$): network dislocations, impurity atoms in fcc metals;
- intermediate barriers ($1/4 < \cos(\varphi_b/2) < 1/2$): coherent precipitates, interstitial impurity atoms in bcc metals;
- strong barriers ($\cos(\varphi_b/2) > 1/2$): incoherent precipitates , Frank loops, voids.

The values of critical angles can be obtained experimentally, since σ_y is nothing else than the yield stress. For example, for Frank dislocation loops an experimental estimate gives $\cos(\varphi_b/2) \approx 0.5\text{-}0.8$, while for voids $\cos(\varphi_b/2) \approx 1$ [371,372]. The estimate for voids correlates nicely with the numerical simulation prediction of $\cos(\varphi_b/2) \approx 0.95$ [364].

One should keep in mind, however, that when a material contains several different barrier types, the selection of the obstacle systems dominating the dislocation stopping depends not only on the strength of individual obstacles, but also on their density in the glide plane, because, as follows from (2.48), a large number of weak barriers can hinder the glide of a dislocation more effectively, than a small number of strong obstacles.

Let us estimate the value σ_y for the principal components of defect structure present in the material at various stages of irradiation creep.

- For *network dislocations* $L_b \approx (\pi\rho)^{-1/2}$, which gives $\sigma_y/\mu \approx 10^{-3}$ -10^{-4} at typical values of $\varphi_b = 5\pi/6$ [347] and $\rho = 10^8$:- 10^{10} cm^{-2}. These estimates correspond to the lower limit of loads used in irradiation creep experiments, so the stopping of gliding dislocations by dislocation "forest" is rather of theoretical interest.
- For *three-dimensional barriers* (point defects, small clusters thereof, phase particles, voids, faulted loops, etc.), which are randomly distributed in the bulk of the material and have characteristic size h and volume density N_b, the average distance between barriers in a glide plane is given by

$$L_b \approx (N_b h)^{-1/2} \qquad (2.52)$$

  So for voids and faulted dislocation loops, which are strong barriers for dislocation glide ($\cos(\varphi_b/2) \approx 1$) and have characteristic density $N_b \sim 10^{15}$ cm^{-3} and sizes $h \sim$ 10-100 nm, we have $\sigma_y/\mu \geq 10^{-3}$, i.e. at relevant experimental stresses such sinks efficiently hinder dislocation glide only when they are sufficiently large. Indeed, measurements of material hardness (the most direct indication of dislocation mobility) show that a certain increase of hardness in void-containing alloys occurs only at higher swelling levels [373].
- In the case of *impurity atoms*, $h \sim b$ and $\sigma_y/\mu \approx C_s^{1/2} \cos(\varphi_b/2)$, where C_s is the atomic concentration of impurity. If the barrier strength of the impurity is not extremely low and the impurity concentration is in the percent range, impurity atoms act as the principal barriers for dislocation glide. At the same time, if in the course of irradiation the impurity atoms precipitate in the form of secondary phases (such that $N_b h^3 \sim C_s$), one gets $\sigma_y/\mu \propto h^{-1}$, i.e. with the increase

of the size of precipitates and, correspondingly, with the solid solution depletion (at the fixed total impurity content) the efficiency of material hardening by impurity falls down.

3.2.2.1.2 The average dislocation glide distance

Let us consider an edge dislocation, oriented with respect to coordinate system as shown in Fig. 3.2. Initially (in an unloaded material) it is assumed to be straight and not fixed by barriers. Application of a shear stress σ_{13} (sufficient to overcome the Peierls barrier) makes the dislocation glide until it is reaches the nearest obstacles and bends forward between them. When the barriers are sufficiently strong to pin the dislocation at the applied stress level, no further glide in the same plane is allowed and the strains due to dislocation segment bending are recoverable. If the barrier system is ordered and the critical angle φ_b for dislocation unpinning from barriers is not too close to zero, the average deflection ΔL_e of a pinned dislocation segment grows linearly with the stress level [374,375]

$$\Delta L_e = \frac{L_b^2}{4b}\frac{\sigma_{13}}{\mu} \sim \frac{\sigma_{13}}{\sigma_y}. \qquad (2.53)$$

Following [359], this average deflection ΔL_e is often treated as the dislocation glide distance (see e.g. [358]). However, such assumption is incorrect. Indeed, overcoming (e.g. by climb) the first chain of barriers, the dislocation hangs up on a similar set of barriers in the new glide plane, keeping, on the average, the same deflection. Hence, **the dislocation glide distance is simply the average distance between barriers in the glide plane** ($L_g = L_b \sim C_b^{-1/3}$, where C_b is the atomic concentration of the barriers) and does not depend on the load level up to $\sigma_{13} = \sigma_y$.

A more complicated situation arises, **when the barriers are randomly distributed in space**. In this case the force acting on each particular barrier can vary depending on the positions of neighbouring barriers. As a result, **the stresses necessary to overcome some of the barriers can be less than the critical stress and the athermal unpinning of a dislocation from these barriers occurs even before the stress level of σ_y is achieved**. In turn, the released dislocation segments act with increased force on the neighbouring barriers (since these forces are proportional to the length of the free dislocation segment), **resulting in a series of correlated unpinning acts** ("unzipping" effect [376]). Due to the unzipping effect, **the dislocation unpinned from the obstacles can glide, on the average, further than the average inter-barrier distance before it is captured by barriers in the new glide plane**. It is clear, however, that **this effect should be noticeable only for stresses sufficiently close to σ_y**. Indeed, numerical simulations of a dislocation break-through through a randomly distributed system of obstacles [347,377] indicate that at low stresses the progress of dislocation is limited by the deflection of its pinned segments according to relation

(2.53), whereas at sufficiently large stresses ($\sigma_{13} > 0.5\sigma_y$) the dislocation can cover after a single unpinning act the distances exceeding L_b.

Thus, the dislocation glide distance in the case $\sigma_{13} < \sigma_y$ can be described by relation

$$L_g = L_b \Psi\left(\frac{\sigma_{13}}{\sigma_y}\right), \qquad (2.54)$$

where $\Psi(x) = 1$ at x up to unity in the case of ordered obstacle system. In the case of random obstacle distribution $\Psi(x) = 1$ only provided $x < 0.5$, while for higher values of x the increase of Ψ with increasing x is predicted, as shown in Fig. 3.3.

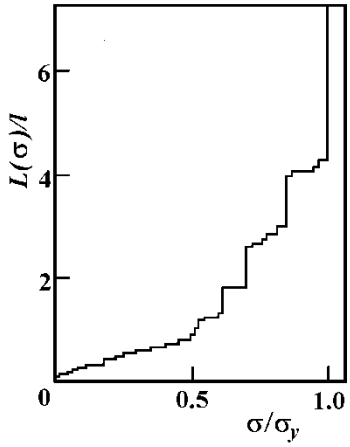

Fig. 3.3. The average dislocation glide distance as a function of shear stress in the dislocation glide plane (according to [347])

3.2.2.1.3 Barrier heights

The **height of barriers *h* is determined** by two factors, namely **by the actual geometrical size of the barrier and by the strength and extension of its elastic field**. In the subsequent discussion it makes sense to distinguish between two-dimensional barriers ("forest" dislocation) and three-dimensional ones (impurity atoms, secondary phase precipitates, dislocation loops, voids, etc.).

For "forest" dislocations the principal contribution to h comes, obviously, from the own length of a dislocation. In the literature it is usually postulated that h is of the order of the average distance between dislocations, i.e. $h \approx (\pi\rho)^{-1/2}$ [359]. However, such choice is arbitrary. It seems more consistent to assume that in this case h is infinite (in real-life materials - comparable to the grain size), and so "forest" dislocations are overcome, most likely, by mechanisms providing no contribution to the irradiation component of creep.

In the case of three-dimensional obstacles the barrier height can be limited either by the own size of the barrier, or by the size of its elastic field. The latter is more typical for barriers with small cross-section, but strong elastic fields, such as dislocation loops and some kinds of precipitates. The same situation is met when a gliding dislocation interacts with a parallel dislocation in a nearby gliding plane.

In the case of stopping by elastic fields the barrier height can be estimated according to the approach proposed in [359]. Let us assume that a dislocation glides in a plane located at distance h from the center of a barrier, such that h exceeds the characteristic barrier size R_b. The dislocation is under the action of an external shear stress σ_{13} and the resistance force from the barrier, $F_b(h)$, which changes as the dislocation moves in the glide plane. Since the stresses from a three-dimensional stress source fall down as h^{-3} and act on a dislocation segment of length ~ h, we get $F_b(h) \propto h^{-2}$. Accordingly, the maximum force of dislocation pinning by the barrier can be written down as

$$F_b^{max} = A_b \frac{\mu |\Delta V_b| b}{h^2}, \qquad (2.55)$$

where ΔV_b is the volume misfit of the obstacles causing elastic stresses in the matrix, and A_b is a numerical factor determined by a particular kind of the interaction law between the barrier and the gliding dislocation. Fig. 3.4 shows the simplest law of interaction of an edge dislocation with a point center of dilatation in an isotropic material. Here, as can be easily checked, $A_b = \frac{3\sqrt{3}}{8\pi} \sim 0.2$. However, the account of anisotropy of both the force tensor of a point defect and the elastic constants of material can result in much more complicated forms of the interaction law [378]. In such cases, the calculation of parameter A_b is a separate task requiring the application of numerical methods.

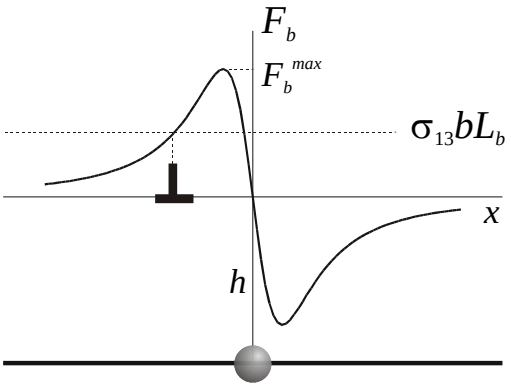

Fig. 3.4. The force acting on an edge dislocation, gliding past an isotropic dilatation center

The minimum distance from the glide plane to the barrier that allows the dislocation to pass by the barrier without being pinned up (i.e. the height of the barrier h) is defined by the exact balance between the maximum pinning force $F_b^{max}(h)$ and the force from the external loading, i.e.

$$F_b^{\max}(h) = \sigma_{13} b L_b. \tag{2.56}$$

Combining relations (2.49), (2.52) and (2.56), we get

$$h = \chi_0 \left[\frac{N_b \Delta V_b^3}{b} \right]^{1/5} \left(\frac{\mu}{\sigma_{13}} \right)^{2/5}, \tag{2.57}$$

where $\chi_0 = (A_b^3/3\chi_s^3)^{1/5}$.

Relation (2.57) for the barrier height remains valid as long as the stress remains below a certain critical value σ_{yh}, which can be easily determined by substitution of (2.57) into the relation $h = \xi R_b$, where the factor ξ accounts for the relative orientation of the dislocation and the barrier ($\xi = 1$ for spherically symmetric stress sources and $\xi < 1$ for dislocation loops). For the most interesting case of point-size barriers (impurity atoms) it is possible to set $\xi = \chi_s = 1$, $A_b = 0.2$, $R_b = b$, and $\Delta V_b = e_b \omega$, where e_b is the absolute value of the point defect dilatation, so that

$$\frac{\sigma_{yh}}{\mu} \sim 0.55 e_b^{3/2} C_b^{1/2}. \tag{2.58}$$

Note that at $e_b \sim 1$ the value of σ_{yh} is comparable to σ_y.

At $\sigma_{13} > \sigma_{yh}$ the elastic fields of the barriers do not stop dislocation glide and the dislocation can be stopped only by the barriers themselves, i.e. at high stresses one has

$$h \approx \xi R_b. \tag{2.59}$$

3.2.2.1.4 The glide factor

Remaining at stresses not too close to σ_y, it is possible to set $\Psi = 1$ in equation (2.54). Then, taking into account (2.52),

$$L_g / h \approx (N_b h^3)^{-1/2}. \tag{2.60}$$

For the case of dislocation pinning by elastic fields of barriers (that is - at low stresses, $\sigma_{13} < \sigma_{yh}$)

$$\frac{L_g}{h} = \chi_0^{-3/2} \left(\frac{b}{\Delta V_b^3} \right)^{0.3} N_b^{-0.8} \left(\frac{\sigma_{13}}{\mu} \right)^{0.6}, \tag{2.61}$$

A relation similar to (2.61) was first proposed in [234].

When dislocations are stopped by the barriers themselves and the load is not too close to σ_y, one has

$$\frac{L_g}{h} = \xi^{-3/2}\left(N_b R_b^3\right)^{-1/2} \tag{2.62}$$

independentLY of the applied load.

In addition to the laws above, one can find other expressions for the glide factor, which are generally presented in the form of power laws in stress, that is

$$\frac{L_g}{h} = \vartheta_g \left(\frac{\sigma_{13}}{\mu}\right)^m, \tag{2.63}$$

where both the prefactor ϑ_g and the power m depend on the particular system considered of glide barriers and on the possibility for gliding dislocation to form pile ups. Most often m =1 is suggested, though one can find other values as well (e.g. m = 0.5 [235] or m = 1.2 [234]).

3.2.2.2 Irradiation creep rates due to climb-controlled dislocation glide

The obtained expressions for the "glide factor" make it possible to estimate the contribution to irradiation creep from the climb-controlled glide (CCG). Substituting (2.19) and (2.63) into (2.46), and using the general representation of bias factors in the form of (2.33), one obtains for the climb-induced glide contribution to irradiation creep

$$\dot{\varepsilon}_{kl}^I = B_{kl}^G \left(\frac{\sigma}{\mu}\right)^{1+m} G\Phi\left(\frac{G}{G_R}\right), \tag{2.64}$$

where the creep compliance B_{kl}^G is

$$B_{kl}^G = \frac{\vartheta_g}{2}\left\langle (\hat{b}_k n_l + n_k \hat{b}_l)\left|\delta_i - \delta_v - \left\langle \delta_i - \delta_v \right\rangle\right|\left((\mathbf{ts})(\hat{\mathbf{bs}})\right)^m \right\rangle. \tag{2.65}$$

The most important feature of the irradiation creep rate in the case of climb-controlled glide is the non-linear dependence on the stress. Due to the relation σ/μ « 1, **the CCG mechanism is weaker than SIPA type mechanisms at sufficiently low stresses, but a change of dominating mechanism of irradiation creep is possible at large stresses,** due to both the stress nonlinearity and the fact that the prefactor ϑ_g usually noticeably exceeds unity. This mechanism change is usually invoked to rationalize the stress exponents in the range 1<m<2, as observed at the stresses above a certain level σ* (see sect. 2.2.2.2). An example of such situation is presented in Fig. 3.5.

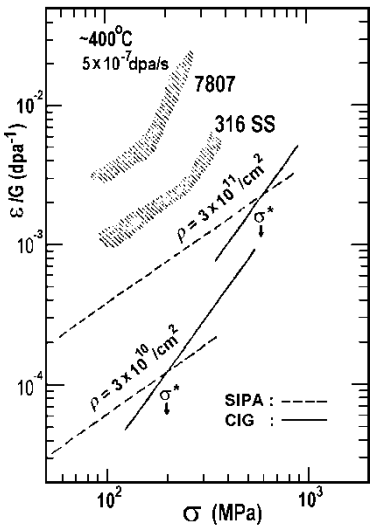

Fig. 3.5. Comparison of creep rate between theoretical values and the experimental ones, as a function of stress. The hatched area indicates the experimental values of the 7807 alloy and type 316 SS. The symbol σ* denotes the critical stress. (From [278]).

As an example of determination of the creep compliance, let us consider the case in which the dislocation distribution over orientations is completely isotropic and the stress affects dislocation bias factors via the modification of point defect elastic moduli. Then the following estimate for the creep compliance component in the stress direction B_{nn}^G holds

$$B_{nn}^G = S_{nn}^G \vartheta_g \left(\frac{Z_i^0 p_i^\mu}{2\pi e_i^0} - \frac{Z_v^0 p_v^\mu}{2\pi e_v^0} \right),$$

where S_{nn}^G is the structure factor. The estimates of the structure factor are not as trivial as in the case of SIPA-type mechanisms and are not found in the literature. One can expect, however, that it is noticeably less than for SIPA creep compliance.

3.3 Primary (transient) irradiation creep

3.3.1. Dislocation loop kinetics

As discussed in sect. 2, at the transient stage of irradiation creep the strain rate is determined by a combined effect from the dislocation network and the growing dislocation loops. The addition of dislocation loops to the defect microstructure can influence irradiation creep in two ways. First of

all, **the volume densities of nucleated Frank loops can depend on loop orientation with respect to the loading direction**. Usually this effect is described as [379]:

$$N^k = N_0^k \exp\left(\frac{m\tilde{\sigma}_{nn}\omega}{k_B T}\right), \qquad (2.66)$$

where N^k_0 is the volume density of *k*-type loops without loading, $\tilde{\sigma}_{nn}$ is the component of stress deviator tensor normal to the loop extra-plane, and m = 2-3. It is interesting that such dependence is observed in some electron microscopy studies [145,168,177,250,380-385] (though not always [91,93,129]), but its explanation is not at all obvious. Initially this kind of stress dependence was assumed to result from the effect of the stress on the free energy barrier for loop nucleation (stress-induced preferential nucleation, SIPN). However, in the case of interstitial dislocation loops the formation of a critical nucleus (di-interstitial) involves no kinetic barrier. **Probably, more adequate is to relate this effect [111] to rotation of small interstitial clusters (of only several interstitial atoms) into an energetically more favourable orientation with respect to the applied load**. Indeed, a possibility of thermally activated changes of the Burgers vector of di- and tri-interstitial clusters were observed in MD simulation studies [386-389].

The SIPN of dislocation loops was one of the first microstructural mechanisms proposed for the explanation of irradiation creep [390]. However, **being considered as an independent creep mechanism, SIPN is a poor alternative to mechanisms of SIPA type**. Indeed, the nucleation of extra loops with a preferred orientation contributes only weakly to the strain of material [234,379]. The subsequent growth of these loops can result in a certain amount of creep [236], but the creep rate of a material in this model (as well as in any model based on the initial anisotropy of loop orientations, such as models where the loop anisotropy is a consequence of preferred unfaulting reaction of small Frank loops [391]) should depend only on stresses acting during loop nucleation, and not on the instantaneous stress values. **Since loop nucleation occurs for very short time, such models would predict no creep if the material is loaded at some time after the onset of irradiation** [236]. **The load variation during irradiation (down to complete unloading) should also have no effect on the creep rate. Both these consequences of SIPN model contradict observations. Moreover, the anisotropic nucleation of loops can be manifested only as long as the loops are present, i.e. SIPN can not operate beyond the transient stage of irradiation creep**. **A contribution of SIPN can be expected, at best, at small doses of irradiation in well annealed materials with very low initial density of other point defect sinks** [392].

Much more productive seems to be the idea to combine SIPN with SIPA-type mechanisms, which ensure the sensitivity of point defect absorption to the loop orientation and thus affect the growth of differently oriented loops.

For the analytical description of dislocation loop kinetics at the early stages of irradiation creep it is necessary to modify the point defect balance equations (2.15), so as to include the growth of dislocation loops. Since the majority of loops nucleate at very short times, one can assume that the loop number density N_L instantly saturates at a constant value and the distribution of loops over sizes is sufficiently narrow in order to assign all loops of the same orientation m approximately the same size R^m. Then the rate of growth for dislocation loops can be written down as

$$V^m \equiv \frac{dR^m}{dt} = b^{-1}\left(\eta_i^m D_i C_i - \eta_v^m D_v (C_v - C_{v0})\right), \tag{2.67}$$

where $\eta^m{}_\alpha$ is the dislocation loop bias factor for point defects of type α at the loops with orientation m. The balance equations can be rewritten as

$$G - k_\alpha^2 D_\alpha (C_\alpha - C_{\alpha 0}) - \sigma_R (D_i + D_v) C_i C_v = 0, \tag{2.68}$$

where $k_\alpha{}^2 = \langle Z_\alpha \rangle \rho + 2\pi N_L \langle \eta_\alpha R \rangle$ is the total sink strength for point defects that takes into account both network dislocations and dislocation loops. Since here we are not interested in the contribution of loops to thermal creep, the dependence of thermal vacancy concentration on the loop size and orientation is neglected.

Combining these equations, the following expression for the dislocation loop growth rate can be obtained [393]:

$$V^m(R) = \frac{G\Phi(G/G_R)}{b k_i^2 k_v^2}\left(A^m \rho + B^m \rho_L\right), \tag{2.69}$$

where $A^m = \eta_i^m \langle Z_v \rangle - \eta_v^m \langle Z_i \rangle$; $B^m = (\eta_i^m \langle R\ \eta_v \rangle - \eta_v^m \langle R\ \eta_i \rangle)/\langle R \rangle$; $G_R = k_i^2\ k_v^2 D_v / 4\sigma_R$; $\rho_L = 2\pi N_L \langle R \rangle$ is the total dislocation density in loops and function Φ is the same as in equation (2.19).

Looking at eq. (2.69) it is easy to notice the loop kinetics is defined by the competition of two processes:

(i) diffusional interaction of loops with network dislocations, specified by the parameter A^m. Usually $A^m > 0$ because dislocation loops interact with interstitials more efficiently than network dislocations [111,394]. The preferential interstitial absorption of loops with respect to network dislocations contributes to the growth of all loops, independently of their orientation

(ii) diffusional interaction between loops of different orientations, specified by the parameter B^m. the value of B^m is depends only on the loop bias factors and is the measure of diffusional interaction between the loops. When the external load is absent, η_α are independent of loop orientation and $B^m = 0$. Under the effect of external stress, the loop bias factors become sensitive to the loop orientations and B^m becomes non zero. As a result, there occurs a redistribution of point defects between "favourably" (at $B^m > 0$) and "unfavourably" ($B^m < 0$) oriented loops with respect to the loading direction.

At the early stages of irradiation, when ρ_L is low, the first mechanism dominates and all loops grow due to their preferential absorption of interstitials with respect to network dislocations. For example, when network dislocations are perfect sinks for point defects and the temperature is sufficiently high to neglect the recombination of point defects, the dependence of the average loop radius R^m on the irradiation dose φ is given by relation [393]

$$R^m \approx R_c \left[(1+\varphi/\varphi_c)^{1/3} - 1 \right], \qquad (2.70)$$

where $R_c \approx 0.1$, $\rho/N_L \approx$ 1-10 nm and $\varphi_c \approx 10^2$- $10^3 \rho^2 a/N_L \approx 10^{-5}$- 10^{-1} dpa at $\rho \approx 10^8$ -10^{10} cm^{-2}, $N_L \approx 10^{15}$ cm^{-3} and $a \approx 0.2$ nm. In other words, at small irradiation doses the growth of loops proceeds linearly with time, whereas at higher dose the growth rate slows down and at rather large doses $R^m \propto \varphi^{1/3}$. Such qualitative behaviour of the loop sizes is quite typical for the experimental observations of loop kinetics in irradiated materials [150,395,396].

As loops become larger, the redistribution of point defects between loops becomes important. Accordingly, the unfavourably oriented loops tend to grow more slowly than those oriented favourably. This effect was also demonstrated experimentally [383,384], as well as in numerical calculations using cluster dynamics methods [397] (see Fig. 3.6).

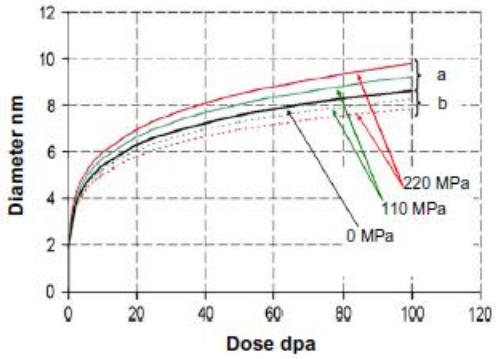

Fig. 3.6. Calculated dependencies of loop radius variation under the effect of uniaxial stresses of 0, 110 and 220 MPa. Solid curves are for favourably oriented loops, dashed curves for unfavourably oriented loops. At zero stress the curves are superposed. (From [397])

Moreover, as shown in [393], when the external tension exceeds some critical value $\sigma*$, the defect redistribution between loops of different orientations can be so strong that at some dose the growth rate of unfavourably oriented loops becomes negative even before these loops build into the dislocation network. At larger doses of irradiation these loops can dissolve completely, creating strongly anisotropic dislocation distribution over orientations. The characteristic doses of loop dissolution are of the order of $\varphi_R \approx 10^{-9}\rho\sigma^3/N_L\mu^3$, while the maximum size of unfavourably oriented loops is $R_{max} \sim 2\times10^{-3}\ \rho\mu/N_L\sigma$. The shrinkage of unfavourably oriented loops is possible, where $R_{max} < (\pi\rho)^{1/2}$, or, equivalently

$$10\frac{N_L}{\rho^{3/2}}\frac{\sigma}{\mu} \sim 1. \qquad (2.71)$$

This relation gives immediately the estimate of $\sim 5\times10^{-3}\mu$ for the minimum stress required for the observation of loop dissolution [393]. At $\rho \approx 10^8$ cm^{-2}, $\sigma/\mu \approx 5\times10^{-3}$ and $G = 10^{-3}$ dpa/s the characteristic time of loop redistribution is of the order of 10^4-10^5 s, that is, this effect can be demonstrated in annealed materials under irradiation in HVEM.

The dissolution of dislocation loops was experimentally observed in annealed nickel samples, irradiated in electron microscope [396]. The rate of damage creation in that experiment reached 2×10^{-3} dpa/s and the loads reached 50 MPa (corresponding to $\sigma/\mu \approx 6\times10^{-3}$). Though the volume density of loops was not reported, a rough estimate based on electron micrographs presented in [396] gives $N_L \approx 10^{15}$ cm^{-3}. In other words, the set of experimental parameters satisfied relation (2.71). The kinetics of growth of several separate loops is shown in Fig. 3.7.

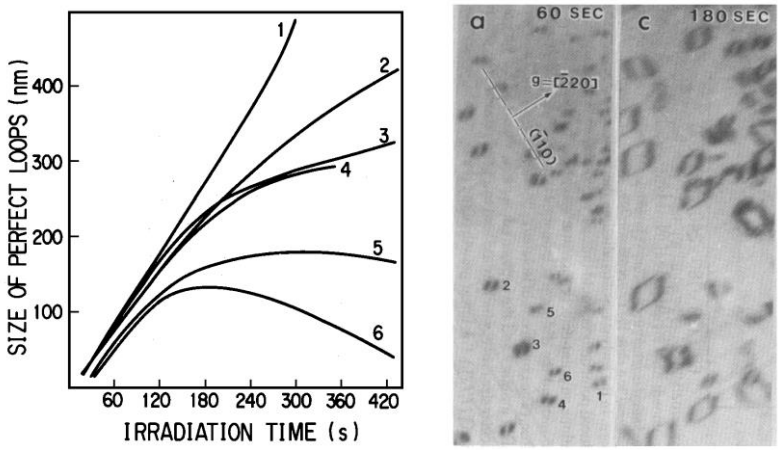

Fig. 3.7. The dependence of individual loop sizes in electron irradiated Ni on irradiation time. Numbers at the curves indicate the loops shown in TEM micrographs (From [396]).

3.3.2 Irradiation creep rate

The first stage of loop kinetics, when loops grow mainly due to their diffusional interaction with dislocations, corresponds to the transient creep [393]. The character of dose dependence of irradiation creep is highly sensitive at this stage to the mechanisms, leading to point defect absorption bias for loops and dislocations, and to the possible orientational anisotropy of loop nucleation. Fig. 3.8 shows some trends that are predicted by the theoretical investigation of irradiation creep at the transient stage.

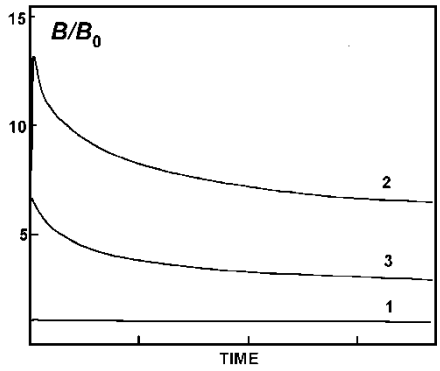

Fig. 3.8. The qualitative behaviour of irradiation creep modulus (normalized per steady-state value) as a function of time t at the transient stage, as predicted by different models. (1) no preferential nucleation of aligned dislocation loops; (2) preferential nucleation of aligned dislocation loops; (3) accounting for dislocation core effects on point defect absorption (from [393]).

When the mechanisms leading to absorption bias are identical for loops and dislocations and the orientational dependence of loop nucleation is neglected, than the creep rate is weakly sensitive to dose. Physically this is evident, because in this case there is no difference between loops and dislocations with respect to their ability to capture point defects (i.e. $\eta_\alpha \approx Z_\alpha$), while the variations of relative densities f^m of dislocation loops and dislocations at the initial stage of loop growth is insignificant (even though the absolute values of dislocation densities, ρ and ρ_L, can vary rather strongly).

In fact, in many papers dealing with irradiation creep the dislocations and loops are not even considered as alternative point defect sinks. The basic drawback of such models is the lack of any intrinsic reason why dislocation loops would grow. To overcome this problem, the presence of other sinks is postulated. Usually voids are considered to play the role of alternative sinks, but this does not seem reasonable, because dislocation loops and voids are microstructural components, characteristic for different stages of creep. In order to be successful in the explanation of the

transient creep, the models should take into account (one way or another) some essential differences between network dislocations and dislocation loops.

For example, a strong dose dependence of irradiation creep at the transient stage is predicted when the loop nucleation dependence on stress orientation is taken into account (see curve 2 in Fig 3.8). At sufficiently high temperature, when the recombination of point defects is negligible, the rate of irradiation creep during some time of irradiation (~$0.1\Phi_c$) grows practically linearly with dose, and then gradually decreases. It is interesting to compare this analytical prediction to results of Ref. [257], where the creep of annealed Al was investigated at 40-150^{o}C during irradiation with 2 MeV electron beam (defect production rate $G \sim 10^{-9}$ dpa/s). The authors of [26] unequivocally assign the observed irradiation creep to the processes of interstitial loop growth (with loop density $N_L \sim 10^{15}$ cm^{-3}) and to the climb of dislocations. It is easy to check that the experimental conditions allow point defect recombination to be neglected. Accordingly, the general behaviour of the dose dependence of irradiation creep rate, observed in this paper (see Fig. 2.1(b)), resembles very much that in Fig. 3.8. The measured time of the creep rate increase also correlates well with the theoretical estimate, which for the specified values of G and N_L and for dislocation density of 10^8 cm^{-2} (as typical for annealed metals) constitutes ~10^4 s.

The irradiation creep rate noticeably falls with increasing dose also where the mechanisms of point defect absorption bias differ for loops and dislocations. In particular, curve 3 in Fig. 3.8 shows the behavior of irradiation creep rate when the bias of loops is due to point defect elastic modulus anisotropy effects, while the bias of dislocations is sensitive to the limitation in the point defect capture by dislocation core. In the latter case the asymmetry of loop nucleation changes only the magnitude, but not the general behavior of irradiation creep rate. In any case, **the effect of orientational dependence of loop nucleation is manifested only at the transient stage of irradiation creep**.

3.4 Accelerated creep and the interrelation between irradiation creep and swelling

The evolution of the dislocation system is often accompanied by the evolution of other defects (voids, bubbles, secondary phases) in irradiated materials and this evolution can cuase the deformation of the material, resulting in volume change. Sometimes this deformation is completely elastic. A typical example involves the volume changes accompanying irradiation-induced phase precipitation in alloys [85,247, 398-400]. Such volume changes are not related to dislocation motion and are not taken into account here. One should, however, be aware of such possibility when

comparing the theoretical predictions with experimental results, in order to avoid data misinterpretation [204].

However, **defect microstructure kinetics can also directly affect the dislocation climb rate. This happens, in particular, at the third stage of irradiation creep, which involves void and gas bubble growth.** Let us discuss, how the development of void ensembles at large irradiation doses affects the rate of material deformation. Similar to the case of steady state creep, we start with the effect of voids on the dislocation climb and after that consider climb-controlled dislocation glide.

3.4.1 The effect of swelling on SIPA-type creep mechanisms

3.4.1.1 Separation of the total strain rate into contributions from creep and swelling

Let us restrict ourselves to a simple model, where only dislocations and voids constitute the defect microstructure of a material. Like before, we assume that there are K different dislocation orientations and the corresponding partial dislocation densities ρ^k ($1 \leq k \leq K$) are maintained at a constant level. All voids are assumed to have the same radius R_c, and the volume density of voids N_c is assumed to reach a saturation value. The latter is not too strong an approximation, because the void density saturation occurs relatively quickly after the swelling onset.

The climb velocity of a dislocation of the k-th orientation is given by equation (2.14), while the rate of void growth is described by common relations

$$\frac{dR_c}{dt} = \frac{1}{R_c}\left[D_v(C_v - C_{v0}) - D_i C_i\right]. \qquad (2.72)$$

The average point defect concentrations, C_α, are given by the balance equations

$$G - k_\alpha^2 D_\alpha (C_\alpha - C_{\alpha 0}) = 0, \qquad (2.73)$$

where $k_\alpha^2 = \langle \underline{Z}_\alpha \rangle \rho + 4\pi N_c R_c$ is the sink strength for the α-type point defects. In writing down (2.73) we neglected point defect recombination, since it is of secondary importance in the temperature range where swelling arises. Also, the dependence of thermal emission of vacancies from sinks on sink parameters is neglected, since it gives no contribution to SIPA irradiation creep.

The total strain rate of the material due to dislocation climb, $\dot{\varepsilon}_{ij}$ (i,j = 1,2,3), is determined by the first term in the r.h.s. of equation (2.11), while the rate of volume change (the swelling rate) $\dot{S}$ is equal to

$$\dot{S} = Tr\dot{\varepsilon}_{ij} = \rho b\langle V\rangle, \tag{2.74}$$

where <*V*> is the average dislocation climb rate.

Equation (2.74) deserves a short comment, which is important for the discussion below. It is very often assumed that the swelling of material is caused by vacancy agglomeration into voids. However, from the microscopic point of view, neither vacancies, nor voids *per se* lead to the swelling of material. The real reason for the volume increase comes from the fact that dislocations capture interstitials more efficiently than vacancies, while the excess vacancies are consumed by void. As a result, the average dislocation climb rate is non-zero and contributes to the swelling according to (2.74). The total volume increase is, of course, equal to the total amount of vacancies in the material, the absolute majority of which at the steady-state swelling stage is collected in voids.

Equation (2.11) gives **the total strain rate of the irradiated material,** which **is usually the only measurable quantity and comprises the contributions from both swelling,** $\dot{\varepsilon}_{ij}^{S}$ **, and irradiation creep itself,** $\dot{\varepsilon}_{ij}^{I}$ **. Though such separation of volume conserving (creep) and non-conserving (swelling) strains is a common practice** (see the discussion of swelling and creep correlation in-sect. 2.1.3), **one should be aware that it is largely arbitrary**. Following this convention, the irradiation creep term is usually written as

$$\dot{\varepsilon}_{ij}^{I} = \rho b(\left\langle \hat{b}_i \hat{b}_j V_c \right\rangle - \frac{1}{3}\delta_{ij}\langle V_c\rangle). \tag{2.75}$$

where δ_{ij} is Kronecker's delta. Writing this relation, one implicitly assumes that swelling is completely isotropic. This assumption seems quite evident, supported by a long-term tradition to associate swelling with the growth of voids, which are spherical. Nonetheless, it is not the best choice even when the dislocation structure is isotropic [103]. When it is anisotropic, additional complications arise, because the swelling-induced strains can become anisotropic as well.

Indeed, let us assume that no external stress is acting on the material. Then all dislocations climb at the same rate V_c = <*V*> irrespective to their orientation and thus the equation for the total strain rate (which coincides now with the rate of macroscopic strain variation due to swelling $\dot{\varepsilon}_{ij}^{S}$) can be re-written as

$$\dot{\varepsilon}_{ij}^{S} = \rho b\left\langle \hat{b}_i \hat{b}_j \right\rangle V_c, \tag{2.76}$$

Note that, when the dislocation structure is isotropic, this equation is reduced to the familiar relation $\dot{\varepsilon}_{ij}^{S} = \delta_{ij}\dot{S}/3$. However, if for some reason the dislocation structure is anisotropic, the swelling can be responsible not only for volume changes, but for a shape change as well.

When an external load is applied, it still seems reasonable to retain (2.76) as a definition of the swelling-induced strain rate. Then the irradiation creep rate can be written as [103]

$$\dot{\varepsilon}_{ij}^{I} = \rho b(\left\langle \hat{b}_i \hat{b}_j V_c \right\rangle - \left\langle \hat{b}_i \hat{b}_j \right\rangle \langle V_c \rangle). \tag{2.77}$$

As will be shown below, **different definitions of the "pure" creep strains can result in quite different conclusions concerning the irradiation creep behaviour at the late stages of irradiation**.

3.4.1.2. Irradiation creep rate

Substituting the values of point defect concentrations, as defined by equation (2.73), into (2.72) and (2.11), one easily obtains the relation between irradiation creep rate and swelling rate in the form of equation (2.3):

$$\dot{\varepsilon}_{kl}^{I} = P_{kl} \frac{\langle Z_i \rangle \langle Z_v \rangle \rho^2}{k_i^2 k_v^2} G + Q_{kl}\dot{S}, \tag{2.78}$$

where the swelling rate is defined by a common relation

$$\dot{S} = \langle Z_i - Z_v \rangle \frac{4\pi N_c R_c \rho}{k_i^2 k_v^2} G, \tag{2.79}$$

and the structure factors P_{kl} and Q_{kl} are

$$P_{kl} = \left\langle \hat{b}_k \hat{b}_l \left(\frac{Z_i}{\langle Z_i \rangle} - \frac{Z_v}{\langle Z_v \rangle} \right) \right\rangle \tag{2.80}$$

and

$$Q_{kl} = . \left\langle \frac{Z_i - Z_v}{\langle Z_i - Z_v \rangle} \hat{b}_k \hat{b}_l \right\rangle - \left\langle \hat{b}_k \hat{b}_l \right\rangle \tag{2.81}$$

If no external stress is applied to the material, then $Z_\alpha^{\,k} = Z_\alpha^{\,0}$ and, since the stress-free bias factors $Z_\alpha^{\,0}$ are independent of the dislocation orientations, both structural factors vanish and no irradiation creep occurs.

Suppose now that the material is under the action of an external uniaxial stress σ (the discussion of the general loading case can be found in [103]). When these stresses are lower than the characteristic stress value σ^* (equal either to the material shear modulus μ [315], or to k_BT/ω [322,326]), the bias factors can be expanded to the first order in stresses, see eq. (2.33). Substituting this expansion into (2.80) and (2.81), and taking into account that the stress-free dislocation bias for interstitial absorption $\Delta Z = (Z_i^0 - Z_v^0)/(Z_i^0 + Z_v^0) \ll 1$, one obtains for the creep rate component along the loading axis :

$$\dot{\varepsilon}^I = BG\frac{\sigma}{\mu}, \tag{2.82}$$

with the creep compliance B being equal to

$$B = B_0\left(\frac{1}{(1+r_c)^2} + \frac{1}{2\Delta Z}\frac{dS_0}{d\phi}\right), \tag{2.83}$$

where $\phi = Gt$ is the irradiation dose, $\dot{S}_0$ is the stress-free swelling rate,

$$\dot{S}_0 = \frac{2\Delta Z G r_c}{(1+r_c)^2}, \tag{2.84}$$

$r_c = R_c/R^*$ is the normalized void radius, $R^* = 4\pi N_c/\bar{Z}\rho$, $\bar{Z} = (Z_i^0 + Z_v^0)/2$ and B_0 is the value of creep compliance in the absence of swelling, which depends on the selected mechanism of stress-induced dislocation bias anisotropy and, in some cases, on the lattice crystallography. For example, in a completely isotropic material we can use equation (2.23) to get

$$B_0 = \frac{2(2-\nu)}{30\pi}\left(\frac{Z_i^0 p_i^\mu}{e_i} - \frac{Z_v^0 p_v^\mu}{e_v}\right), \tag{2.85}$$

which gives $B_0 \approx 0.05$ for typical parameter values defined in section 3.2.1.2.1.

On the other hand, when the effect of point defect polarization in saddle-points of diffusion jumps (see sect. 3.2.1.2.2) is considered, the crystalline lattice of the metal is cubic and the material is polycrystalline, one can use the bias factor expansion over stresses in the form of equation (2.26) and use the averaging over all possible grain orientations, thus getting

$$B_0 = \frac{(1+\nu)\mu\omega}{45(1-2\nu)k_BT}\left[e_i^s\left(d_i^{(2)} + \frac{2}{3}d_i^{(3)}\right) - e_v^s\left(d_v^{(2)} + \frac{2}{3}d_v^{(3)}\right)\right]. \tag{2.86}$$

Equation (2.83) reveals the advantages of irradiation creep rate definition according to (2.77). First of all, the creep rate thus defined is related to the stress-free swelling rate, which can be measured

much more easily than the swelling rate of a stressed material. Moreover, if the dislocation anisotropy during swelling is maintained only by SIPA-induced point defect partitioning between differently oriented dislocations (or dislocation loops) as suggested in [401,402], the degree of dislocation anisotropy is proportional to external stress. Consequently, the anisotropy of dislocation structure can in this case be neglected.

The dependence of B on the normalized void radius r_c can be converted to the dose dependence with the help of the relation following from (2.72) and (2.73):

$$r_c^2 + \frac{4}{3} r_c^3 + \frac{1}{2} r_c^4 = 4\Delta Z(\phi - \phi_{in}), \tag{2.87}$$

where $\phi = \varphi/\Phi_c$ is the normalized dose, ϕ_{in} is the incubation dose for void nucleation and

$$\Phi_c = \frac{(\bar{Z}\rho)^3}{64\pi^2 \Delta Z N_c^2}. \tag{2.88}$$

At the typical values of $\rho \approx 3\times10^{10}$ cm^{-2} and $N_c \approx 10^{15}$ cm^{-3} one gets $\Phi_c \approx 5$ dpa. The predicted dependencies of the creep compliance and total material strain on irradiation dose are shown in Fig. 3.9. It is seen that **the SIPA-based mechanisms predict the reduction of irradiation creep due to swelling, which correlates to experimental observations of creep cessation at high irradiation doses** [178,251,252,403].

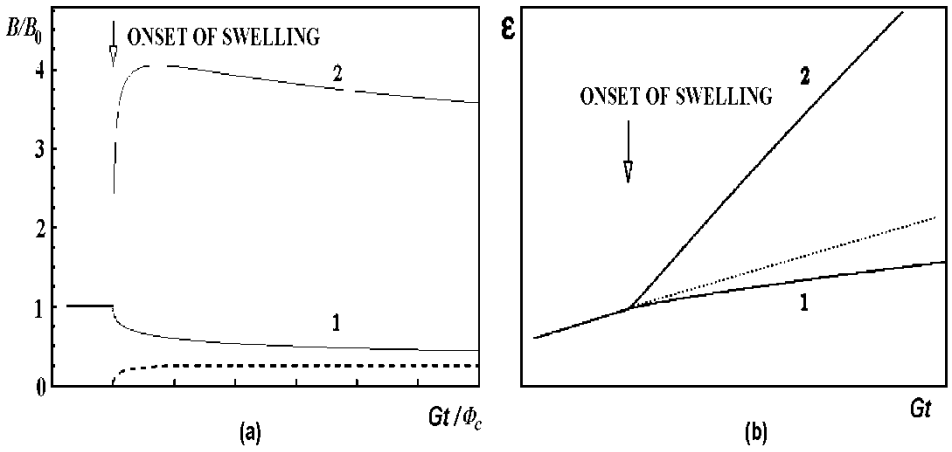

Fig. 3.9. Dose dependence of the normalized creep compliance B/B_0 (a) and the total strain (b) with (curve 1) and without (curve 2) account of the swelling rate enhancement by stress. The dashed line in (a) is the stress-free swelling rate, the dotted line in (b) - the swelling-free trend. (From [103]).

3.4.1.3. Alternative definition of the irradiation creep rate

Let us consider what happens to the creep rate **when the 'usual' definition (2.75) for creep strain rate is applied**. Let us notice, first of all, that after simple transformations equation (2.83) can be reduced to the form, commonly used in experimental studies of irradiation creep - swelling coupling, i.e.

$$B = B_0 + D^c \frac{dS_0}{d\phi}, \tag{2.89}$$

where the creep-swelling coupling factor D^c is

$$D^c = -\frac{B_0}{2\Delta Z}(1 + r_c). \tag{2.90}$$

Note that the absolute value of the coupling factor thus defined does not exceed ~100, while the factor itself is negative. However, when the creep rate is defined using equation (2.75), the creep compliance looks like

$$B = B_0 + D^c \frac{dS_0}{d\phi} + \frac{\mu}{\sigma}\left(\left\langle \hat{b}_1^2 \right\rangle \frac{dS}{d\phi} - \frac{1}{3}\frac{dS_0}{d\phi} \right), \tag{2.91}$$

where $dS/d\phi$ is the actual (i.e. stress-affected) swelling rate. As compared to (2.89), equation (2.91) contains an additional contribution, which can differ from zero for at least two reasons, as described below.

First of all, the swelling rate in the loaded material can differ from the stress-free one. At comparatively low stresses (<100 MPa) the swelling is known to depend on stress as (cf. sect . 2.1.3):

$$S = S_0(1 + D^s \frac{\sigma}{\mu}), \tag{2.92}$$

where D^S is a material constant. There can be several reasons for such effect, including the effect of stress on void number density and on the void growth. Indeed, external loading modifies dislocation biases and the equilibrium vacancy concentration in the bulk, affecting the swelling rate. For example, stress modification of dislocation biases due to the elastodiffusion mechanism leads to [103]:

$$D^s \approx \frac{e_i^s - e_v^s}{6\pi\Delta Z}\frac{\omega}{k_B T}. \tag{2.93}$$

If D^S is time-independent and the dislocation structure is isotropic ($\left\langle \hat{b}_1^2 \right\rangle = 1/3$), equation (2.91) has the form

$$B = B_0 + \left(D^c + \frac{D^s}{3} \right) \frac{dS_0}{d\phi}, \tag{2.94}$$

Equations (2.89) and (2.94) have the same functional form, but now the creep-swelling coupling factor includes a correction $D^S/3$, which can be of the same order of magnitude as the experimentally observed values of ~10^4. Fig. 3.8 shows that **equation (2.94) predicts both the increase of creep compliance and the growth of the total strain with the irradiation dose after the onset of swelling**.

Another reason of **creep acceleration by swelling**, as predicted by eq. (2.91), can be related to anisotropy of dislocation structure, which, according to both experimental observations [170,250,384,404] and theoretical predictions [383,393,405,406], can result from SIPA-induced preferential growth of interstitial loops. A detailed investigation of the anisotropic dislocation structure kinetics and its contribution to creep-swelling coupling was undertaken in [401,402]. Strictly speaking, some of the assumptions used in these papers do not quite fit the experimental picture. For example, the enhanced growth of favourably oriented dislocation loops in the presence of voids is hardly probable, even assuming the continuous interstitial loop nucleation (e.g. in irradiation produced collision cascades [407,408]). Nonetheless, if for some reason the SIPA-induced anisotropy of dislocation orientations arises at the steady-state swelling stage, additional contribution to irradiation creep modulus can be expected.

Indeed, let us assume that the relative density of dislocations with the Burgers vector along the loading direction has the value Δf in excess of the otherwise isotropic dislocation density. Then, even when the swelling rate is not influenced by stress, eq. (2.91) provides an additional contribution to the creep modulus,

$$\Delta B^g = \frac{2\Delta f}{3\sigma} \frac{dS}{d\varphi}. \tag{2.95}$$

The dislocation anisotropy factor Δf can reach values up to 0.8-0.9 [404] and at the usual stresses of the order of 100 MPa the contribution to the creep-swelling coupling factor is again of the same order of magnitude, as its experimentally observed value. Since the dislocation anisotropy is the direct result of dislocation structure evolution under the action of stresses, the contribution (2.95) cannot be eliminated by the swelling measurements on unloaded samples. Moreover, if only one component of strain tensor is measured, one cannot even check whether this systematic error is

present or not.

Summing up, **the way of total strain separation into contributions from the irradiation creep and swelling can crucially influence the correlation between these phenomena. When the irradiation creep rate is defined as the difference between the total strain rate and the stress-modified swelling, the swelling results in decreasing of SIPA irradiation creep rate with the irradiation dose. On the contrary, when the stress-free value of swelling is subtracted from the total strain rate, the predicted correlation between creep and swelling is rather well described by equation (2.91) with the creep-swelling coupling factor of the same order as observed experimentally.**

3.4.2 The effect of voids on the "climb-controlled glide" mechanisms of irradiation creep

As shown above, in the absence of voids the dominant mode of dislocation motion at the steady-state creep stage is climb. Only at stresses close to the irradiation modified yield stress of the material can the contribution from climb-controlled glide play a noticeable role. The situation becomes more complicated, however, when voids appear in the material.

On the one hand, the accumulation of vacancies in voids is accompanied by large currents of uncompensated interstitials to all dislocations, so that the relative role of stress-induced misbalance on interstitial redistribution between differently oriented dislocations becomes less pronounced and the decrease of SIPA-type contributions to irradiation creep is expected [103,406,409]. However, the absolute values of dislocation climb velocities increase, promoting climb-controlled glide. Correspondingly, it is a long-lasting tradition to ascribe irradiation creep acceleration by swelling to the action of CCG creep mechanism [233,234,238,359,410].

Indeed, when the point defect concentrations are defined by eq. (2.73), the absolute value of dislocation climb rate is expressed in terms of the swelling rate dS/dt simply as

$$V_c = \frac{1}{b\rho}\frac{dS}{dt}, \tag{2.96}$$

where we neglected the dislocation bias dependence on dislocation orientation, which is responsible for SIPA creep. Correspondingly, the irradiation creep due to CCG mechanism is

$$\dot{\varepsilon}^I_{kl} = \frac{1}{2}\left\langle (\hat{b}_k n_l + n_l \hat{b}_k)\frac{L_g}{h}\right\rangle \frac{dS}{dt}, \tag{2.97}$$

In contrast to dislocation climb, in the case of the climb-controlled glide it is not necessary to subtract contributions from swelling from the creep strain rate, since dislocation glide is, by definition, volume conservative.

The most striking feature of this relation is that the stress dependence of the creep rate is completely determined by the glide factor. Very often [233,234,238,359,410] a linear stress dependence of the glide factor is postulated and the resulting swelling contribution is reduced to the standard form. However, as discussed in sect. 3.2.2.1.4, quite different stress dependencies of the glide factor can be expected. In particular, glide stopping by impurity atoms involves no stress dependence of the glide factor at all, so that a complete independence of the CCG creep rate on stress can be expected.

On the other hand, the increase of the dislocation mobility is not the only effect of voids on CCG and is counterbalanced by the void blocking of dislocation glide. Indeed, **the efficiency of dislocation pinning by voids increases with the increase of the average void size and at a certain swelling level the voids become the principal obstacle set for gliding dislocations**. In this situation dislocation segments terminate on voids [251,253] and cannot be detached by glide because the voids are very strong obstacles to dislocation motion. The climb of pinned dislocation segments is also largely reduced due to pipe diffusion of point defects to voids along dislocations and the unpinning of dislocation from voids is expected to be practically suppressed when the swelling reaches ~ 30% [411]. Therefore, **the acceleration of irradiation creep thanks to climb-controlled dislocation glide is no more than transient and should be eventually suppressed as the swelling proceeds. It is no wonder, therefore, that the irradiation creep cessation at high swelling levels is observed.**

Conclusions

The safe operation of nuclear reactors requires dimensional stability of their structural and functional materials operating in heavy radiation environment. The radiation resistance of these materials is limited by such physical phenomena as radiation swelling, irradiation creep, radiation embrittlement, etc. All these phenomena are caused by the production of primary radiation damage by external irradiation with fast particles, which in turn promotes the transformation of material microstructure, including nucleation and growth of defect clusters in the form of voids, gas bubbles and dislocation loops.

This review addresses one of the important mechanical effects intensified by irradiation, namely irradation creep. It summarizes the main observed trends of irradiation creep reported in the literature and suggests the ways of their rationalization based on the available theoretical models. In particular, the influence of experimental conditions on parametric dependencies of irradiation creep are discussed and correlated to the underlying microstructual evolution. The analysis of experimental data accumulated by now allows confident correlation of the dislocation structure evolution in irradiated materials with various stages of irradiation creep, thus providing a reliable basis for analytical description of this complicated phenomenon.

The existing theoretical models of irradiation creep are reviewed and their ability to reproduce the dose, stress and temperature dependencies of irradiation creep are critically assessed. It is demonstrated that theoretical models are able to give reasonable description of irradiation creep in a broad range of irradiation doses, external stresses and test temperatures, both qualitatively and often even quantitatively.

The knowledge of the main features of irradiation creep and the microscopic reasons responsible for that or other mode of material response to the combined effect of irradiation and loading is useful not only for the qualitative predictions of irradiated material performance in nuclear facilities, but for the justified interpolation of simulation experiment results to in-reactor operational conditions.

References

1 . R.V.Hesketh, in: Irradiation Embrittlement and Creep in Fuel Cladding and Core Components (BNES, London, 1972) p.221.
2 . F.A.Nichols, J.Nucl.Mater., 69-70, 451 (1978).
3 . G.L.McVay, R.E.Einziger, G.L.Hofman, L.C.Walters, J.Nucl.Mater., 78, 201 (1978).
4 . D.Mosedale, J.Appl.Phys., 33, 3142 (1962).
5 . J.H.Gittus, in: Irradaition Effects in Crystalline Solids, ch.7 (Applied Science, London, 1978).
6 . J.J.Holmes, J.A.Williams, D.H.Nyman, J.C.Tobin, in: Flow and Fracture of Metals and Allows in Nuclear Environments. ASTM STP 380 (ASTM, Phil., 1964) p.385.
7 . V.Fidleris, C.D.Williams, Electrochem.Techn., 4, 258 (1966).
8 . R.V.Hesketh, in: Fragilite et effets de l'irradiation, 10 Colloque de metallurgie, Saclay, 1966, p.185.
9 . E.E.Bloom, J.R.Weir, Trans.ANS, 10, 131 (1967).
10 . G.W.Lewthwaite, D.Mosedale, I.R.Ward, Nature, 216, n.5114, 472 (1967).
11 . K. Fukumoto, S.Takahashi, R.J.Kurtz, D.L.Smith, H. Matsui, J.Nucl.Mater. 341, 83 (2005)
12 . K. Fukumoto, M.Narui, H.Matsui, T.Nagasaka, T.Muroga, M.Li, D.T.Hoelzer, S.J.Zinkle, J.Nucl.Mater. 386-388, 575 (2009)
13 . M.Li, D.T.Hoelzer, M.L.Grossbeck, A.F.Rowcliffe, S.J.Zinkle, R.J.Kurtz, J.Nucl.Mater. 386-388, 618 (2009)
14 . J.Chen, P.Jung, M.Nazmy, W.Hoffelner, J.Nucl.Mater. 346, 120 (2006)
15 . K.Tai, R.S.Averback, P.Bellon, Y.Ashkenazy, Scr.Mater. 65, 163 (2011)
16 . K.Tai, R.S.Averback, P.Bellon, Y.Ashkenazy, B.Stumphy, J.Nucl.Mater. 422, 8 (2012)
17 . L.N.Bystrov, L.I.Ivanov, O.V.Martyshin, Rad.Effects, 24, 111 (1975).
18 . L.I.Ivanov, V.M.Lazorenko, O.V.Martishin, Fiz.Khim.Obrab.Metal., n.3, 3 (1978).
19 . L.I.Ivanov, A.Orlova, V.M.Lazorenko, O.V.Martishin, Czech.J.Phys., B29, 1260 (1979).
20 . E.S.Aitkhozhin, Sh.Sh.Ibragimov, S.K.Kusainov, Yu.S.Pyatiletov, E.V.Chumakov, Izv. AN KazSSR, Ser.: Physics&Mathematics, n.4, 70 (1981).
21 . V.R.Regel, V.A.Alpert, D.Szenes, Yu.A.Fadin, Zh.Tech.Fiz, 51, 134 (1981).
22 . E.S.Aitkhozhin, Sh.Sh.Ibragimov, S.K.Kusainov, Yu.S.Pyatiletov, E.V.Chumakov, Izv. AN KazSSR, Ser.: Physics&Mathematics, n.4, 55 (1983).
23 . E.S.Aitkhozhin, Sh.Sh.Ibragimov, S.K.Kusainov, Yu.S.Pyatiletov, E.V.Chumakov, Voprosy Atomnoi Nauki Techniki, Ser: Physics of Radiation Damage and Radiation Materials Science, n.4(32), 71 (1984).
24 . L.N.Bystrov, M.E.Reznitskyi, Fiz.Khim.Obrab.Metal., n.6, 15 (1985).
25 . E.S.Aitkhozhin, S.P.Vagin, Sh.Sh.Ibragimov, S.K.Kusainov, V.F.Reutov, Izv. AN KazSSR, Ser.: Physics&Mathematics, n.2, 13 (1987).
26 . Yu.M.Platov, S.V.Simakov, A.B.Tsepelev, Fiz.Khim.Obrab.Metal., n.1, 11 (1989).
27 . R.V.Hesketh, in: Proc.Int.Conf. on Solid State Physics Research with Accelerators, BNL 50083(C-52), 1967, p.389.
28 . Sh.Sh.Ibragimov, E.S.Aitkhozhin, E.V.Chumakov, Izv. AN KazSSR, Ser.: Physics&Mathematics, n.2, 25 (1986).
29 . Sh.Sh.Ibragimov, E.S.Aitkhozhin, E.V.Chumakov, Izv. AN KazSSR, Ser.: Physics&Mathematics, n.4, 3 (1986).
30 . Sh.Sh.Ibragimov, E.S.Aitkhozhin, E.V.Chumakov, Izv. AN KazSSR, Ser.: Physics&Mathematics, n.4, 5 (1986).
31 . P.Jung, M.I.Ansari, J.Nucl.Mater., 138, 1, 40 (1986).

32 . P.Jung, J.Nucl.Mater., 200, 138 (1993).
33 . E.S.Aitkhozhin, E.V.Chumakov, J.Nucl.Mater. 233-237, 537 (1996).
34 . R.V.Hesketh, Phil.Mag., 8, 1321 (1963).
35 . D.Mosedale, G.W.Lewthwaite, G.D.Leet, W.Sloss, Nature, 224, n.5226, 1301 (1969).
36 . J.L.Pouchou, L.Zuppiroli, J.Ardonceau, J.Leteurtre, Rad. Effects, 29, 225 (1976).
37 . L.Zuppiroli, J.L.Pouchou, A.Francois, J.Leteurtre, Y.Quere, Phil.Mag., 35, 853 (1977).
38 . D.Mosedale,G.W.Lewthwaite, I.Ramsey, in: Irradiation Embrittlement and Creep in Fuel Cladding and Core Components (BNES, London, 1972) p.233.
39 . D.Mosedale, G.W.Lewthwaite, I.Ramsey, in: Physical Metallurgy of Reactor Fuel Elements, Proc.Int.Conf. CEGB-BNL (The Metals Society, Glouchestershire, 1973) p.132.
40 . D.Mosedale, G.W.Lewthwaite, in: Creep Strength in Steel and High-temperature Alloys, Proc. of a meeting, Univ. of Sheffild, 20-22 Sept. 1972. The Metals Soc., 1974, p.169.
41 . J.A.Hudson, R.J.McElroy, R.S.Nelson, in: Application of Ion Beams to Materials. Inst. of Phys. Conf. Ser. N 28, London, 1975, p. 251.
42 . P.L.Hendrick, D.J.M.Michel, A.G.Pieper, R.E.Surrat, A.L.Bement, J.Nucl.Mater., 59, 229 (1976).
43 . P.L.Hendrick, A.G.Pieper, D.J.M.Michel, R.E.Surrat, A.L.Bement, in: Radiation Effects and Tritium Technology for Fusion Reactors, vol.2. CONF-750989, 1976, p.84.
44 . R.J.McElroy, J.A.Hudson, R.S.Nelson, in: Radiation Effects and Tritium Technology for Fusion Reactors, vol.2. CONF-750989, 1976, p.72.
45 . J.A.Hudson, R.S.Nelson, R.J.McElroy, J.Nucl.Mater., 65, 279 (1977).
46 . R.J.McElroy, J.A.Hudson, Trans. ANS, 26, 195 (1977).
47 . D.J.Michel, P.L.Hendrick, A.G.Pieper, J.Nucl.Mater., 75, 1 (1978).
48 . P.L.Hendrick, Nucl.Instr.Methods, 161, 345 (1979).
49 . E.P.Simonen, P.L.Hendrick, J.Nucl.Mater., 85-86, 873 (1979).
50 . A.R.Causey, G.L.C.Carpenter, S.R.Mac Ewen, J.Nucl.Mater., 90, 216 (1980).
51 . C.H.Henager, J.L.Brimhall, E.P.Simonen, J.Nucl.Mater., 90, 290 (1980).
52 . C.H.Henager, Jr., E.P.Simonen, E.R.Bradley, R.S.Stang, J.Nucl.Mater., 104, 1269 (1981).
53 . J.Nagakawa, V.K.Sethi, A.P.L.Turner, J.Nucl.Mater., 104, 1275 (1981).
54 . E.P.Simonen, C.H.Henager, Jr, J.Nucl.Mater., 104, 1281 (1981).
55 . T.Atkins, R.J.McElroy, in: Effects of Radiation on Materials, 11th Conf. ASTM STP 782, H.R.Brager and J.S.Perrin, Eds., (ASTM, Phil., 1982) p.841..
56 . J.P.Foster, U.P.Nayak, D.L.Porter, J.Nucl.Mater., 110, 95 (1982)..
57 . J.Nagakawa, J.Nucl.Mater., 116, 10 (1983).
58 . L.N.Bystrov, A.B.Tsepelev, in: Structural Materials for Fusion Reactors (Nauka, Moscow, 1983) p.99 (in Russian).
59 . P.Jung, J.Nucl.Mater., 113, 133 (1983).
60 . T.Atkins, R.J.McElroy, in: Dimensional Stability and Mechanical Behaviour of Irradiated Metals and Alloys. Proc. BNES Conf., vol.2 (BNES, London, 1984) p.71.
61 . L.N.Bystrov, L.I.Ivanov, A.B.Tsepelev, Phil.Mag. A, 49, 273 (1984).
62 . C.H.Henager,Jr., E.P.Simonen, E.R.Bradley, R.G.Stang, J.Nucl.Mater., 122, 413 (1984).
63 . P.Jung, in: Dimensional Stability and Mechanical Behaviour of Irradiated Metals and Alloys. Proc. BNES Conf., vol.1 (BNES, London, 1984) p.133.
64 . J.Nagakawa, Trans.Nat.Res.Inst.Met., 26, 183 (1984).
65 . M.I.Ansari, Ber.KFA Juelich - 1991 (1985).
66 . P.Jung, H.Klein, J.Nucl.Mater., 159, 360 (1988).
67 . R.R.Vandervoort, W.L.Barmore, A.K.Mukherjee, Rad.Effects, 41, 113 (1979).
68 . W.Barmore, A.Ruotala, E.Raimond, A.Mukherjee, J.Nucl.Mater., 117, 258 (1983).

69 . G.W.Lewthwaite, K.J.Proctor, J.Nucl.Mater., 46, 9 (1973).
70 . R.E.Nygren, J.Nucl.Mater., 85-86, 861 (1979).
71 . J.Ponsoye, Rad.Effects, 8, 13 (1971).
72 . V.M.Nalesnik, V.A.Pavlov, A.G.Arakelov, V.V.Klyushin, A.E.Kissel, I.N.Kovalev, in: Radiation Physics of Crystals, Trudy Inst. Fiz. Metall., n.34 (Inst. of Metal Physics, Sverdlovsk, 1977) p.99 (in Russian).
73 . V.M.Troyanov, M.G.Bulkanov, A.S.Kruglov, E.A.Krjuchkov, M..Nikulin, J.M.Pevchikh, A.E.Rusanov, A.A.Smirnoff, S.N.Votinov, J.Nucl.Mater. 233-237, 381 (1996).
74 . V.Fidleris, J.Nucl.Mater., 26, 51 (1968).
75 . D.R.Harries, J.Nucl.Mater., 65, 1, 157 (1977).
76 . S.R.MacEwen, V.Fidleris, J.Nucl.Mater., 65, 250 (1977).
77 . J.R.Parsons, C.W.Hoelke, J.Nucl.Mater., 114, 103 (1983).
78 . J.R.Parsons, C.W.Hoelke, AECL-8831, 1985.
79 . F.A.Garner, R.J.Puigh, J.Nucl.Mater., 179-181, 577 (1991).
80 . P.Jung, J.Nucl.Mater., 179-181, 745 (1991).
81 . A.Kohyama, Y.Kohno, K.Asakura, M.Yoshino, C.Namba, C.R.Eiholzer, J.Nucl.Mater., 212-215, 751 (1994).
82 . M.B.Toloczko, F.A.Garner, C.R.Eiholzer, J.Nucl.Mater., 212-215, 604 (1994).
83 . M.L.Grossbeck, L.T.Gibson, S.Jitsukawa, J.Nucl.Mater. 233-237, 148 (1996).
84 . M.B.Toloczko, F.A.Garner, J.Nucl.Mater. 233-237, 289 (1996).
85 . M.B.Toloczko, F.A.Garner, C.R.Eiholzer, J.Nucl.Mater., 258-263, 1163 (1998).
86 . M.B.Toloczko, F.A.Garner, in: Effects of Radiation on Materials: 18th Int.Symp., ASTM STP 1325 (ASTM, Phil., 1999) p.765.
87 . M.B.Toloczko, J.P.Hirth, F.A.Garner, J.Nucl.Mater. 283-287, 409 (2000)
88 . M.B.Toloczko, D.S. Gelles, F.A.Garner, R.J.Kurtz, K.Abe, J.Nucl.Mater. 329-333, 352 (2004)
89 . J.Chen, P.Jung, M.A.Pouchon, T.Rebac, W.Hoffelner, J.Nucl.Mater. 373, 222 (2008)
90 . J.Chen , M.A.Pouchon, A.Kimura, P.Jung, W.Hoffelner, J.Nucl.Mater. 386-388, 143 (2009)
91 . J.Chen, W.Hoffelner, J.Nucl.Mater. 392, 360 (2009)
92 . J.Chen, P.Jung, J.Henry, Y.de Carlan, T.Sauvage, F.Duval, M.F.Barthe, W.Hoffelner, J.Nucl.Mater. 437, 432 (2013)
93 . J.Chen, P.Jung, W.Hoffelner, J.Nucl.Mater. 441, 688 (2013)
94 . J.P.Foster, A.Boltax, J.Nucl.Mater., 183, 115 (1991).
95 . D.L.Porter, G.D.Hudman, FA.Garner, J.Nucl.Mater., 179-181, 581 (1991).
96 . M.B.Toloczko, F.A.Garner, C.R.Eiholzer, J.Nucl.Mater. 191-194, 803 (1992).
97 . I.Shibahara, S.Ukai, S.Onose, S.Shikakura, J.Nucl.Mater., 204, 131 (1993).
98 . A.N.Vorobyev, N.I.Budylkin, E.G.Mironova, S.I.Porollo, Yu.V.Konobeev, F.A.Garner, J.Nucl.Mater., 258-263, 1618 (1998).
99 . A.Uehira, S.Ukai, S.Mizuta, R.J.Puigh, in: Effects of Radiation on Materials: 20th Int.Symp., ASTM STP 1405 (ASTM, Phil., 2001), p..
100 . G.R.Piercy, J.Nucl.Mater., 26, 18 (1968).
101 . F.A.Nichols, J.Nucl.Mater., 37, 59 (1970).
102 . E.R.Gilbert, Reactor Technology, 14, 258 (1971).
103 . V.A.Borodin, J.Nucl.Mater., 225, 15 (1995).
104 . J.Friedel, Dislocations (Pergamon Press, Oxford, 1964).
105 . D.S.Gelles, J.Nucl.Mater. 307-311, 393 (2002)
106 . R.L.Coble, J.Appl.Phys., 34, 1679 (1963).
107 . I.M.Lifshitz, Zh.Eksp.Teor.Fiz., 44, 1349 (1963).

108 . F.R.N.Nabarro, R.Bullough, J.R.Matthews, Acta Met., 30, 1761 (1982).
109 . P.A.Bereznyak, V.I.Ryabukhin, Voprosy Atomnoi Nauki Techniki, Ser: Physics of Radiation Damage and Radiation Materials Science, n.2(25), 41 (1983).
110 . G.Martin, J.P.Poirier, J.Nucl.Mater., 39, 93 (1971).
111 . W.G.Wolfer, J.Nucl.Mater., 90, 175 (1980).
112 M.J. Norgett, M.T. Robinson, I.M. Torrens, Nucl. Eng. Des. 33, 50 (1975).
113 . T.C.Reiley, P.Jung, in: Radiation Effects in Breeder Reactor Structural Materials, Proc.Int.Conf., Scottsdale, AZ, 1977, p.295.
114 . P.Jung, Chr.Schwaiger, H.Ullmaier, J.Nucl.Mater., 85-86, 867 (1979).
115 . F.A.Nichols, J.Nucl.Mater., 84, 207 (1979).
116 . F.A.Nichols, J.Nucl.Mater., 90, 29 (1980).
117 . L.E.Rehn, P.R.Okamoto, R.S.Averback, Phis. Rev. B 30, 3073 (1984).
118 . A.Mueller, V.Naundorf, M.-P.Macht, Mat.Sci.Forum, 15-18, 1275 (1987).
119 . B.N.Singh, S.J.Zinkle, J.Nucl.Mater., 206, 212 (1993).
120 . S.J.Zinkle, B.N.Singh, J.Nucl.Mater., 199, 173 (1993).
121 . B.N.Singh, M.Eldrup, A.Horswell, P.Ehrhart, F.Dworschak, Phil. Mag. A, 80, 2629 (2000).
122 . D.Mosedale, D.R.Harries, J.A.Hudson, G.W.Lewthwaite, R.J.McElroy, in: Radiation Effects in Breeder Reactor Structural Materials. Proc.Int.Conf., Scottsdale, AZ, 1977, p.209.
123 . J.Nagakawa, S.Uchio, Y.Murase, N.Yamamoto, K. Shiba, J.Nucl.Mater. 386-388, 264 (2009)
124 . S.R.MacEwen, V.Fidleris, Phil.Mag., 31, 1149 (1975).
125 . L.N.Bystrov, A.B.Tsepelev, Fiz.Khim.Obrab.Metal., n.4, 22 (1980).
126 . C.H.Henager, E.P.Simonen, E.R.Bradley, R.G.Stang, J.Nucl.Mater., 117, 250 (1983).
127 . J.Nagakawa, H.Shiraishi, H.Kamitsubo, I.Kohno, T.Shikata, J.Nucl.Mater., 136, 238 (1985).
128 V.S. Neustroev, V.K. Shamardin, J.Nucl.Mater. 307-311, 343 (2002)
129 . J.Garnier, Y.Bréchet, M.Delnondedieu, A.Renault, C.Pokor, P.Dubuisson, J.-P. Massoud, J.Nucl.Mater. 417, 70 (2011)
130 . J.Nagakawa, H.Shiraishi, M.Okada, H.Kamitsubo, I.Kohno, T.Shikata, J.Nucl.Mater., 133-134, 497 (1985).
131 . E.R.Gilbert, J.Nucl.Mater., 26, 105 (1968).
132 . E.F.Ibrahim, in: Application Related Phenomena for Zirconium and its Alloys. ASTM STP 458 (ASTM, Phil. 1969) p.18.
133 . S.D.Harkness, F.L.Yaggee, F.V.Nolfi, in: Irradiation Embrittlement and Creep in Fuel Cladding and Core Components (BNES, London, 1972) p.259.
134 . V.V.Andreev, E.S.Aitkhozhin, V.V.Kirsanov, G.A.Naumenko, S.S.Ogorodnik, A.S.Oryschenko, V.D.Yaroshevich, in: Radiation Defects in Metals (Nauka, Alma-Ata, 1981), p.156.
135 . V.A.Safonov, E.N.Loguntzov, S.N.Tyumetzev, A.M.Katel'tzev, V.M.Nalesnik, V.V.Klyushin, M.I.Solonin, Voprosy Atomnoi Nauki Techniki, Ser: Physics of Radiation Damage and Radiation Materials Science, n.2(25), 47 (1983).
136 . J.P.Foster, E.R.Gilbert, K.Bunde, D.L.Porter, J.Nucl.Mater., 252, 89 (1998).
137 . E.K.Opperman, J.L.Straalsund, G.L.Wire, R.H.Howell, Nucl.Technology, 42, 71 (1979).
138 . W.N.McElroy, R.E.Dahl, E.R.Gilbert, Nucl.Eng.Des., 14, 319 (1970).
139 . E.R.Gilbert, D.C.Kaulitz, J.J.Holmes, T.T.Claudson, in: Irradiation Embrittlement and Creep in Fuel Cladding and Core Components (BNES, London, 1972) p.239.
140 . E.F.Ibrahim, J.Nucl.Mater., 46, 169 (1973).
141 . D.S.Wood, in: Irradiation Behaviour of Fuel Cladding and Core Component Materials, Proc.Eur.Conf. Karlsruhe, 1974, p.123.
142 . P.A.Bereznyak, N.M.Kiryukhin, Voprosy Atomnoi Nauki Techniki, Ser: Physics of Radiation Damage and Radiation Materials Science, n.2(10), 1979, p.55.

143 . G.E.Lucas, M.Surprenant, J.DiMarzo, G.J.Brown, J.Nucl.Mater., 101, 78 (1981).
144 . D.Caillard, J.L.Martin, B.Jouffray, Ann.Chim., 6, 37 (1981).
145 . D.Caillard, J.L.Martin, J.Microsc.Spectrosc.Electron., 6, 361 (1981).
146 . E.N.Loguntzov, V.A.Safonov, S.N.Tyumetzev, A.V.Kozlov, V.M.Nalesnik, Fiz.Met.Metalloved., 57, 802 (1984).
147 . D.J.Mazey, J.A.Hudson, J.Nucl.Mater., 37, 13 (1970).
148 . H.R.Brager, J.L.Straalsund, J.Nucl.Mater., 47, 105 (1973).
149 . H.R.Brager, E.R.Gilbert, J.L.Straalsund, Rad.Effects, 21, 1, 37-50 (1974).
150 . M.J.Makin, in: Electron Microscopy 1978, vol.3, J.M.Sturgess, ed. (Microstructural Society of Canada, Toronto, 1978) p.330.
151 . P.Jung, T.C.Reiley, W.Kesternich, in: Fusion Technology 1980, vol.2. (Pergamon Press, Oxford, 1980) p.1287.
152 . V.V.Bryk, V.N.Voevodin, B.V.Matvienko, I.M.Neklyudov, P.V.Platonov, Voprosy Atomnoi Nauki Techniki, Ser: Physics of Radiation Damage and Radiation Materials Science, n.5(28), 12 (1983).
153 . H.Kusanagi, H.Kimura, M.Tokiwai, T.Suzuki, J.Nucl.Mater., 133-134, 473 (1985).
154 . K.V.Botvin, S.P.Vagin, V.F.Reutov, Fiz.Khim.Obrab.Metal., n.1, 14 (1989).
155 . A.S.Kruglov, V.N.Bykov, Yu.M.Pevchikh, Atomnaya Energiya, 54, 57 (1983).
156 . R.A.Johnson, Phys.Rev., 152, 629 (1966).
157 . P.H.Dederichs, C.Lehmann, H.R.Schober, A.Scholz, R.Zeller, J.Nucl.Mater., 69-70, 176 (1978).
158 . F.A.Nichols, in: Annual Review of Material Science, vol. 2, Palo Alto, CA, USA, 1972, p.463.
159 . V.I.Tscherbak, Fiz.Met.Metalloved., 50, 1315 (1980).
160 . N.Igata, Y.Kohno, H.Tsunakawa, T.Fujihira, in: Effects of Radiation on Materials. 12th Int. Symp. ASTM STP 870, vol.1 (ASTM, Phil., 1985) p.265.
161 . T.M.Williams, J.Nucl.Mater., 79, 28 (1979).
162 . P.T.Heald, M.V.Speight, Acta Met., 23, 1389 (1975).
163 . M.R.Hayns, R.C.Perrin, in: The Physics of Irradiation Produced Voids. AERE-R7934, 1975, p.188.
164 . M.R.Hayns, J.Nucl.Mater., 56, 267 (1975).
165 . J.N.Alhajji, N.M.Ghoniem, Trans. ANS, 41, 251 (1982).
166 . H.R.Brager, J.F.Bates, Trans.ANS, 13, 1, 146 (1970).
167 . P.J.Barton, B.L.Eyre, D.A.Stow, J.Nucl.Mater., 67, 181 (1977).
168 . D.Caillard, J.L.Martin, B.Jouffray, Acta Met., 28, 1059 (1980).
169 . S.Jitsukawa, Y.Katano, K.Shiraishi, J.Nucl.Sci.Tecn., 21, 671 (1984).
170 . F.A.Garner, D.S.Gelles, J.Nucl.Mater., 159, 286 (1988).
171 . J.Delaplace, N.Azam, L.LeNaour, C.Fiche, Bull.Inform.Sci. Tech., 216, 29 (1976).
172 . J.A.Hudson, J.Nucl.Mater., 60, 89 (1976).
173 . H.R.Brager, F.A.Garner, E.R.Gilbert, J.E.Flinn, W,G.Wolfer, in: Radiation Effects in Breeder Reactor Structural Materials, Proc.Int.Conf., Scottsdale, AZ, 1977, p.727.
174 . R.A.Weiner, J.P.Foster, A.Boltax, in: Radiation Effects in Breeder Reactor Structural Materials, Proc.Int.Conf., Scottsdale, AZ, 1977, p.865.
175 . F.A.Garner, W.G.Wolfer, Preprint UWFDM - 484 (1982).
176 . F.A.Garner, J.Nucl.Mater., 122, 459 (1984).
177 . L.Le Naour, P.Grosjean, V.Levy, CEA-CONF-7170 (1984).
178 . F.A.Garner, in: Materials Science and Technology, vol.10. Nuclear Materials (VCH, Weinheim,1994) p.419.
179 . F.A.Garner, B.J.Makenas, S.A.Chastain, J.Nucl.Mater. 413, 53 (2011)
180 . D.J.Michel, P.L.Hendrick, A.G.Pieper, Trans. ANS, 26, 195 (1977).

181 . L.C.Walters, W.E.Ruther, J.Nucl.Mater., 68, 324 (1977).
182 . M.Griffith, J.Nucl.Mater. 205, 225 (1993)
183 P.T.Heald, M.V.Speight, J.Nucl.Mater., 64, 139 (1977).
184 . P.T.Heald, in: Radiation Effects in Breeder Reactor Structural Materials, Proc.Int.Conf., Scottsdale, AZ, 1977, p.781.
185 . L.K.Mansur, J.Nucl.Mater., 83, 109 (1979).
186 . Sh.Sh.Ibragimov, Yu.S.Pyatiletov, in: Radiation Defects in Metals (Nauka, Alma-Ata, 1981), p..
187 . G.W.Lewthwaite, J.Nucl.Mater., 61, 313 (1976).
188 . Yu.S.Pyatiletov, Fiz.Met.Metalloved., 51, 641 (1981).
189 . P.T.Heald, J.Nucl.Mater., 74, 221 (1978).
190 . P.Blanchard, P.Jary, J.Delaplace, J.Nucl.Mater., 74, 267(1978).
191 . R.B.Jones, in: Dimensional Stability and Mechanical Behaviour of Irradiated Metals and Alloys. Proc. BNES Conf., vol.2 (BNES, London, 1984) p.57.
192 . F.A. Garner, M.L. Hamilton, C.R. Eiholzer, M.B. Toloczko, A.S. Kumar, J. Nucl. Mater. 191–194 (1992) 813.
193 E.R. Gilbert, F.A. Garner, J.Nucl.Mater. 367-370, 954 (2007)
194 . D.Mosedale, J.W.Barnaby, J.I.Bramman, D.I.Bell, D.R.Harries, in: Fuel and Fuel Elements for Fast Reactors, Proc.Symp.IAEA, vol.2 (IAEA, Vienna, 1974) p.131.
195 . L.C.Walters, C.M.Walter, M.A.Pugacz, J.Nucl.Mater., 43, 133 (1972).
196 . P.Jung, Chr.Schwaiger, H.Ullmaier, J.Viehweg, in: Irradiation Behaviour of Metallic Materials for Fast Reactor Core Components, Proc.Int.Conf., Ajaccio, France, 1979, p.415.
197 . E.R.Gilbert, J.F.Bates, J.Nucl.Mater., 65, 204 (1977).
198 . Chr.Schwaiger, P.Jung, H.Ullmaier, J.Nucl.Mater., 90, 268 (1980).
199 . A.S.Kruglov, V.N.Bykov, M.G.Bulkanov, V.D.Dmitriev, Yu.M.Pevchikh, V.A.Fazkullin, O.G.Yurin, in: Radiation Defects in Metals (Nauka, Alma-Ata, 1981), p.136.
200 . P.Jung, in: Fusion Technology 1982 (Pergamon Press, Oxford, 1982) p.779.
201 . V.S.Neustroev, V.K.Shamardin, L.S.Ozhigov, Voprosy Atomnoi Nauki Techniki, Ser: Physics of Radiation Damage and Radiation Materials Science, n.1(52), 20 (1990).
202 . M.B.Toloczko, F.A.Garner, J.Standring, B.Munro, S.Adaway, J.Nucl.Mater., 258-263, 1606 (1998).
203 . C.Xu, G.S.Was, J.Nucl.Mater. 441, 681 (2013)
204 . F.A.Garner, M.B.Toloczko, M.L.Grossbeck, J.Nucl.Mater., 258-263, 1718 (1998).
205 . A.S.Kruglov, M.G.Bulkanov, V.N.Bykov, Yu.M.Pevchikh, Atomnaya Energiya, 48, 258 (1980).
206 . G.W.Lewthwaite, D.Mosedale, in: Irradiation Behaviour of Metallic Materials for Fast Reactor Core Components, Proc.Int.Conf., Ajaccio, France, 1979, p.399.
207 . E.A.Little, D.R.Arkell, D.R.Harries, G.W.Lewthwaite, T.M.Williams, in: Irradiation Behaviour of Metallic Materials for Fast Reactor Core Components, Proc.Int.Conf., Ajaccio, France, 1979, p.32.
208 . G.W.Lewthwaite, D.Mosedale, J.Nucl.Mater., 90, 205 (1980).
209 . K.Ehrlich, J.Nucl.Mater., 100, 149 (1981).
210 . M.M.Paxton, B.A.Chin, E.R.Gilbert, R.E.Nygren, J.Nucl.Mater., 80, 144 (1979).
211 . J.E.Flinn, G.L.McVay, L.C.Walters, J.Nucl.Mater., 65, 210 (1977).
212 . K.D.Closs, K.Herschbach, Tagungsberichte Reaktortagung Duesseldorf (1974) p.790..
213 . J.Lehmann, J.M.Dupouy, H.Broudeur, J.L.Boutard, A.Maillard, in: Irradiation Behaviour of Metallic Materials for Fast Reactor Core Components, Proc.Int.Conf., Ajaccio, France, 1979, p.409.
214 . J.Erler, A.Maillard, G.Brun, J.Lehmann, J.M.Dupouy, in: Irradiation Behaviour of Metallic Materials for Fast Reactor Core Components, Proc.Int.Conf., Ajaccio, France, 1979, p. 11.
215 . H.J.Bergmann, W.Dietz, D.Haas, J.Nucl.Mater., 65, 224 (1977).

216 . H.J.Bergmann, D.Haas, K.Herschbach, in: Radiation Effects in Breeder Reactor Structural Materials. Proc.Int.Conf., Scottsdale, AZ, 1977, p.241.
217 . G.L.Wire, J.L.Straalsund, J.Nucl.Mater., 64, 254 (1977).
218 . K.Herschbach, W.Schneider, K.Ehrlich, J.Nucl.Mater., 101, 326 (1981).
219 . R.J.Puigh, E.R.Gilbert, B.A.Chin, in: Effects of Radiation on Materials, 11th Conf. ASTM STP 782, H.R.Brager and J.S.Perrin, Eds., (ASTM, Phil., 1982) p.108..
220 . J.L.Straalsund, in: Radiation Effects in Breeder Reactor Structural Materials, Proc.Int.Conf., Scottsdale, AZ, 1977, p.191.
221 . L.C.Walters, G.L.McVay, G.D.Hudman, in: Radiation Effects in Breeder Reactor Structural Materials, Proc.Int.Conf., Scottsdale, AZ, 1977, p.277.
222 . H.J.Bergmann, G.Knoblauch, D.Haas, K.Herschbach, in: Irradiation Behaviour of Metallic Materials for Fast Reactor Core Components, Proc.Int.Conf., Ajaccio, France, 1979, Suppl., p.37.
223 . G.L.McVay, L.C.Walters, G.D.Hudman, J.Nucl.Mater., 79, 395 (1979).
224 . J.P.Foster, R.V.Strain, W.G.Wolfer, Nucl.Eng.Des., 31, 117 (1973).
225 . W.Schneider, K.Herschbach, K.Ehrlich, in: Effects of Radiation on Materials, 11th Conf. ASTM STP 782, H.R.Brager and J.S.Perrin, Eds., (ASTM, Phil., 1982) p.30..
226 . E.R.Gilbert, B.A.Chin, Trans. ANS, 28, 141 (1978).
227 . M.M.Paxton, B.A.Chin, E.R.Gilbert, J.Nucl.Mater., 95, 185 (1980).
228 . B.A.Chin, R.J.Puigh, in: Effects of Radiation on Materials, 11th Conf. ASTM STP 782, H.R.Brager and J.S.Perrin, Eds., (ASTM, Phil., 1982) p.122..
229 . J.L.Boutard, Y.Carteret, R.Cauvin, Y.Guerin, A.Maillard, in: Dimensional Stability and Mechanical Behaviour of Irradiated Metals and Alloys. Proc. BNES Conf., vol.1 (BNES, London, 1984) p.109.
230 . J.F.Bates, R.W.Powell, E.R.Gilbert, in: Effects of Radiation on Materials, 10th Conf. ASTM STP 725 (ASTM, Phil., 1981) p.713.
231 . B.A.Chin, J.L.Straalsund, G.L.Wire, J.Nucl.Mater., 75, 274 (1978).
232 . A.D.Brailsford, R.Bullough, in: Irradiation Embrittlement and Creep in Fuel Cladding and Core Components (BNES, London, 1972) p.221.
233 . S.D.Harkness, R.Grappel, S.G.McDonald, Nucl.Techn., 16, 25 (1972).
234 . W.G.Wolfer, J.P.Foster, F.A.Garner, Nucl.Techn., 16, 55 (1972).
235 . W.G.Wolfer, A.Boltax, in: Irradiation Embrittlement and Creep in Fuel Cladding and Core Components (BNES, London, 1972) p.283.
236 . A.D.Brailsford, R.Bullough, Phil.Mag., 27, 49 (1973).
237 . W.G.Wolfer, M.Ashkin, A.Boltax, in: Properties of Reactor Structural Alloys after Neutron or Particle Irradiation. ASTM STP 570 (ASTM, Phil., 1975) p.233.
238 . P.T.Heald, J.E.Harbottle, J.Nucl.Mater., 67, 229 (1977).
239 . Yu.S.Pyatiletov, Fiz.Met.Metalloved., 54, 1080 (1982).
240 . F.A.Garner, D.L.Porter, J.Nucl.Mater., 155-157, 1006 (1988).
241 . A.Boltax, J.P.Foster, R.A.Weiner, A.Biancheria, J.Nucl.Mater., 65, 174 (1977).
242 . R.A.Weiner, A.Boltax, J.Nucl.Mater., 65, 1 (1977).
243 . J.P.Foster,J.F.Bates, J.Nucl.Mater., 55, 119 (1975).
244 . D.L.Porter, F.A.Garner, HEDL-SA-3615 (1986).
245 . J.F.Bates,E.R.Gilbert, J.Nucl.Mater., 59, 95 (1975).
246 . J.L.Boutard, G.Brun, J.Lehmann, J.L. Seran, J.M.Dupouy, in: Irradiation Behaviour of Metallic Materials for Fast Reactor Core Components. Proc.Int.Conf., Ajaccio, France, 1979, p. 137.
247 . K.Herschbach, W.Schneider, H.-J. Bergmann, in: Effects of Radiation on Materials: 14th Int. Symp., ASTM STP 1046, vol. 2 (ASTM, Phil., 1990) p.570.
248 . S.Ya.Lebedev, V.G.Bagdinov and S.Ya.Surkov, Fiz.Met.Metallov. 54, 595 (1982).
249 . F.A.Garner, E.R.Gilbert, D.L.Porter, in: Effects of Radiation on Materials, 10th Conf. ASTM

STP 725 (ASTM, Phil., 1981) p.680.
250 . H.R.Brager, F.A.Garner, G.L.Gutrie, J.Nucl.Mater., 66, 301 (1977).
251 . F.A.Garner, D.L.Porter, B.J.Makenas, J.Nucl.Mater., 148, 279 (1987).
252 . K.Herschbach, H.-J. Bergmann, J.Nucl.Mater., 175, 143 (1990).
253 . D.L.Porter, F.A.Garner, in: Influence of Radiation on Material Properties : 13th Int. Symp. (Part II) ASTM STP 956 (ASTM, Phil., 1988) p. 11.
254 . J.M.Dupouy, J.Erler, G.Allegrand, A.Bisson, P.Blanchard, M.Vouillon, J.Sagot, M.Weisz, in: Fuel and Fuel Elements for Fast Reactors, Proc.Symp.IAEA, vol.2. (IAEA, Vienna, 1974) p.253.
255 . R.J.Puigh, J.Nucl.Mater., 141-143, 954 (1986).
256 . J.M.Dupouy, J.Lehmann, J.L.Boutard, in: Reactor Materials Science (Moscow, 1978) p.280.
257 . K.Herschbach, J.Nucl.Mater., 127, 239 (1985).
258 . K.Ehrlich, J.Nucl.Mater., 133-134, 119 (1985).
259 . D.H.Kreyns, M.W.Burkart, J.Nucl.Mater., 26, 87 (1968).
260 . D.E.Fraser, P.A.Ross-Ross, A.R.Causey, J.Nucl.Mater., 46, 281 (1973).
261 . A.R.Causey, J.Nucl.Mater., 54, 64 (1974).
262 . C.E.Colman, A.R.Causey, V.Fidleris, J.Nucl.Mater., 60, 185 (1976).
263 . B.A.Chin, J.L.Straalsund, J.Nucl.Mater., 74, 260 (1978).
264 . B.A.Chin, J.L.Straalsund, G.L.Wire, J.Nucl.Mater., 83, 324 (1979).
265 . A.R.Causey, V.Fidleris, R.A.Holt, J.Nucl.Mater., 139, 3, 277 (1986).
266 . G.W.Lewthwaite, D.Mosedale, Brit.J.Appl.Phys., 17, 821 (1966).
267 . I.Finnie, W.R.Heller, Creep of Engineering Materials (Mc Graw Hill, NY, 1959).
268 . V.Fidleris, J.Nucl.Mater., 159, 22 (1988).
269 . J.P.Foster, K.Bunde, M.L.Grossbeck, E.R.Gilbert, J.Nucl.Mater., 270, 357 (1999).
270 . J.P.Foster, W.G.Wolfer, A.Biancheria, A.Boltax, in: Irradiation Embrittlement and Creep in Fuel Cladding and Core Components (BNES, London, 1972) p.273.
271 . F.A.Nichols, Trans.ANS, 12, 572 (1969).
272 . D.S.Gelles, R.J.Puigh, in: Effects of Radiation on Materials. 12th Int. Symp. ASTM STP 870, vol.1 (ASTM, Phil., 1985) p.19.
273 . R.J.Puigh, in: Effects of Radiation on Materials. 12th Int. Symp. ASTM STP 870, vol.1 (ASTM, Phil., 1985) p.7.
274 . D.S.Gelles, J.Nucl.Mater., 149, 192 (1987).
275 . M.L.Grossbeck, J.A.Horak, J.Nucl.Mater., 155-157, 1001 (1988).
276 . M. Ando, M. Li, H. Tanigawa, M.L. Grossbeck, S. Kim, T. Sawai, K. Shiba, Y. Kohno, A. Kohyama, J. Nucl. Mater. 367–370 (2007) 122.
277 . T.C.Reiley, R.L.Auble, R.H.Shannon, J.Nucl.Mater., 90, 271 (1980).
278 . N.Kishimoto, H.Shiraishi, N.Yamamoto, J.Nucl.Mater., 155-157, 1014 (1988).
279 . R.Scholz, R.Mueller, J.Nucl.Mater. 233-237, 169 (1996).
280 . A.S.Kruglov, V.N.Bykov, Yu.M.Pevchikh, O.G.Yurin, M.G.Bulkanov, Atomnaya Energiya, 50, 342 (1981).
281 . A.R.Causey, R.A.Holt, Trans. ANS, 44, 235 (1983).
282 . L.N.Bystrov, L.I.Ivanov, A.B.Tsepelev, Voprosy Atomnoi Nauki Techniki, Ser: Physics of Radiation Damage and Radiation Materials Science, n. 1(34), 56 (1985).
283 . B.Watkins, D.S.Wood, in: Application Related Phenomena for Zirconium and its Alloys. ASTM STP 458 (ASTM, Phil. 1969) p.226.
284 . J.Hirth, J.Lothe, Theory of Dislocations (McGraw-Hill, NY, 1967).
285 . A.M.Kosevich, Z.K.Saralidze, V.V.Slyozov, Fiz.Tv.Tela, 9, 895 (1967).
286 . F.R.Nabarro, Phil.Mag., 16, 231 (1967).
287 . N.A.Demin, Yu.V.Konobeev, Voprosy Atomnoi Nauki Techniki, Ser: Physics of Radiation

Damage and Radiation Materials Science, n.2(13), 3 (1980).
288 . G.W.Lewthwaite, J.Nucl.Mater., 38, 118 (1971).
289 . E.R.Gilbert, B.Mastel, Trans.ANS, 12, 132 (1969).
290 . V.Fidleris, J.Nucl.Mater., 36, 343 (1970).
291 . K.D.Closs, K.Hershbach, L.Schmidt, H.Van den Boorn, J.Nucl.Mater., 65, 244 (1977).
292 . M.L.Grossbeck, J.A.Horak, Trans. ANS, 55, 299 (1987).
293 . A.de Bremaecker, J.-J.Huet, in: Dimensional Stability and Mechanical Behaviour of Irradiated Metals and Alloys. Proc. BNES Conf., vol.1 (BNES, London, 1984) p.117.
294 . Y.S.Kim, K.S.Im, Y.M.Cheong, S.B.Ahn, J.Nucl.Mater. 346, 120 (2005)
295 . K.Fukumoto, H.Matsui, M.Narui, M.Yamazaki, J.Nucl.Mater. 437, 341 (2013)
296 . E.R.Gilbert, N.E.Harding, Trans.ANS, 13, 143 (1970).
297 . W.A.Coghlan, L.K.Mansur, J.Nucl.Mater., 104, 1245 (1981).
298 . K.Herschbach, J.Nucl.Mater., 131, 303 (1985).
299 . M.L.Grossbeck, L.L.Horton, L.K.Mansur, Trans. ANS, 60, 295 (1989).
300 . E.R.Gilbert, A.J.Lovell, in: Radiation Effects in Breeder Reactor Structural Materials. Proc.Int.Conf., Scottsdale, AZ, 1977, p.269.
301 . E.R.Gilbert, B.A.Chin, in: Effects of Radiation on Materials. 12th Int. Symp. ASTM STP 870, vol.1 (ASTM, Phil., 1985) p.52.
302 . F.A.Garner, E.R.Gilbert, D.S.Gelles, J.P.Foster, in: Effects of Radiation on Materials, 10th Conf. ASTM STP 725 (ASTM, Phil., 1981) p.665.
303 . T.Mura, Int.J.Eng.Sci., 1, 371 (1963).
304 . W.G.Wolfer, M.Ashkin, J.Appl.Phys., 47, 791 (1976).
305 . W.G.Wolfer, Phil.Mag. A, 43, 61 (1981).
306 . A.J.E.Foreman, W.J.Phytian, C.A.English, Phil.Mag.A, 66, 671 (1992).
307 . B.D.Wirth, G.R.Odette, D.Maroudas, G.E.Lucas, J.Nucl.Mater., 244, 185 (1997).
308 . Yu.N.Osetsky, D.J.Bacon, A.Serra, Phil.Mag.Lett., 79, 273 (1999).
309 . A.J.E.Foreman, C.A.English, W.J.Phytian, Phil.Mag.A, 66, 655 (1992).
310 . T.Diaz de la Rubia, M.W.Guinan, A.Caro, P.Scherrer, Rad.Eff.Def.Sol., 130-131, 39 (1994).
311 . W.J.Phytian, R.E.Stoller, A.J.E.Foreman, A.F.Calder, D.J.Bacon, J.Nucl.Mater., 223, 245 (1995).
312 . A.D.Brailsford, J.Nucl.Mater., 60, 257 (1976).
313 . V.A.Borodin, Physica A, 211, 279 (1994).
314 . P.T.Heald, M.V.Speight, Phil.Mag., 29, 1075 (1974).
315 . R.Bullough, M.R.Hayns, J.Nucl.Mater., 57, 348 (1975).
316 . R.Bullough, J.R.Willis, Phil.Mag., 31, 855 (1975).
317 . E.J.Savino, Phil.Mag., 36, 323 (1977).
318 . Z.K.Saralidze, Fiz.Tv.Tela, 20, 2716 (1978).
319 . N.A.Demin, Yu.V.Konobeev, in: Radiation Defects in Metals (Nauka, Alma-Ata, 1981), p.128.
320 . C.H.Woo, U.Gosele, J.Nucl.Mater., 119, 219 (1983).
321 . B.C.Skinner, C.H.Woo, Phys.Rev. B, 30, 3084 (1984).
322 . C.H.Woo, J.Nucl.Mater., 120, 55 (1984).
323 . V.A.Borodin, A.I.Ryazanov, J.Nucl.Mater., 210, 258 (1994).
324 . A.I.Ryazanov, V.A.Borodin, Rad.Effects, 55, 157 (1981).
325 . A.I.Ryazanov, V.A.Borodin, Rad.Effects, 56, 179 (1981).
326 . V.A.Borodin, A.I.Ryazanov, J.Nucl.Mater., 135, 46 (1985).
327 . V.A.Borodin, A.I.Ryazanov, in: Effects of Radiation on Materials. 15th Int. Symp. ASTM STP 1125 (ASTM, Phil., 1992) p.530.
328 . E.Kroner, Physik der Kondensierten Materie, Band 2. 1964, s.262.
329 . C.H.Woo, AECL-6791 (1980).

330 . E.Kuramoto, J.Nucl.Mater., 122, 422 (1984).
331 . J.Holder, A.V.Granato, L.E.Rehn, Phys.Rev. B, 363 (1974).
332 . H.Wenzl, in: Vacancies and Interstitials in Metals, Eds. A.Seeger et al. (North-Holland, Amsterdam, 1970) p.363.
333 . F.S.Ham, J.Appl.Phys., 30, 915 (1959).
334 . P.H.Dederichs, K.Schroder, Phys.Rev. B, 17, 2524 (1978).
335 . E.J.Savino, C.N.Tome, J.Nucl.Mater., 108-109, 405 (1982).
336 . M.P.Puls, C.H.Woo, J.Nucl.Mater., 139, 48 (1986).
337 . H.R.Schober, J.Nucl.Mater., 126, 220 (1984).
338 . E.Ya.Mikhlin, V.V.Nelaev, in: Computer Modeling of Defects in Crysatals (LFTI, Leningrad, 1979) p.166 (in Russian).
339 . H.Saka, T.Kondo, N.Kiba, Phil.Mag. A, 44, 1213 (1981).
340 . A.D.Brailsford, R.Bullough, in: Vacancies'76 (The Metals Society, London, 1977) p.108.
341 . A.Seeger, in: Defects in Crystalline Solids, Proc.Int.Conf., Univ. of Bristol, July 1954 (London, 1955), p. 392.
342 . V.A.Borodin, A.I.Ryazanov, Atomnaya Energiya, 63, 127 (1987).
343 . V.A.Borodin, A.I.Ryazanov, C.Abromeit, J.Nucl.Mater., 207, 242 (1993).
344 . V.A.Borodin, V.V.Kolomytkin, U.R.Kevorkyan, A.I.Ryazanov, J.Nucl.Mater., 187, 131 (1992).
345 . R.A.Johnson, J.Phys. F, 3, 295 (1973).
346 . Yu.S.Pyatiletov, Fiz.Met.Metalloved., 50, 646 (1980).
347 . V.V.Kirsanov, Yu.S.Pyatiletov, O.G.Tyupkina, Phys.Stat.Sol.(a), 64, 735 (1981).
348 . A.I.Bondarenko, V.M.Chernov, Preprint FEI-1475 (FEI, Obninsk, 1983).
349 . C.H.Henager,Jr., E.P.Simonen, in: Effects of Radiation on Materials. 12th Int. Symp. ASTM STP 870, vol.1 (ASTM, Phil., 1985) p.75.
350 . H.Gurol, N.M.Ghoniem, W.G.Wolfer, J.Nucl.Mater., 99, 1 (1981).
351 . L.K.Mansur, W.A.Coghlan, T.C.Reiley, W.G.Wolfer, J.Nucl.Mater., 104, 1257 (1981).
352 . H.Gurol, W.G.Wolfer, Trans. ANS, 44, 251 (1983).
353 . H.Gurol, W.G.Wolfer, J.Nucl.Mater., 117, 244 (1983).
354 . J.Weertman, J.Appl.Phys., 26, 1213 (1955).
355 . G.S.Ansell, J.Weertman, Trans. AIME, 215, 838 (1959).
356 . S.D.Harkness, J.A.Tesk, Che-Yu Li, Nucl.Appl.Techn., 9, 24 (1970).
357 . W.I.Duffin, F.A.Nichols, J.Nucl.Mater., 45, 302 (1972/73).
358 . L.K.Mansur, Phil.Mag. A, 39, 497 (1979).
359 . J.H.Gittus, Phil.Mag., 25, 345 (1972).
360 . D.O.Northwood, L.E.Bahen, R.G.Fleck, J.Nucl.Mater., 66, 209 (1977).
361 . B.Burton, Phil.Mag., A43, 1, 1 (1981).
362 . C.C.Dollins, Rad.Effects, 11, 123 (1971).
363 . C.C.Dollins, R.R.Tucker, J.Nucl.Mater., 52, 277 (1974).
364 . R.O.Scattergood, D.J. Bacon, Acta Met., 30, 1665 (1982).
365 . A.H.Cotterill, Dislocations and Plastic Flow in Crystals (Oxford Univ.,Oxford, 1953).
366 . A.J.E.Foreman, M.J.Makin, Phil.Mag., 14, 911 (1966).
367 . R.Labusch, Z.Phys., 167, 452 (1962).
368 . A.S.Argon, Phil.Mag, 25, 1053 (1972).
369 . A.I.Landau, V.N.Vydashenko, Metallofizika, 4, 3 (1982).
370 . A.L.Bement, Rev.Roum.Phys., 17, 361 (1972).
371 . J.J.Holmes, R.E.Robbins, J.L.Brimhall, B.Mastel, Acta Met., 26, 955 (1968).
372 . M.B.Toloczko, G.E.Lucas, G.R.Odette, R.E.Stoller, M.L.Hamilton, in: Effects of Radiation on Materials: 17th Int.Symp., ASTM STP 1270 (ASTM, Phil., 1996), p.902.

373 . F.A.Garner, M.L. Hamilton, N.F. Panayotou, G.D.Johnson, J.Nucl.Mater., 103-104, 803 (1981).
374 . N.V.Mott, Phil.Mag, 43, 1151 (1952).
375 . J.Friedel, Phil.Mag., 44, 444 (1953).
376 . J.E.Dorn, P.Guyot, T.Stefansky, in: Physics of Strength and Plasticity, A.S.Argon, ed. (MIT, Cambridge, 1969) p.133.
377 . A.J.E.Foreman, M.J.Makin, Canad.J.Phys., 45, 511 (1967).
378 . V.M.Chernov, M.M.Savin, Phis.Stat.Sol. (a), 53,113 (1979).
379 . G.W.Lewthwaite, J.Nucl.Mater., 46, 324 (1973).
380 . P.R.Okamoto, S.D.Harkness, J.Nucl.Mater., 48, 204 (1973).
381 . Yu.N.Socursky, L.N.Protsenko, J.Br.Nucl.En.Soc. 14, 137 (1975).
382 . T.Tabata, Y.Nakajima, T.Hida, H.Fujita, in: High Voltage Electron Microscopy 1977 (Tokyo 1977) p.519.
383 . F.A.Garner, W.G.Wolfer, Trans. ANS, 28, 144 (1978).
384 . F.A.Garner, W.G.Wolfer,H.R.Brager, in: ASTM STP 683, Eds. J.A.Sprague and D.Kramer (ASTM, Phil., 1979) p.160.
385 . M.Suzuki, S.Sato, J.Nucl.Mater., 172, 97 (1990).
386 . B.J.Whiting, D.J.Bacon, Mat. Res. Soc. Symp. Proc., 439, 384 (1997).
387 . Yu.N.Osetsky, A.Serra, V.Priego, Mat. Res. Soc. Symp. Proc.., 527, 59 (1998).
388 . A.V.Barashev, Yu.N.Osetsky, D.J.Bacon, Mat. Res. Soc. Symp. Proc., 540, 697 (1999).
389 . A.V.Barashev, Yu.N.Osetsky, D.J.Bacon, Phil. Mag. A, 80, 2709 (2000).
390 . R.V.Hesketh, Phil.Mag., 7, 1417 (1962).
391 . G.W.Lewthwaite, Scripta Met., 7, 75 (1973).
392 . R.Bullough, M.H.Wood, J.Nucl.Mater., 90, 1 (1980).
393 . A.I.Ryazanov, V.A.Borodin, Rad.Effects, 59, 13 (1981).
394 . L.A.Maximov, A.I.Ryazanov, Rad.Effects, 33, 7 (1977).
395 . K.Nakai, C.Kinoshita, Y.Muroo, S.Kitajama, Phil.Mag., A48, 215 (1984).
396 . S.Jitsukawa, Y.Katano, K.Shiraishi, F.A.Garner, in: Effects of Radiation on Materials. 15th Int. Symp. ASTM STP 1125 (ASTM, Phil., 1992) p.1034.
397 . J. Garnier, Y.Bréchet, M.Delnondedieu, C.Pokor, P.Dubuisson, A.Renault, X.Averty, J.-P. Massoud, J.Nucl.Mater. 417, 63 (2011)
398 . H.Hausen, W.Schuele, M.R.Cundy, Fusion Techn. 88, 905 (1988).
399 . W.Schuele, H.Hausen, J.Nucl.Mater., 212-215, 388 (1994) .
400 . H.Hausen, W.Schuele, in: Effects of Radiation on Materials: 18th Int.Symp., ASTM STP 1325 (ASTM, Phil., 1999) p.742.
401 . C.H.Woo, F.A.Garner, J.Nucl.Mater., 191-194, 1309 (1992).
402 . C.H.Woo, F.A.Garner and R.A.Holt, in: Effects of Radiation on Materials: 16th Int.Symp., ASTM STP 1175 (ASTM, Phil., 1994), p. .
403 . M.B.Toloczko, F.A.Garner, J.Nucl.Mater., 212-215, 509 (1994).
404 . D.S.Gelles, in: Effects of Radiation on Materials. 12th Int. Symp. ASTM STP 870, vol.1 (ASTM, Phil., 1985) p.98.
405 . W.G.Wolfer, L.K.Mansur, J.A.Sprague, in: Radiation Effects in Breeder Reactor Structural Materials, Proc.Int.Conf., Scottsdale, AZ, 1977, p.841.
406 . C.H.Woo, Phil.Mag., A42, 551 (1980).
407 . C.A.English, W.J.Phytian and A.J.E.Foreman, J.Nucl.Mater., 174, 135 (1990).
408 . T.Diaz de la Rubia, M.W.Guinan, Mat.Sci.Forum, 97-99, 23 (1992).
409 . R.Bullough, M.R.Hayns, J.Nucl.Mater., 65, 184 (1977).
410 . L.K.Mansur, W.A.Coghlan, in: Dimensional Stability and Mechanical Behaviour of Irradiated Metals and Alloys. Proc. BNES Conf., vol.2 (BNES, London, 1984) p.65.

411 V.A.Borodin, A.I.Ryazanov, J.Nucl.Mater., 165, 164 (1989).

Annex I: Irradiation creep behavior of ODS steels

Jiachao Chen, PSI

Irradiation creep studies, due to their high technical and financial cost, were mostly limited to candidate structural steels. Investigation on ODS steels only took off when these materials came into the scope for application in advanced nuclear devices due to their excellent high temperature strength, low irradiation-induced swelling and potential resistance to helium embrittlement. Here a summary will be drawn based on limited results available in the literature [1-6].

1. Parametric dependence of irradiation creep compliance

The study of the parametric dependence of irradiation creep on materials (lattice structures and compositions), damage spectrum (K, $T_{1/2}$, He et al.), and loading states (T, σ), is essential for both engineering application and basic understanding. The most common experimental method of irradiation creep study are "pressurized tubes" in reactor experiments [7] and uniaxial loading in accelerator experiments [8]. The former is closer to real service condition of reactor components. But the latter offers the possibility to perform experiments under well-defined conditions which will

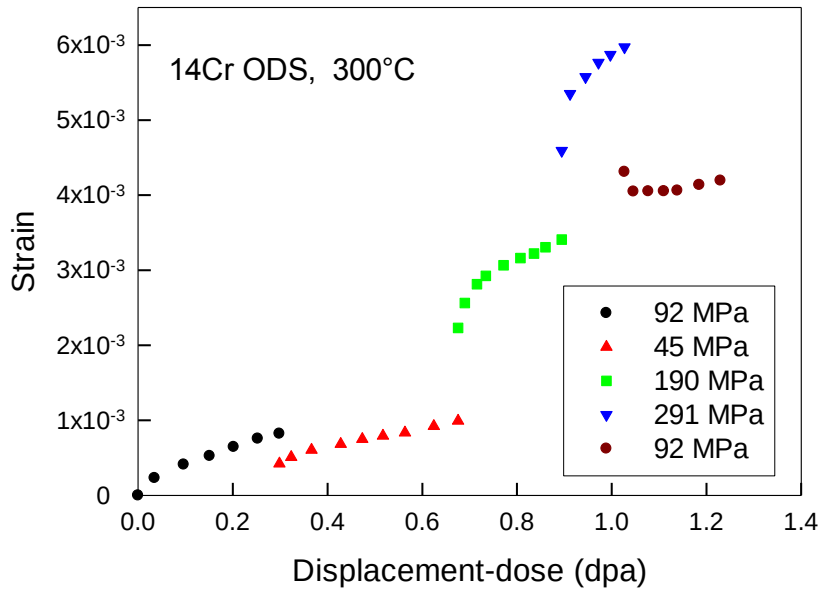

Fig 1: Creep strain of 14Cr ODS steels during He-implantation at 300°C as a function of displacement dose at different stresses.

simplify the data analysis. The following summary is mainly based on the results from accelerator experiment. However, a comparison to reactor experiment will be mentioned.

Irradiation creep is observed at temperatures far below the typical thermal creep regime. In most cases irradiation-creep strain rate $\dot{\varepsilon}$ is proportional to irradiation displacement damage rate K and to stress σ (at least at low to intermediate applied stresses), i.e.:

$$\dot{\varepsilon} = B \cdot \sigma \cdot K \qquad (1)$$

The irradiation creep compliance B, i.e. creep rate per unit dose rate and stress, can be written in the form $B = B_0 + D \cdot \dot{S}$, where B_0 is the compliance without swelling, D is the creep-swelling coupling coefficient, and $\dot{S}$ is the instantaneous volumetric swelling rate per dpa. Ferritic/martensitic steels under neutron irradiation showed negligible swelling up to doses in the 20 dpa range.

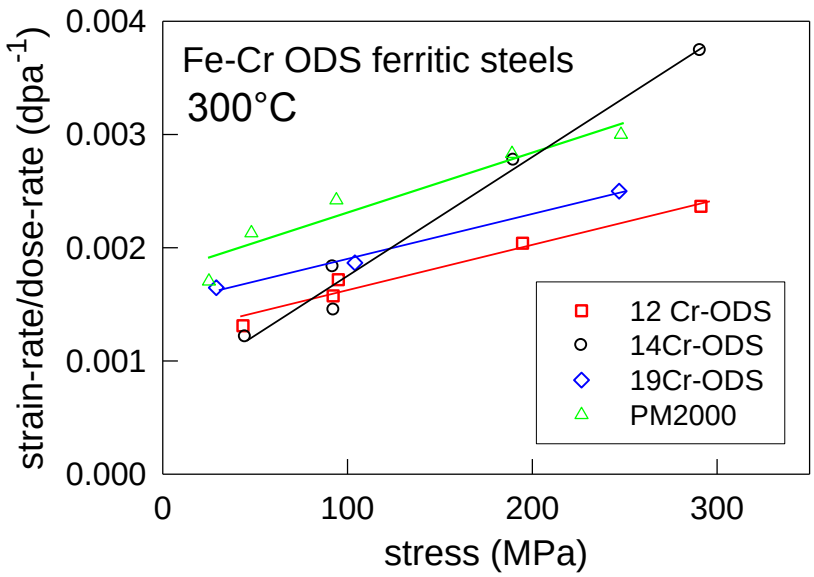

Fig 2: Irradiation creep rates per displacement rates of 12Cr ODS, 14Cr ODS, 19Cr and PM2000 steels as a function of tensile stress under He-implantation at 300°C. Linear fits give irradiation creep compliances.

The linear strain $\varepsilon(\sigma) = \frac{\Delta l}{l_0}$ during implantation was measured as a function of displacement dose under uniaxial applied stresses. As an example, Fig. 1 shows a typical strain-displacement dose curve of 14Cr-ODS steel during implantation at 300°C. According to the results from PM2000 [1], it is fair to assume that thermal creep is negligible at 300°C. Each stress change caused, aside from elastic strain, also a short transient stage before stationary creep was reached. Those transient strains are similar to observations in other ODS steels [1-4]. They are ascribed to irradiation-induced relaxation. It is worth to notice that in all steels a contraction of the specimen against the applied tensile stress occurred at the beginning of irradiation when the applied stress was reduced (e.g. from 300 to 100 MPa), but already after a dose of less than 0.03 dpa, creep proceeds again in the stress direction.

Irradiation induced strain rates $\varepsilon' = \frac{\dot{\varepsilon}}{K}$, i.e. strain-rate/damage-dose-rate (in unit of dpa^{-1}) were obtained by fitting straight lines to the stationary parts of the curves in Fig. 1. These values were further plotted against applied stress. Here an example is given in Fig. 2 for the 4 ODS steels. The ε' versus σ data can be fitted by a linear stress dependence at least up to 300 MPa (solid line):

$$\varepsilon'(\sigma) = B_0 \sigma \qquad (2)$$

This behaviour is similar to pure metals [9], nickel-based alloys and austenitic stainless steels [10].

Table 1: Result on irradiation creep

materials	grain size (μm)^3	ODS particle size (nm)	ODS particle density(m^{-3})	$\sigma_{0.2}$ at 300°C (MPa)	creep compliance (10^{-6}dpa^{-1}MPa^{-1})	offset ε'_0 (10^{-3} dpa^{-1})
12Cr ODS	1.3x1.3x8.0	2.2	1.6x10^{23}	992	4.0	1.2
14Cr ODS	0.5x0.5x2	4.8	4.5x10^{22}	1087	10.	0.72

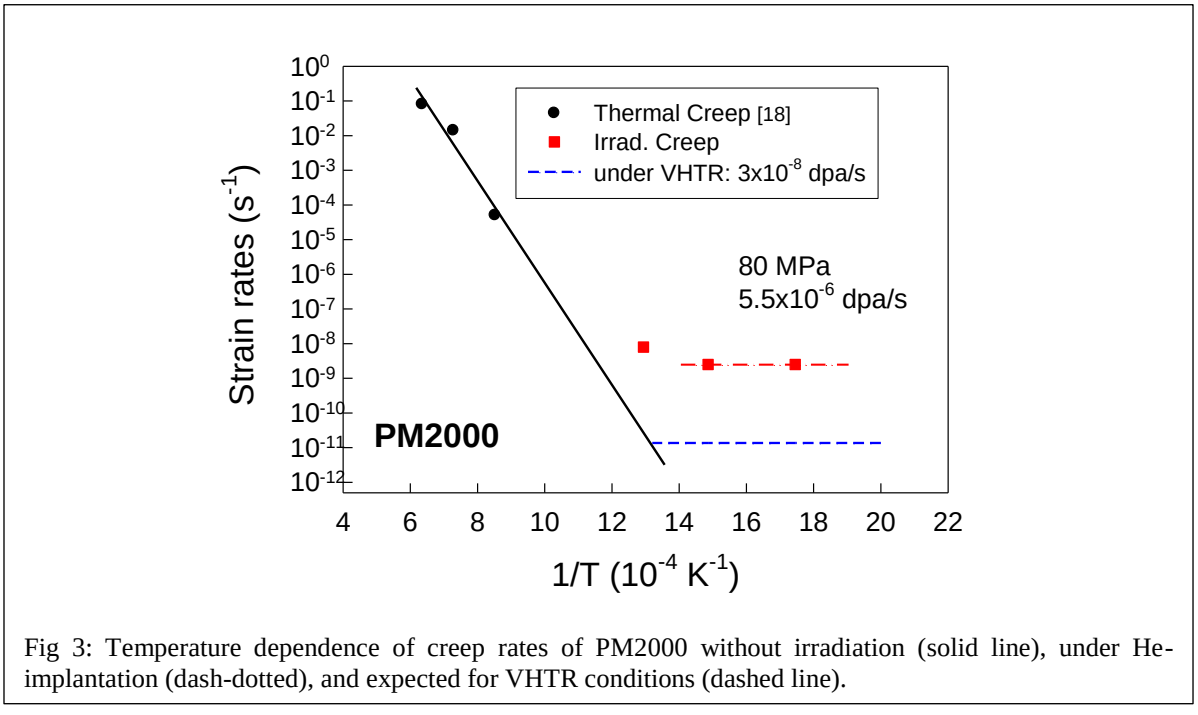

Fig 3: Temperature dependence of creep rates of PM2000 without irradiation (solid line), under He-implantation (dash-dotted), and expected for VHTR conditions (dashed line).

The measured irradiation creep compliances B_0 for the investigated materials are summarized in Table 1. **The results reveal that size and distribution of dispersoids have no significant influence on irradiation creep behaviour of ODS steels. It might thus be inferred that irradiation creep is a pure matrix phenomenon**.

The temperature-dependence of creep strain rates with and without He-implantation [11] is given in Fig.3. The thermal creep data are from standard bulk specimens [11]. The effect of miniature size of the present specimens on creep cannot be precisely assessed, as literature on this topic is contradictory [12, 13]. Expected creep rates under conditions close to those encountered in future very high temperature reactors (VHTR) are included. The present data show that the irradiation creep rate of PM2000 is the same for 573 K and for 673 K. Extrapolation of irradiation data at 80 MPa and $3x10^{-8}$ dpa/s match the thermal creep line at about 760 K. From the results, B_0 is almost independent of temperature and becomes dominant in comparison to thermal creep at temperatures below about 800 K in PM2000 [1] for dose rates typical of fast reactors. According to earlier experimental findings [14] and theoretical understanding [15, 16], irradiation creep dominates at low temperatures when the thermal vacancy concentration is negligible. Only a minor temperature dependence is expected in this area. When thermal creep dominates at high temperatures, irradiation will have no major influence on creep rates [14] except possibly via irradiation induced microstructural or compositional changes.

The irradiation creep data from the He-bombardments [1-4], and from previous proton [17] and neutron irradiations [18-20] of ferritic/martensitic and ODS steels are summarized in Fig. 4. Strains and stresses of pressurized tubes in reactor experiments are effective values obtained by the Soederberg formalism. The comparison shows that **the compliances from neutron irradiations are by almost one order of magnitude lower than that from light ions**. This difference is ascribed to three contributions:

1) Light ions (and electrons) produce defects with a much softer recoil spectrum than fast neutrons (and heavy ions). Experiments on defect production showed that the NRT model, commonly used to calculate damage rates in reactor experiments overestimate the efficiency of defect production at high recoil energies by about a factor of three [15], thus giving compliances which are too low by this factor.
2) Various creep experiments in reactors show that creep rates are decreasing by factors in the order of 2 even above ≈5 dpa (typically the lowest dose investigated in reactor experiments) [18, 19]. This means that the present light ion creep strains (at doses far below 1 dpa), though apparently linear in dose, may still be not completely stationary.
3) All neutron data in Fig. 4 are obtained from pressurized tubes, i.e. from triaxially stressed samples, in contrast to the uniaxially stress state in the light ion irradiations. In spite of the meagre data base on uniaxial in-pile experiments, there are some indications that

irradiation creep rates in pressurised tubes may be slightly lower than under uniaxial loading [21, 22].

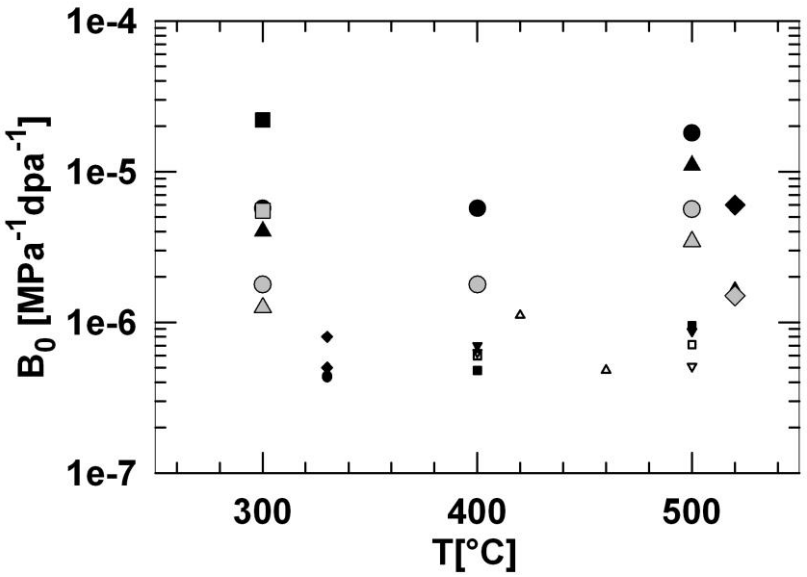

Fig.4: Comparison of irradiation creep compliances B_0 as a function of irradiation temperature T. Big, black and gray filled symbols indicate light ion irradiations before and after damage efficiency correction, respectively: He-implanted ODS PM2000 (●,●) and 19Cr-ODS (▲,▲), p-irradiated ODS Ni-20Cr-1ThO_2 (■,■), p-irradiated martensitic DIN1.4914 (◆,◆). Small symbols indicate neutron irradiations to doses below 25 dpa (filled symbols) and above 25 dpa (empty symbols): ODS MA957 (▼,▽), HT9 (▪,▫), HT9 (•), F82H (△), Fe-16Cr (•).

2. Irradiation creep models versus experimental evidence

A variety of models for irradiation creep has been proposed, for extensive reviews see the theoretical parts of this report. But up to now it was not possible to unambiguously identify the underlying mechanism. Various criteria may be taken into consideration to discriminate between these models:

1) Effect of irradiation particle and/or energy: For example the above result, showing that irradiation creep compliances under light ion irradiation are higher or - after the above corrections - at least equal to those under fast neutron irradiation, contradicts models which emphasize effects of cascades or inhomogeneity (in space or time) of defect production.

2) Dependence on experimental parameters (dose, dose rate, stress, temperature, etc.): Unfortunately many models predict similar parametrical dependencies, e.g. linear dependence of

strain on dose (at least after some initial transient), of strain rate on dose rate and stress, and weak increase with temperature (at least up to temperatures where thermal creep contributes).

3) Parameter transients: Intentional parameter changes are difficult to perform in reactor irradiations. On the other hand, so far very limited results are reported from light ion experiments. Dose rate and temperature transients apparently have a negligible effect on creep compliance [23], again ruling out models based on inhomogeneity of defect production. Also the small initial transient of irradiation creep indicates that glide processes give no major contribution. On the other hand, the fast response of creep rate on stress changes strongly contradicts models based on stress induced preferential nucleation (SIPN) of dislocation loops.

4) Material composition, including precipitates and dispersed particles: There is a clear tendency of reduction of irradiation creep compliance with increasing content of minor elements in steels. But this effect is much less under irradiation compared to thermal creep. In total the overall dependence on material (for pure metals see ref.[24]), composition, alloying and precipitation or segregation is relatively weak.

5) Effect of microstructure: Ferritic/martensitic steels apparently show systematically lower creep compliances than austenitic, but the difference in irradiation creep seems to be smaller than for example in swelling. Also the effect of dislocation density on creep rate is rather weak, as well as the effect of spatial homogeneity of dislocation structure [25]. Vice versa the dependence on stress of the microstructural record after irradiation also allows discrimination between different mechanisms, as will be shown in the next section.

3. Impact of microstructural findings on irradiation creep models

The most discussed irradiation creep models are based on preferential interaction of interstitials with those dislocations which are favourably oriented with respect to the external stress. All of these models predict an imprint of irradiation creep on the microstructure.

A detailed study on dislocation structure was performed in PM2000 [2], where the evolution of dislocation loops was analysed by transmission electron microscopy. To identify the effect of stress, the Burgers vectors and habit planes of the dislocation loops were determined for the specimens at various temperatures by systematically tilting the specimens to several low-index orientations of the bcc lattice, such as [001], [$\bar{1}$ 11] and especially [011]. All loops are approximately circular. Two set of pure edge loops of type <100>(100), and type ½<111>(111) were identified. By using ±***g***

technique, both sets of loops produced by He-implantation under uniaxial tensile stresses at different temperatures are observed to be of interstitial type.

In PM2000, implanted at 573 K to 0.75 dpa, ½<111> loops are dominant, with an average diameter of 3.6 ±1 nm and an apparent number density of 2.4×10^{23} /m^3, only few <100> loops of 5.5±1.1 nm in diameter can be observed. At 673 K (0.74 dpa), the average diameter of the ½<111> loops increased to 69 nm, while that of the <100> loops increased to 44 nm and their number density was higher. At 773 K (0.46 dpa), sizes of <111> and <100> loop reach 34 nm and 28 nm, respectively. At that temperature, some loops start to glide and climb to form dislocation fragments. The most important result was, however, that the loops showed no correlation in terms of orientation or geometry with the direction of applied stress, as illustrated in Fig. 5. The characteristics (habit planes, diameters, number densities) of the observed loop families at the three temperatures are summarized in Table 3, together with their orientation with respect to the applied external stress direction.

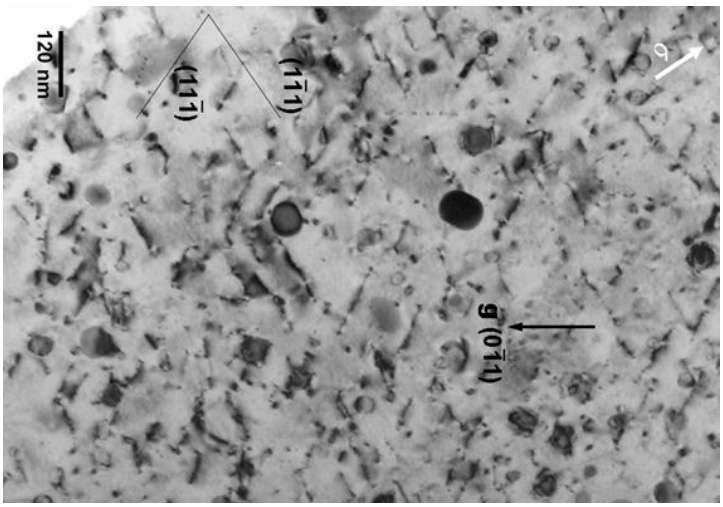

Fig. 5: Bright-field TEM images taken from ***z***=[011] under 2-beam dynamical conditions for a PM2000 specimen implanted at 673 K. The ***g***-vector is shown as black arrow. The (1 $\bar{1}$ 1) and (11 $\bar{1}$) planes are indicated by thin lines. The direction of applied stress is indicated by the white arrow. Note the equal distribution of loop sizes and of loop densities in the image.

Table 3: Diameters and densities of interstitial dislocation loops and their orientation with respect to external stress in PM2000 after He-bombardment. The errors of the diameter and density give standard deviation. The errors of the angle give the precision of applied stress direction.

T(K)	loop family	habit plane	diameter d (nm)	density N (m^{-3})	angle (***b***, σ)

573	½<111> <100>	{111} {100}	3.6±1.0 5.5±1.1	$4.8\pm1.1\times10^{23}$ Very low	- 54.74±4°
673	½[1$\underline{1}$1] ½[11$\underline{1}$] ½<111> <100>	(1$\underline{1}$1) (11$\underline{1}$) {111} {100}	70±25 67±21 68±23 44±15	$7.0\pm1.6\times10^{20}$ $6.7\pm1.5\times10^{20}$ $27.4\pm6.2\times10^{20}$ $4.7\pm1.1\times10^{20}$	0±4° 70.52±4° - 54.74±4°
773	½<111> <100>	{111} {100}	34±15 28±11	$3.5\ \pm0.8\ \times\ 10^{20}$ $2.4\ \pm0.5\ \times\ 10^{20}$	- 54.74±4°

The finding that neither the size nor the density of the irradiation-induced dislocation loops shows any dependence on the direction of the applied stress is at variance with the predictions of the most prominent irradiation creep models, based on stress-induced preferential absorption of interstitial loops (SIPA) or stress-induced preferential nucleation (SIPN). While SIPN should show up in an anisotropic distribution of loop densities, SIPA should produce an anisotropy of loops sizes. A similar study on TiAl [26] yielded irradiation creep rates of the same order of magnitude as in PM2000, while no dislocations and only a meagre population of black-dots or loops were detectable by TEM in the TiAl alloy.

4. Conclusions

1. Irradiation creep rates of ODS ferritic steels show linear stress dependence at temperature from 300 to 500°C.

2. Irradiation compliance is constant at and below 400°C and increases slowly at 500°C.

3. Irradiation creep is insensitive to material structures (lattice, grain size, ODS particles, dislocation densities et. al.).

4. There exist no significant effects of bombarding particles (He and H) on irradiation creep.

5. In a ferritic ODS steel (bcc lattice) implanted with helium, two sets of loops were completely identified, having Burgers vectors of ½<111> and <100>, and habit planes of {111} and {100}, respectively. Both types of loops are interstitial in nature.

6. No differences in size and number density of loops with different orientations relative to the applied stress could be found. This contradicts predictions made by models such as SIPA and SIPN and calls for additional experimental and theoretical studies to eventually modify or replace existing irradiation creep models.

Reference

[1] J. Chen, P. Jung, M.A. Pouchon, T. Rebac, W. Hoffelner, Journal of Nuclear Materials 373 (2008) 22
[2] J. Chen, P. Jung, W. Hoffelner, H. Ullmaier, Acta Materialia 56 (2008) 250
[3] J. Chen, M.A. Pouchon, A. Kimura, P. Jung, W. Hoffelner , Journal of Nuclear Materials 386-388 (2009) 143
[4] J. Chen, P. Jung, J. Henry, Y. de Carlan, T. Sauvage, F. Duval, M.F. Barthe, W. Hoffelner, Journal of Nuclear Materials 437 (2013) 432
[5] P. Jung and P.B. Chilson, Journal of Nuclear Materials 149 (1987) 1
[6] M.B. Toloczko, D.S. Gelles, F.A. Garner, R.J. Kutz, K. Abe, Journal of Nuclear Materials 329-333 (2004) 352
[7] F.A. Garner, D.S. Gelles, Journal of Nuclear Materials 159 (1988) 286
[8] P. Jung, A. Schwarz and H.K. Sahu, Nucl. Instr. and Meth. A234 (1985) 331
[9] P. Jung and M.I. Ansari, J. Nucl. Mater. 138 (1986) 40
[10] P. Jung, J. Nucl. Mater. 113 (1983) 133
[11] J. Wunder, in “Mikrostrukturelle Beschreibung der Warmfestigkeit ferritischer Superlegierungen” Fortschr. –Ber. VDI Reihe 5 Nr. 510, Duesseldorf: VDI Verlag 1997, p. 84
[12] N.Igata, K.Miyahara, C.Tada, D.Blasl and G.Lucas, Radiat.Effects 101 (1986) 131
[13] D.G.Rickerby, P.Fenici, P.Jung, G.Piatti and P.Schiller, ASTM-STP 888 (1986) 220
[14] P. Jung and N.M. Afify, J. Nucl. Mater. 155-157 (1988) 1019
[15] H. Ullmaier and W. Schilling, Radiation Damage in Metallic Reactor Materials in “Physics of Modern Materials”, Vol.1, International Atomic Energy Agency, Vienna, 1980, p301.
[16] L.K. Mansur, in: G.R. Freeman (Ed.), Kinetics of Non-homogeneous Processes, Wiley-Interscience, New York, 1987
[17] Zh. Zhu, Peter Jung and Horst Klein, J. Nucl. Mater. 202 (1993) 222
[18] M.B. Toloczko, D.S. Gelles, F.A. Garner, R.J. Kurtz and A. Abe, J.Nucl.Mater. 329-333(2004) 352
[19] M.L. Grossbeck, L.T. Gibson and S. Jitsukawa, J. Nucl. Mater. 233-237 (1996) 148
[20] A. Kohyama, Y. Kohno, K. Asakura, M. Yoshino, C. Namba andC.R. Eiholzer, J. Nucl. Mater. 212-215 (1994) 751
[21] A.J. McSherry, M.R. Patel, J. Marshall and E.R. Gilbert, Trans ANS 28 (1978) 146
[22] E.R. Gilbert, D.C. Kaulitz, J.J. Holomes and T.T. Claudson, in Proc.Conf. on Irrad. embrittlement and creep in fuel cladding and core components, London, BNES (1972) 239
[23] P. Jung and H. Ullmaier, Radiat. Effects 103 (1987) 21
[24] P. Jung and M.I. Ansari, J. Nucl. Mater. 138 (1986) 40
[25] P. Jung, T.C. Reiley and W. Kesternich, Fusion Technology 1980, SOFT, Proc. 11th Symposium, Oxford, p.1287
[26] J. Chen, P. Jung, M. Nazmy, W. Hoffelner, J. Nucl. Mater. 352 (2006) 36

Annex II: Irradiation creep behavior of ferritic and martensitic steels

Maxime Sauzay, DEN-DMN-SRMA, CEA Saclay

During the last two decades, several studies of the irradiation creep properties of ferritic and martensitic steels have been reported in literature. These materials are used in components of nuclear power plants and are candidates for some applications concerning the next generation of power plants. Their properties are compared to the ones of FCC metals and alloys as well as ODS steels based on the previous appendix. Finally, the different irradiation creep mechanisms proposed in literature are discussed in the light of the macroscopic and microscopic observations. A model close to the SIPAG, where G stands for glide, in agreement with the most recent observations, is proposed for being developed in the framework of the MOIRA project.

1. Parametric dependence of irradiation creep compliance

As for other materials, tubes under internal pressure are used for the experiments. The hoop strain measured without pressure is usually substracted from the one measured under pressure. This allows a crude correction of the swelling effect if active. Von Misès equivalent viscoplastic strain and stress are used in the plots. In some of the experiments described below (thin plate specimen loaded in situ), very thin specimens are used which may lead to surface effects introducing some possible bias.

Neutron, proton or He are used in the irradiations. The flux is usually about a few 10^{-6} dpa/s. It should be noticed that the irradiation dose is sometimes too low to allow the saturated strain rate to be reached (stationary creep stage) which introduces another possible bias in some of the comparisons.

2. Stage I or non stationary stage

For all the considered martensitic and ferritic steels, a non-stationary stage is first observed before strain rate reaches its minimum, if the applied irradiation dose is high enough.

This holds for all the considered martensitic steels or ferritic steels [Figs. 1-3].

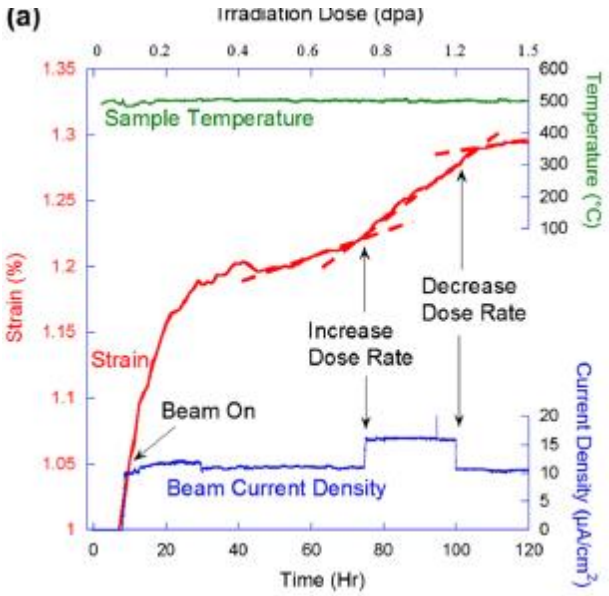

Fig. 1: In-situ irradiation creep experiment, thin sample, grade 91 steel (tempered ferritic martensitic steel) [Xu and Was, 2013].

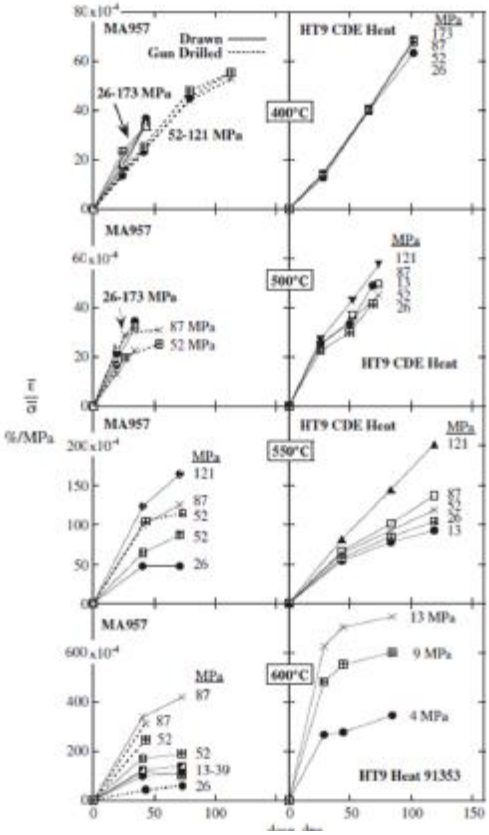

Fig. 2: Strain evolution with irradiation dose, measured for various stress and ferritic / martensitic steels. Materials : MA957 (ODS ferritic steel) and HT9 (martensitic steel). Temperature range: 400-600°C [Toloczko et al., 2012].

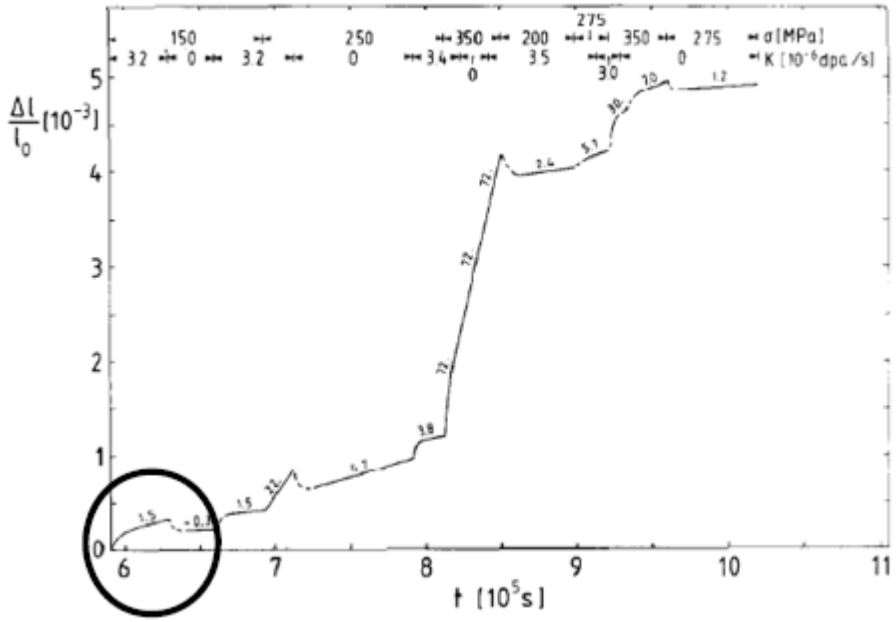

Fig. 3: Strain evolution with time, during a test including change in irradiation dose and stress magnitude. Martensitic steel: DIN 1.4914 [Jung and Afify, 1988].

3. Stationary creep stage

Provided the irradiation dose reaches at least ten dpa, the minimum creep strain rate is reached and the creep deformation becomes saturated. This means that the measured creep strain increases linearly with the irradiation dose. Then, the effect of stress and temperature can be studied.

As observed for many other metals and alloys, such as FCC ones, the stationary creep strain rate is proportional to the applied stress (Fig. 4).

In the following, the well-known expression of stationary creep strain rate is adopted (Eq. 1), using the creep compliance, B_0, which is a material and temperature dependent parameter (unit/ 10^{-6} MPa^{-1} dpa^{-1}). Table 1 sums up the results of the measurements of the recent studies concerning ferritic and martensitic steels.

Table 1 shows that the order of magnitude of the **compliance is the same in all the ferritic and martensitic steels. Therefore, the microstructure features are generally not significant. The addition of Y_2O_3 / ODS particles has minor effects as well**.

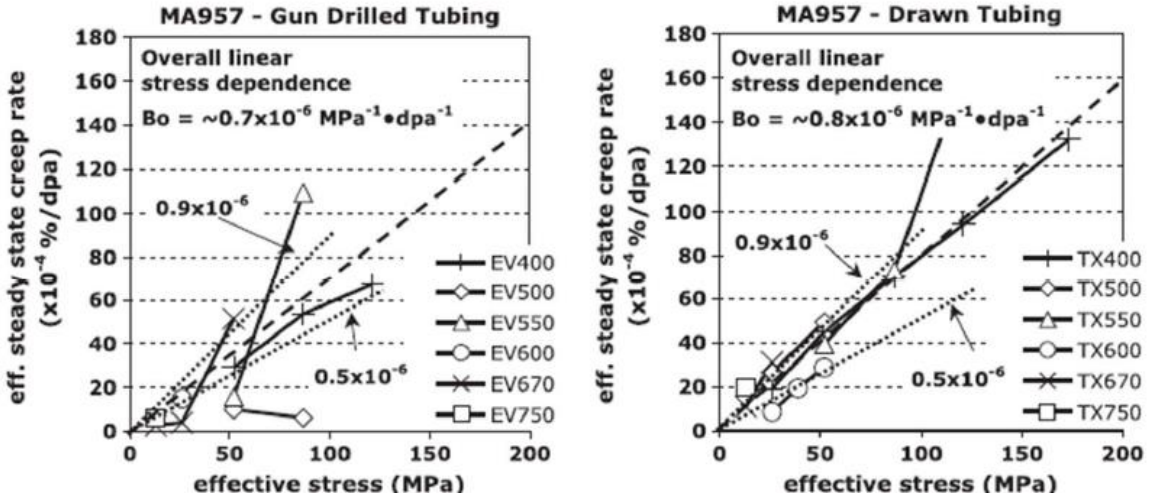

Fig. 4: influence of the effective stress on the effective stationary creep strain rate. Various temperatures have been applied (from 400°C up to 750°C). ODS ferritic steel MA957 [Toloczko et al., 2012].

Material	**B_0 (unit/ 10^{-6} MPa^{-1} dpa^{-1})**	**Authors**
HT9 (ferritic martensitic steel)	0.95	[Toloczko et al., 1998]
D57 (dispersion hardened ferritic steem)	0.4-0.6	[Toloczko et al., 1998]
MA957 (ODS ferritic steel)	0.25-0.6	[Toloczko et al., 1998]
11Cr (ferritic-martensitic steel)	0.5-0.75	[Uehira et al., 2000]
T91 (ferritic martensitic steel)	3-7 (the stationary creep deformation regime is not reached and surface effects may have introduced a bias)	
JLF (ferritic steel), 410-430°C	~0.7	[Koyama et al., 1994]
F82H (ferritic steel), 410-430°C	~0.7	[Koyama et al., 1994]

Table 1: summary of the measured creep compliance values for various BCC steels. Temperature and irradiation conditions are given in the mentioned references.

In the temperature range 400-550°C, it varies only slightly with temperature (Figs. 5 and 6). A similar observation has been made on ODS steel (see this report). But at higher temperature, an increase is observed. At high irradiation dose (36 / 60 dpa) and high temperature (460 and 520°C), a non linear dependence of strain with respect to stress is reported by Koyama et al. even if the dependence is linear at 410-430°C.

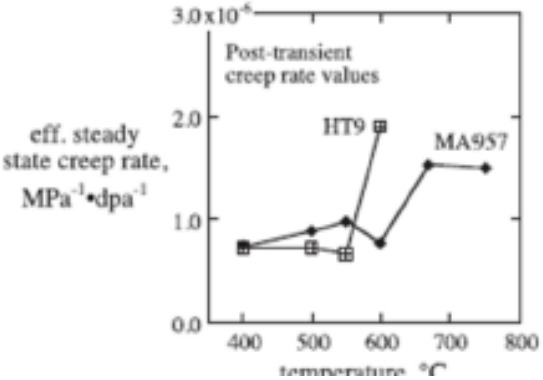

Fig. 5: effect of temperature on the measured value of the compliance, B_0. Materials : HT9 (ferritic martensitic steel) and MA957 (ODS ferritic steel).

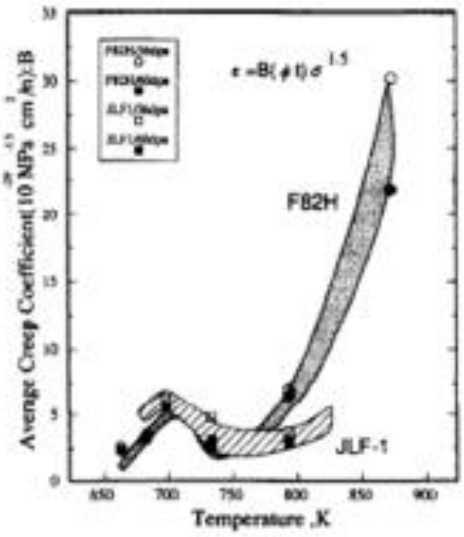

Fig. 6: effect of temperature on the measured value of the compliance (defined differently from the linear equation). Materials : F82H (ferritic steel) and JLF-1 (ferritic steel) [Koyama et al., 1994].

It should be noticed that the effect of the chemical content of Cr is almost negligible as shown by the study of Koyama et al. on a ferritic steel, provided it varies between 7 and 12%. But a very low

content of 2% leads to a much lower creep compliance value at 773K [Koyama et al., 1994]. In this case, the corresponding microstructure is bainitic.

Therefore, **provided the stationary creep deformation regime is reached, the creep compliance depends only slightly on temperature and Cr content**. The measured value of the compliance is rather weakly dependent on the microstructure (ferritic grains or tempered martensitic-ferritic microstructure).

4. *Comparison of the irradiation creep of various materials*

Non stationary creep stage has been sometimes reported for austenitic stainless steels [Gilbert et al., 1972]. It is more easily observed at high temperature. It is observed in ODS steels as well (see this report).

As shown in this report, the creep compliance of ODS steels is only slightly dependent on temperature. This has been shown earlier for austenitic stainless steels. This is a generic property of irradiation creep, provided temperature is lower than about 500°C.

The creep compliance of ferritic and ferritic-martensitic steels is about three times lower than the compliance measured in austenitic stainless steels. Nevertheless, the order of magnitude is the same.

5. *Irradiation creep versus thermal creep*

During stage I, experiments show that the ferritic and martensitic steels deform more quickly under irradiation creep than thermal creep [Xu and Was, 2013; Toloczko et al., 2004]. The considered temperatures are 500 and 600°C. The mechanical tests carried out by applying change in dose rate and stress magnitude show clearly that **irradiation creep strain rates are much higher than thermal creep ones** (Fig. 3).

During stationary stage, the irradiation creep strain rate is higher than the thermal one, provided the stress magnitude is not too high (Fig. 7).

These comparisons are in agreement with the ones shown by Chen et al. concerning ODS steels which deform much faster during irradiation creep than thermal creep under the doses and temperatures of interest.

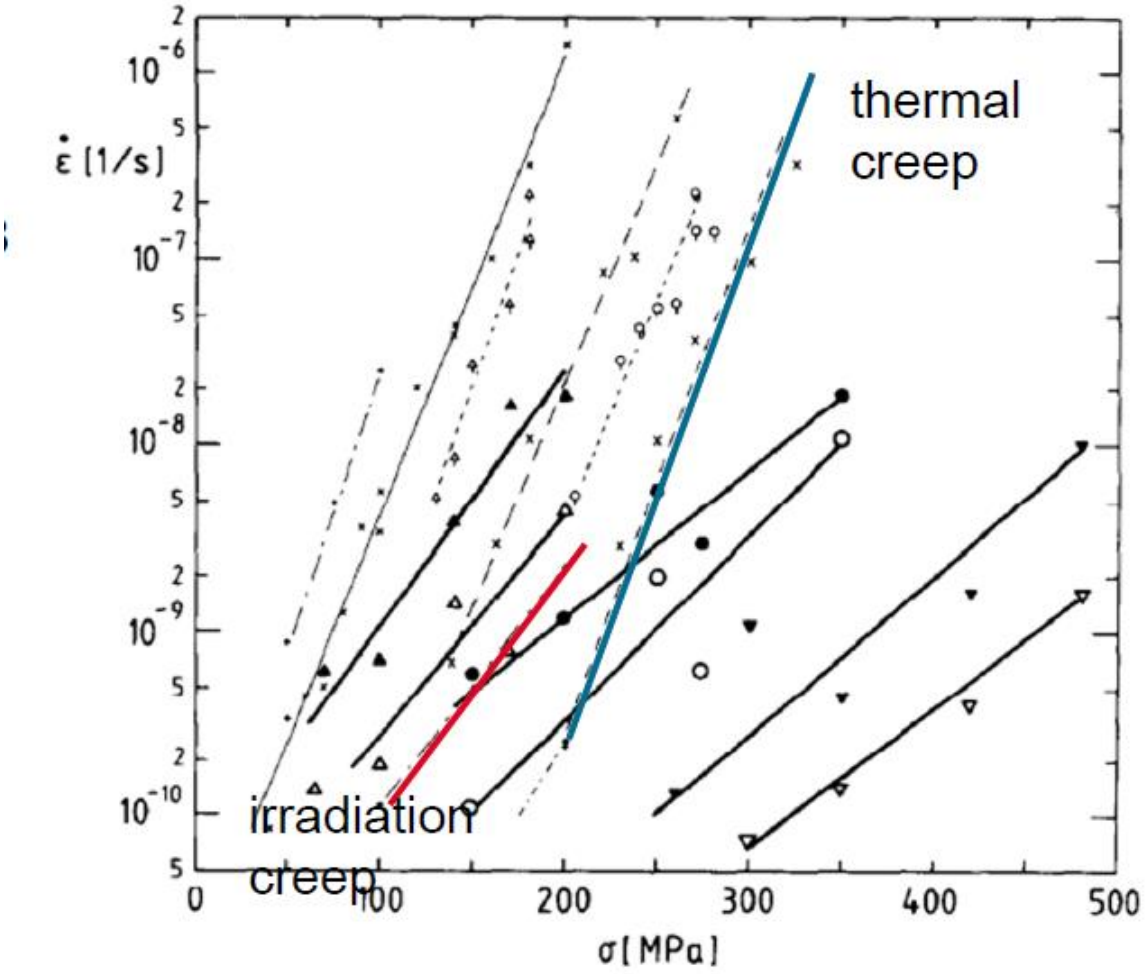

Fig. 7: minimum creep strain rates measured under either irradiation creep (red curve, irradiation flux: 10^{-6} dpa/s) or thermal creep (blue curve) at 450°C. Dependence with respect to stress. Martensitic steel: DIN 1.4914 [Jung and Afify, 1988].

6. Irradiation creep mechanisms

From the macroscopic point of view, the application of the SIPN model leads to predicted values of creep strain rates which are lower than the experimental ones. The application of the SIPA model leads to overestimations [Garnier, 2007], even if refined cluster dynamics computations are carried out [Jourdan, 2014].

From the point of view of the irradiation microstructure, the TEM observations of Chen et al. carried out on an ODS steel allow him to provide the following conclusions:

- No preferential orientation of the loops is observed, which is in contradiction with the SIPN hypothesis;
- No size dependence of the loops with respect to the tensile axis is observed, in contradiction with the SIPA model.

It should be noticed that similar observations have been reported in literature concerning austenitic stainless steels [Garnier, 2007] and TiAl, even if the same early observations support the SIPN hypothesis.

All these observations show that neither the SIPN model nor the SIPA model predictions agree with experimental observations at macroscopic or microscopic scales.

TEM observations show clearly that the density of free dislocations segments is rather high during an irradiation creep tests carried out on:

- The ferritic martensitic steel, grade 91 at 500°C (Fig.8);
- The ODS steel observed by Chen et al. at 500°C;
- The austenitic stainless steel observed in [Garnier, 2007].

These free dislocations should be taken into account in the modelling of the deformation mechanisms occurring during irradiation creep. As proposed by the SIPAG model, the plastic deformation should be at least partially carried out by the glide of these free dislocations between two obstacles, e.g. irradiation loops. The waiting time at each obstacle may be computed using the dislocation climb expression and the obstacle height. Such modeling will be carried out during the MOIRA project by coupling cluster dynamics and crystal plasticity.

The observations of Chen and co-authors concerning the effect of ODS particles on irradiation creep deformation should nevertheless be discussed with respect to the interest of the SIPAG modeling. It was clearly shown that neither the ODS particle size or its density affect irradiation creep strain rate. If ODS particles are obstacles which should be taken into account in the SIPAG modeling, these observations seem to invalidate it. As a matter of fact, the combination of climb and glide between two obstacles leads to the well-known modified Orowan equation:

$$\gamma^{creep} = \rho v_{climb} \frac{L_{obst}}{h_{obst}} b$$

With ρ the density of (mixed and edge) free dislocation segments, v_{climb} the climb velocity, and b the length of the Bürgers vector. The obstacle characteristic lengths are its average height, h_{obst}, and its average interspacing L_{obst}. In an ODS steel subjected to irradiation creep, which obstacles are the most influent: the ODS particles or the irradiation loops? Following the modified Orowan equation, **the creep slip rate is more affected by the population of obstacles with the lowest L_{obst}/h_{obst} ratio**. This is why, we compare in the following the characteristic obstacle ratio between the two populations: ODS particles versus irradiation loops. We use the data measured by Chen et al. for different ODS steels including both size and density for both ODS particles and irradiation loops [Chen et al., 2009 and 2013].

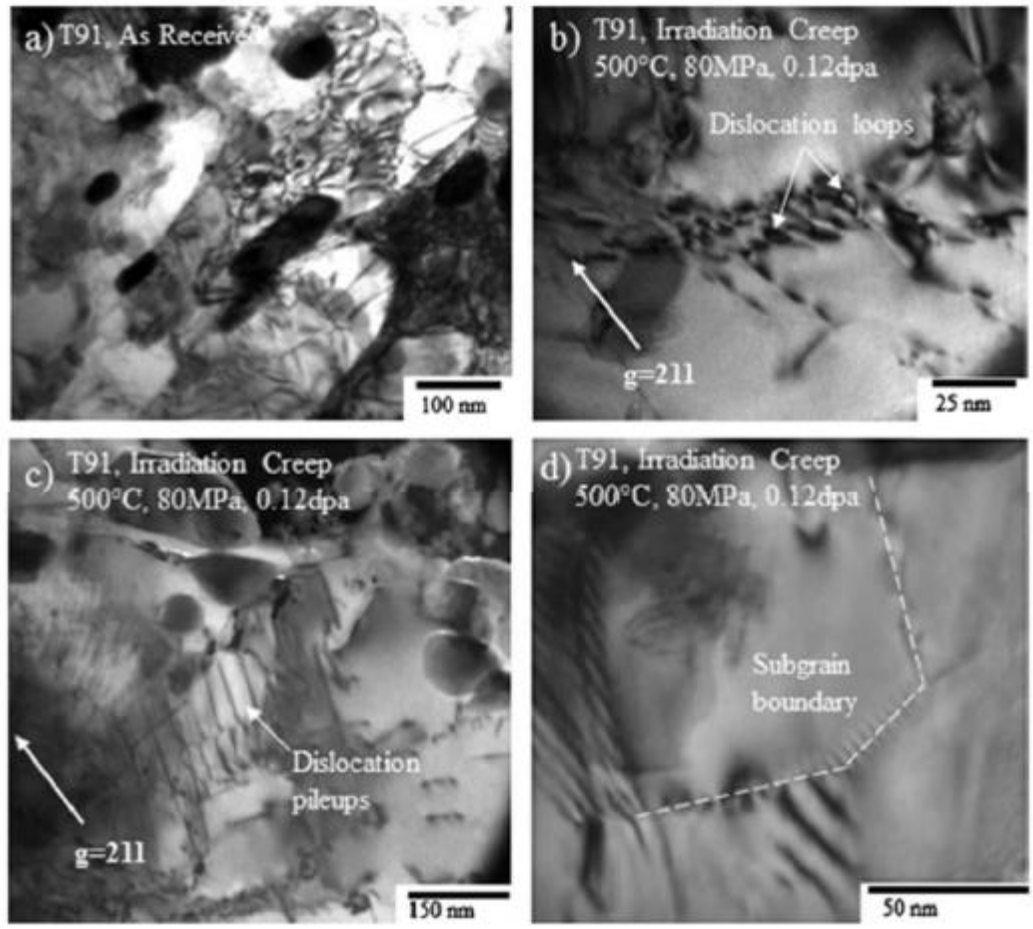

Fig. 8: TEM bright field image of samples following irradiation creep at 500°C, 80MPa to 0.12dpa. (a) as-received T91, (b) dislocation loops, (c) dislocation pile-up and (d) subgrain boundary (denoted with dashed lines) [Xu and Was, 2013].

Table 2 shows clearly that whatever the irradiation temperature, the characteristic obstacle length ratio is much lower for irradiation loops than ODS particles. The ratio which affects strongly the irradiation creep rate is at least ten times lower for irradiation loops than for ODS particles.

These conclusions hold for a particular ODS steel, PM2000, tested at various temperatures. What about the other ODS steels? Table 3 summarizes the obstacle lengths and ratio measured by Chen and co-workers for oxide particles in four different ODS steels. The obstacle ratios are generally lower than the one measured in the ODS steel PM2000. Nevertheless, the obstacle ratio of all ODS steels is generally higher than the one computed for each populations of the two or three kinds of irradiation loops considered in Table 2. A more rigorous computation taking into account the two or

three populations of irradiation loops observed at each temperature would confirm that generally, **irradiation loops are more influent than ODS particles**.

Therefore, the conclusions of Chen and co-authors about the low effect of ODS particle features on irradiation creep are not in contradiction with the SIPAG modeling because **irradiation loops seem to affect more strongly irradiation creep mechanisms and rate than ODS particle do**.

T (°C)	h_{obst} (nm) oxide	L_{obst} (nm) oxide	L_{obst}/h_{obst} oxide	h_{obst} (nm) loop	L_{obst} (nm) loop	L_{obst}/h_{obst} loop
300	2.8	144.5	44.5	3.6 70.	12.7 112.1	3.5 1.6
400	2.8	144.5	44.5	67. 68. 44.	114.3 71.2 128.	1.7 1. 2.9
500	2.8	144.5	44.5	34. 28.	141.2 160.1	4.2 5.7

Table 2: size, interspacing and characteristic obstacle length ratio calculated for either ODS particles or irradiation loops. Several kinds of irradiation loops are considered at each temperature. Materials: PM2000 ODS steel. TEM data [Cheng et al., 2009].

ODS steel	h_{obst} (nm) oxide	L_{obst} oxide	L_{obst}/h_{obst} oxide
12Cr	2.2	18.4	8.3
14Cr	4.8	28.	5.8
19Cr	2.1	9.4	4.5
PM2000	2.8	144.5	44.5

Table 3: size, interspacing and characteristic obstacle length ratio calculated for ODS particles in various ODS steels. TEM data [Chen et al., 2013].

7. Conclusions

- Irradiation creep rates of ferritic and ferritic martensitic steels show linear stress dependence at temperatures from 300 to 500°C.

- Irradiation compliance is constant at and below 500°C and increases at higher temperature.

- Irradiation creep is only slightly sensitive to material microstructures (grain size, low-angles boundaries, dislocation densities, precipitates and particles). The measured compliances are about three times lower than the ones measured in austenitic stainless steels.

- Non stationary creep is observed in most of the ferritic and martensitic steels.

- In the considered ranges of temperature and stress and for the irradiation flux usually applied, irradiation creep leads to much faster deformation than thermal creep does

- Many macroscopic and microscopic observations are in contradiction with the SIPN and SIPA modeling. Non neglible densities of free dislocations segments are observed at 500°C in different steels. These dislocations may glide between obstacles and pass than by climbing. This corresponds to the SIPAG hypothesis. The low effect of ODS particle size and interspacing on irradiation creep strain rates do not contradict the SIPAG modeling because the comparison with the mean size and interspacing of irradiation loops show that these ones should affect more irradiation creep strain rates than ODS particles do.

References

[Xu and Was, 2013] C. Xu, G. S. Was, Journal of Nuclear Materials 441 (2013) 681.
[Toloczko et al., 2004] M. B. Toloczko, D. S. Gelles, F. A. Garner, R. J. Kurtz, K. Abe, Journal of Nuclear Materials 329-333 (2004) 352.
[Toloczko et al., 1998] M. B. Toloczko, F. A. Garner, C. R. Eiholzer, Journal of Nuclear Materials 258-263 (1998) 1163.
[Uehira et al., 2000] A. Uehira, S. Mizuta, S. Ukai, R.J. Puigh, Journal of Nuclear Materials 283-287 (2000) 396.
[Koyama et al., 1994] A. Koyama, Y. Kohno, K. Asakura, M. Yoshino, C. Namba, C. R. Eiholzer, Journal of Nuclear Materials 212-215 (1994) 751.
[Jung and Afify, 1988] P. Jung and N.M. Afify, J. Nucl. Mater. 155-157 (1988) 1019.
[Gilbert et al., 1972] E.R. Gilbert, D.C. Kaulitz, J.J. Holomes and T.T. Claudson, in Proc.Conf. on Irrad. embrittlement and creep in fuel cladding and core components, London, BNES (1972) 239.
[Garnier, 2007] J. Garnier, PhD thesis, Université de Grenoble (INPG) and CEA Saclay (2007).
[Jourdan, 2014] Th. Jourdan, private communication, 2014.
[Chen et al., 2009] Journal of Nuclear Materials 392 (2009) 360.
[Chen et al., 2013] Journal of Nuclear Materials 437 (2013) 432.